國 立 交 通 大 學

機 械 工 程 學 系

碩 士 論 文

R-134a 和 R-407C 冷媒在水平多排小圓管內蒸發熱傳及壓降特性之實驗研究

Experimental Study of Evaporation Heat Transfer and Pressure Drop Characteristics of R-134a and R-407C in Horizontal Small Tubes

研 究 生：蘇 峯 慶

指 導 教 授：林 清 發 博士

中 華 民 國 九十三 年 六 月

R-134a 和 R-407C 冷媒在水平多排小圓管內蒸發熱傳及壓降特性之實驗研究

Experimental Study of Evaporation Heat Transfer and Pressure Drop Characteristics of R-134a and R-407C in Horizontal Small Tubes

研 究 生：蘇 峯 慶　　Student：Feng-Qing Su

指導教授：林 清 發　　Advisor：Tsing-Fa Lin

國立交通大學

機械工程學系

碩士論文

A Thesis

Submitted to Institute of Mechanical Engineering

College of Engineering

National Chiao Tung University

In Partial Fulfillment of the Requirements

For the degree of

Master of Science

In

Mechanical Engineering

June 2004

Hsinchu, Taiwan, Republic of China

中 華 民 國 九 十 三 年 六 月

誌 謝

時光飛逝，想當初才剛進交大，對於一切總是那麼地陌生。由於學長與學弟的關心與幫助，讓我在這兩年的研究所生活過得非常充實與開心。在這兩年的研究過程中，林清發老師的教學態度與研究精神都是值得我學習的對象，相信對於往後不管是工作或是學習上都是很有幫助的。然而，從一開始對於冷凍空調方面的知識一竅不通，直到現在本論文的完成，要感謝的人很多，若不是有祐民學長和瑞琳學長的細心教導，以及召漢學弟與家銘學弟的從旁協助，可能我要花兩倍甚至更多的時間才能完成。在此，我由衷的感謝老師、學長與學弟。

當然在研究室的兩年中，實驗室的好夥伴是不可少的，佳鴻、榮源(小白)與信介(介哥)不管在修課或做實驗的過程都是亦師亦友。其次對研究室成員瑞青學長、威伸學長、尚緯學長、汎鈞學長、文賢、及立傑等人感謝他們分享在實驗室的低潮與喜悅。

還要感謝清華大學潘欽主任、核能所李堅雄教授與工研院能資所顏貽乙學長在口試中提出各項建設性的建議，使得本論文更趨於完備。

最後要感謝家人與所有好朋友在背後的的默默關心與支持，對於每一個人的好，我一直心存感謝著。

蘇峯慶　2004, 6 於新竹交大

R-134a 和 R-407C 冷媒在水平多排小圓管內蒸發熱傳及壓降特性之實驗研究

研究生：蘇峯慶　　指導教授：林清發 博士

國立交通大學機械工程學系

摘要

本論文是分別針對 R-134a 和 R-407C 兩種冷媒在 0.83 mm 和 2.0 mm 兩種內徑的 28 根水平小圓管內蒸發熱傳及壓降特性之實驗研究。實驗的目的是探討改變冷媒的飽和溫度、冷媒的質通量、測試段的熱通量及測試段的進口蒸氣乾度對R-134a和R-407C兩種冷媒在此兩種小管熱交換器的影響。在實驗參數的範圍上，冷媒的飽和溫度 T_{sat} 被設定從 5 到 15℃，測試段熱通量 q 從 5 到 15 kW/m^2，進口蒸氣乾度 x_{in} 大約從 0.2 到 0.8。在冷媒的質通量 G 方面，由於管徑從 2.0 mm 縮小到 0.83 mm，因此在系統迴路的穩定性考量上，我們設定 G 在 2.0-mm 小管是從 200 到 400 kg/m^{2}s，在 0.83-mm 小管是從 800 到 1500 kg/m^{2}s。

經由實驗的結果可知，R-134a 和 R-407C 兩種冷媒在 0.83-mm 和 2.0-mm 兩種管徑中，我們發現除了在較低的質通量和較高的熱通量，蒸發熱傳係數與摩擦壓降係數皆會隨著進口乾度的增加而明顯地上升。另外，在熱通量的影響方面，熱傳係數也會隨著熱量的增加而

上升。但是相較摩擦壓降係數的影響則是很微弱的。而在飽和溫度的影響上，蒸發熱傳係數會隨著系統的飽和溫度上升而增加；但是對於摩擦壓降係數則會隨著飽和溫度的上昇而減少。此外，R-134a 和 R-407C 的蒸發熱傳與摩擦壓降均隨著冷媒質通量的增加而增加。值得一提的是，R-134a 冷媒在 0.83-mm 小管中，若供給較低的冷媒質通量和較高的熱通量，蒸發熱傳係數可能會隨著乾度的增加而下降。這是由於冷媒在小管內流動時，產生部分乾化的現象，因此影響蒸發熱傳係數的下降。

在相同的實驗條件與管徑的比較下，我們發現 R-407C 冷媒其整體的蒸發熱傳係數會比 R-134a 冷媒來得高。然而，在摩擦壓降係數方面，則較 R-134a 冷媒低。

最後，我們將蒸發熱傳係數與摩擦壓降係數在 0.83-mm 和 2.0-mm 小管中的實驗資料作分析，並求出經驗公式。

Experimental Study of Evaporation Heat Transfer and Pressure Drop Characteristics of R-134a and R-407C in Horizontal Small Tubes

Student：Feng-Qing Su　　Advisor：Prof. Tsing-Fa Lin

Institute of Mechanical Engineering
National Chiao Tung University

ABSTRACT

An experiment is carried out in the present study to investigate the characteristics of the evaporation heat transfer and frictional pressure drop for refrigerants R-134a and R-407C flowing in horizontal small tubes having the same inside diameter of 0.83 mm or 2.0 mm. In the experiment for the 2.0-mm small tubes, the refrigerant mass flux G is varied from 200 to 400 kg/m^{2}s, imposed heat flux q from 5 to 15 kW/m^2, inlet vapor quality x_{in} from 0.2 to 0.8 and refrigerant saturation temperature T_{sat} from 5 to 15℃. While for the 0.83-mm small tubes, G is varied from 800 to 1500 kg/m^{2}s with the other parameters varied in the same ranges as those for D_i=2.0 mm. In the study the effects of the refrigerant vapor quality, mass flux, saturation temperature and imposed heat flux on the measured evaporation heat transfer coefficients and frictional pressure drops are examined in detail.

For R-134a and R-407C in the 2.0-mm or 0.83-mm small tubes, the experimental data clearly show that both the R-134a and R-407C evaporation heat transfer coefficients and frictional pressure drops increase almost linearly and significantly with the vapor quality of the refrigerant, except at low mass flux and high heat flux. Besides, the evaporation heat transfer coefficients also increase substantially with the rise in the imposed heat flux. But the effect of q on the frictional pressure drop is rather weak. Moreover, a significant increase in the evaporation heat transfer

coefficients results for a rise in T_{sat}, but an opposite trend is noted for the frictional pressure drop. Furthermore, both the R-134a and R-407C evaporation heat transfer coefficients and frictional pressure drops increase substantially with the refrigerant mass flux. At low R-134a mass flux and high imposed heat flux the evaporation heat transfer coefficient in the small tubes (D_i=0.83 mm) may decline at increasing vapor quality when the quality is high. This decline of h_r at rising x is attributed to the partial dryout of the refrigerant flow in the small tubes at these conditions.

We also note that under the same x_{in}, T_{sat}, G, q and D_i, refrigerant R-407C has a higher evaporation heat transfer coefficient and a lower frictional pressure drop when compared with that for R-134a.

Finally, the empirical correlations for the R-134a and R-407C evaporation heat transfer coefficient and friction factor in 0.83-mm and 2.0-mm small tubes are proposed.

TABLE OF CONTENTS

LIST OF FIGURES

Experiment Apparatus

R-407C & R-134a Single-Phase Heat Transfer in 2.0 & 0.83-mm Small tubes

R-134a & R-407C Evaporation Heat Transfer in 2.0 & 0.83-mm Small tubes

R-134a in 2.0-mm small tubes

For T_{sat} effects

For G effects

R-407C in 2.0-mm small tubes

R-134a in 0.83-mm small tubes

R-407C in 0.83-mm small tubes

For T_{sat} effects

For G effects

For q effects

LIST OF TABLE

NOMENCLATURE

A	heat transfer area of the small tube, m^2
Bo	Boiling number, $Bo=\frac{q}{G \cdot i_{fg}}$, dimensionless
C_c	coefficient of contraction
Co	Convective number, $Co=(\frac{\rho_g}{\rho_l})^{0.5}(\frac{(1-x)}{x})^{0.8}$, dimensionless
c_p	specific heat, J/kg°C
D	diameter of small tube, mm
E	enhancement factor
f	friction factor
G	mass flux, kg/m^2s
h	heat transfer coefficient, $W/m^2°C$
i_{fg}	enthalpy of vaporization, J/kg°C
I	measured current from DC power supply, A
L	length of small tube, m
N_{conf}	Confinement number, $N_{conf}=\frac{[\frac{\sigma}{g(\rho_l-\rho_g)}]^{0.5}}{D_i}$, dimensionless
Nu	Nusselt number, $Nu=\frac{hD}{k}$, dimensionless
P	system pressure, kPa
Pr	Prandtl number, $Pr=\frac{\mu \cdot c_p}{k}$, dimensionless
P_r	reduced pressure
q	average imposed heat flux, W/m^2
Q	heat transfer rate, W
Re	Reynolds number, $Re=\frac{G \cdot D_i}{\mu}$, dimensionless

S	suppression factor
T	temperature,℃
$T_{r,sat}$	bubble point temperature of the refrigerant R-134a or R-407C, ℃
V	measured voltage from DC power supply, V
W	mass flow rate
We_l	Weber number based on liquid, $We_l = \frac{G^2 \cdot D}{\rho_l \cdot \sigma}$, dimensionless
x	vapor quality
X	Martinelli parameter

Greek Symbols

ΔP	pressure drop
ΔT	temperature difference, ℃
Δx	total quality change in the small tube
ρ	density, kg/m^3
ν	specific volume, m^3/kg
σ	surface tension
σ_c	contraction ratio
α	void fraction, dimensionless
ε	relative heat loss

Subscripts

a	acceleration
ave	average
conv	convection boiling
cs	cross-section of small tube
eq	equilibrium
evp	evaporation heat transfer

exp	experiment
f	friction or liquid phase
fg	difference between liquid phase and vapor phase
g	vapor phase
hom	homogeneous
i	inside diameter of the tube
i,o	at inlet and exit of the test section
l	all-liquid nonboiling heat transfer
lat,sen	latent and sensible heats
m	average value for the two phase mixture or between the inlet and exit
n	net power input to the refrigerant R-134a or R-407C
nb	nucleate boiling
p	preheater
pool	pool boiling
r	refrigerant
s	heater surface for area or single phase for heat transfer rate
sat	saturation
t	total
tp	two phase
tt	both liquid and vapor phases in turbulent flow
w	water
wall	the inner wall of small tube

CHAPTER 1

INTRODUCTION

1.1 Motivation of the Present Study

The Montreal Protocol signed in 1987 allowed the use of the chlorofluorocarbons refrigerants (CFCs) such as CFC-11, CFC-12, CFC-113, CFC-114 and CFC-115 up to 1996, due to the presence of chlorine and carbon in these refrigerants which were found to destruct the ozone layer in the outer atmosphere around the earth and increase the Total Equivalent Warming Impact (TEWI) [1]. Moreover, refrigerant R-22 which is widely used in medium- and small-sized air conditioning system is scheduled to be phased out at the year 2030. Thus, the search for the replacement of CFCs and R-22 becomes very urgent since 1987. Several new refrigerants have been developed for this purpose. For examples the hydrofluorocarbons refrigerants (HFCs) such as R-134a, R-410A, R-407C, R-409A, R-401A and R-290 have been considered to be suitable and some are currently in use.

It is well known that R-134a is a single-component HFC refrigerant and has similar thermophysical properties to R-12. However, R-407C is a multicomponent HFC mixture consisting of R-32/R-125/R-134a (23/25/52 wt%) with its thermophysical properties close to R-22. The operating conditions of refrigerants R-134a, R-410A and R-407C are given in Table 1.1.

In air conditioning system design, the use of compact heat exchangers to promote the performance of the air conditioning is beneficial. Ultra-compact heat exchangers also called microchannel heat exchangers or compact high intensity coolers. Such heat exchangers are distinguished by a very high ratio of surface area to volume, low thermal resistances, small volumes, lower total mass and low inventory of working

fluids [2]. The understanding of heat transfer and flow characteristics in the small channels consisted in compact heat exchangers are therefore very important. In the present study we plan to investigate the heat transfer and pressure drop characteristics for the evaporation of refrigerants R-134a and R-407C in small pipes.

1.2 Literature Review - Boiling Heat Transfer and Pressure Drop in Small Channels

The size of the channels in a compact heat exchanger can significantly affect the performance of the exchanger when it is small enough. Mehendale et al. [2] suggested to use the hydraulic diameter D_h of the channels to classify the compact heat exchangers: (1) micro heat exchangers for D_h =1 ~ 100 μm, (2) meso heat exchangers for D_h =100 μm ~ 1 mm, (3) compact heat exchangers for D_h =1 ~ 6 mm, and (4) conventional heat exchangers for D_h >6 mm. Another classification from Kandlikar [3] proposed a different criterion: D_h >3 mm for the convectional channels, 0.2 mm< D_h <3 mm for the mini-channels, and 0.01 mm< D_h <0.2 mm for the micro channels.

1.2.1 Single Phase heat transfer in small tubes

Before reviewing the works on the flow boiling heat transfer, several studies on the single-phase heat transfer in small tubes are reviewed first. A decade age, Peng and Wang [4] investigated single-phase heat transfer for liquid methanol in a duct made of small rectangular channels with D_h=0.31, 0.51 and 0.646 mm. Their experimental data showed that the liquid velocity, liquid subcooling, liquid properties and geometry of the channels all exhibited significant effects on the heat transfer performance. Enhancement in heat transfer was noted at increasing liquid velocity, subcooling and channel number. In a continuing study for water [5] they also found

that the geometric configuration of channels had a significant effect on the single-phase convective heat transfer and flow characteristics. Specifically, the heat transfer was noted to depend on the aspect ratio and the ratio of the hydraulic diameter to the center-to-center distance of the channels. Furthermore, the turbulent heat transfer depends on a new dimensionless variable, Z, defined as $\frac{\min(H, W)}{\max(H, W)}$, H and W are the height and width of the channel, respectively.

Recently in an experiment for R-134a liquid flow in mini-channels, Agostini et al. [6] compared their heat transfer data with some existing correlations. They concluded that the correlation of Shah and London [7] was good for Re <500 and the Gnielinsky correlation [8] was appropriate for 2,300< Re <10^6 and 0.6< Pr <10^5. Moreover, the Dittus-Boelter correlation [9] was suitable for Re >10^5 and 0.7< Pr <16,700.

1.2.2 Flow boiling heat transfer in small tubes

Heat transfer associated with flow boiling in a conventional channel is normally considered to result from two mechanisms: nucleate boiling and convective boiling. In the situation with a dominant nucleate boiling mechanism, the boiling heat transfer coefficient is mainly dependent on the imposed heat flux and the refrigerant saturated temperature or pressure. While for the cases with a predominated convective boiling mechanism, heat transfer coefficient is mainly dependent on the refrigerant mass flux and vapor quality. Therefore in the study of flow boiling heat transfer in mini- and micro- channels, which mechanism is prevalent is the main issue of many investigations.

Yu et al. [10] recently examined flow boiling heat transfer for water in a 2.98 mm diameter channel. They found that the boiling heat transfer of water in the small channel (vapor quality above 0.5) was dependent on the heat flux but was independent of the mass flux. They concluded that the nucleate boiling was dominant over the

convective boiling in small channels. The results are significantly different from these for the conventional channels, where the mass flux effect can be substantial. Similarly, Sumith et al. [11] measured the saturated flow boiling heat transfer and pressure drop of water in the test section which was made of a stainless steel tube with an inner diameter of 1.45 mm. They indicated that the dominant flow pattern in the tube was a slug-annular or an annular flow, and liquid film evaporation dominated the heat transfer.

An experimental measurement carried out by Yan and Lin [12, 13] to study the evaporation heat transfer and pressure drop of R-134a in a tube bank forming by 28 small pipes (D_i=2.0 mm) revealed that both the nucleate and convective boiling mechanisms were important and the evaporation heat transfer in the small pipes was significantly higher than that in large tubes. A visualization investigation was presented by Nino et al. [14] to examine R-134a refrigerant in a multiport microchannel tube with D_h=1.5 mm. They proposed a method to describe the fraction of time or the probability that a flow pattern existed in a particular flow condition. A recent study from Fujita et al. [15] for R-123 boiling in a horizontal small tube with an inside diameter of 1.12 mm suggested that heat transfer in the flow was dominated by the nucleate boiling and the effects of the refrigerant mass flux and vapor quality to the boiling heat transfer were very weak. A similar study for R-113 boiling conducted by Lazarek and Black [16] noted the negligible variation of the boiling heat transfer coefficient with the local vapor quality, which implied that the wall heat transfer process was again controlled by nucleate boiling. In a vertical small tube with an inside diameter of 1 mm with R-141b refrigerant flowing in it, Lin et al. [17] found that at low quality, nucleate boiling dominated. But at higher quality, convective boiling dominated. In a further study [18], they examined the same refrigerant in four tubes with diameters of 1.1, 1.8, 2.8, 3.6 mm and one square tube of cross section 2×2

mm^2. Their results indicate that the mean heat transfer coefficient in a tube or channel is independent of the mass flux and tube diameter but is a function of the imposed heat flux. Cornwell and Kew [19] observed boiling in refrigerant R-113 flow and measured the heat transfer for two geometries: one had 75 channels with D_h=1.03 mm and other had 36 channels with D_h=1.64 mm. Their experimental work suggested the presence of three two-phase flow patterns in the channels: isolated bubble, confined bubble and annular-slug flow. In a continuing study [20], they investigated refrigerant R-141b boiling in a horizontal tube with its inner diameter ranging from 1.39 to 3.69 mm and proposed that flow boiling in a narrow channel might be through one of four mechanisms: nucleate boiling, confined bubble boiling, convective boiling and partial dry-out. They further indicated that, except at very low heat flux, the boiling showed a strong dependence on the heat flux, a weak dependence on the mass flux, and independence of the quality. Besides, they introduced a new dimensionless group named as the confinement number, $N_{conf} \equiv \frac{[\sigma/(g(\rho_l - \rho_g))]^{1/2}}{D_h}$, which represented the importance of the restriction of the flow by the small size of the channel. The dimensionless number N_{conf} can be used to find the transition from the isolated to confined bubble regimes. To a first approximation, they showed that the confined boiling occurred when N_{conf} >0.5. The effects of the tube confinement were found to be significant for micro- and mini-channels.

Examining the boiling of refrigerants in a small circular tube (D=2.46 mm) and a rectangular duct (D_h=2.40 mm) with nearly the same hydraulic diameters, Tran et al. [21] showed that there was no significant geometry effect for the two channels tested. Furthermore, their results implied that the nucleation mechanism dominated over the convection mechanism in small-channel evaporators over the full range of quality (0.2 ~ 0.8), which was contrary to the situations in larger channels where the convection

mechanism dominates at qualities typically above 0.2. Bao et al. [22] also found that the boiling heat transfer coefficient was a strong function of the heat flux and system pressure in a 1.95 mm diameter tube with R-11 and R-123, while the effects of the mass flux and vapor quality were very small, suggesting that the heat transfer was mainly through the nucleate boiling. Wambsganss et al. [23] studied boiling heat transfer of refrigerant R-113 in a small diameter (2.92 mm) tube and evaluated 10 different heat transfer correlations. They found that the high boiling number and slug flow pattern led to the domination by the nucleation mechanism and the two-phase correlations based on this dominance also predicted the data best. Moreover, Warrier et al. [24] used FC-84 in five parallel channels with each channel having a hydraulic diameter of 0.75 mm and compared their results with five widely used correlations. They then proposed two new correlations, one for subcooled flow boiling heat transfer and the other for saturated flow boiling heat transfer. Oh et al. [25] examined R-134a in capillary tubes of 500 mm long and 2, 1 and 0.75 mm inside diameters. They concluded that the heat transfer in the forced convective boiling was more influenced by the refrigerant mass flux than by the boiling number and the heat transfer coefficient was controlled by the Reynolds number. Besides, their results also showed that the dry-out point moved to the lower quality with decreasing size of the tubes. Vaporization of CO_2 in 25 flowchannels of 0.8 mm ID was recently examined by Pettersen [26]. He also observed the two-phase flow pattern with another separate test rig with 0.98-mm heated glass tube. The results showed that nucleate boiling dominated at low/moderate vapor fractions, where the boiling heat transfer coefficient increased with the heat flux and refrigerant temperature but was less affected by the mass flux and vapour fraction. Moreover, the dryout effects became very important at higher mass flux and temperature, where the boiling heat transfer coefficient dropped rapidly at increasing x. And the two-phase flow was in intermittent and annular flow

regimes, the latter becoming more important at high mass flux.

More complete information on the two phase flow boiling heat transfer in compact evaporators or microchannels is available from the recent critical review conducted by Ghiaasiaan and Abdel-khalik [27], Thome [28], Sobhan and Garimella [29], Kandlikar [30, 31] and Watel [32].

1.2.3 Flow Boiling Heat Transfer in Conventional Tubes

The experimental data taken from boiling of refrigerants R-22 and R-407C in a conventional tube (D_i=6.5 mm) by Wang and Chiang [33] suggested that the major heat transfer mechanism at low mass flux (G= 100 kg/m^{2}s) was the nucleate boiling. The convective evaporation becomes dominant as the mass flux is increased to 400 kg/m^{2}s. A similar study from Shin et al. [34] showed that the boiling heat transfer coefficients depended strongly on the heat flux in a low quality region. Choi et al [35] examined boiling of several refrigerants in a horizontal tube (D_i=7.75 mm) and found that the boiling heat transfer coefficients increased with the refrigerant temperature and mass flux.

Yu et al. [36] examined the relations between the flow patterns and local heat transfer coefficient for the flow boiling of R-134a in a 10.7 mm diameter smooth tube and a micro-fin tube. The results showed that the flow pattern changed from wavy, intermittent, semi-annular to annular patterns at increasing mass flux and quality, and the heat transfer could be enhanced with the microfin surface up to 200% at low mass flux and high quality where the annular flow dominated in the microfin tube while the wavy flow occurred in the smooth tube. Yun et al. [37] investigated the evaporation heat transfer characteristics of CO_2 in a horizontal tube with an inner diameter of 6.0 mm and found that the heat transfer coefficient decreased with an increase in the

quality due to both a lower dryout quality and dominance of nucleate boiling as compared to the conventional refrigerants.

1.2.4 Pressure Drop in Small Tubes

The single phase pressure drop for flow in micro-channels was examined by Peng and Peterson [5]. Their results showed that the laminar friction factor or flow resistance reached a minimum value as the parameter Z approached 0.5. In the turbulent flow, the smaller the resistance, the higher the flow transition Reynolds number.

Lazarek and Black [16] developed empirical correlations for frictional, spatial acceleration and bend pressure drops for saturated boiling of R-113 in a vertical U-tubes with D_h=3 mm. Yan and Lin [12, 13] found that the frictional pressure drop for R-134a evaporation increased with the refrigerant mass flux and imposed wall heat flux in a tube bank with D_h=2 mm for each tube. Similar results were obtained by Fujita et al. [15], Warrier et al. [24] and Tran et al. [38]. Recently Qu and Mudawar [39] investigated the pressure drop in multi-port parallel micro-channels (D_h=0.348 mm). They identified two types of two-phase hydrodynamic instability: severe pressure drop oscillation and mild parallel channel instability. They further noted that the pressure drop increased appreciably upon commencement of boiling in micro-channels.

1.3 Review of Correlation Equations for Two Phase Flow Boiling Heat Transfer

Based on the available experimental data from open literatures, some correlation equations for two phase flow boiling heat transfer and pressure drop were developed.

An early general correlation model for the flow boiling in channels was proposed by Chen [40]. He divided the boiling heat transfer coefficient into two parts: a microconvective (nucleate boiling) contribution which could be estimated by the pool boiling correlations and a macroconvective (non-boiling force convection) contribution which could be estimated by the single-phase correlation such as the Dittus-Boelter equation [9]. A new correlation for boiling heat transfer in small diameter channels was proposed by Kew and Cornwell [19]. They introduced a confinement number in the correlation. Besides, Tran et al. [21] modified the heat transfer correlation of Lazarek and Black [16] with the Reynolds number of the flow replaced by the Weber number to eliminate viscous effects in favor of the surface tension. Similar correlations were proposed by Fujita et al. [41] and Xia et al. [42].

A flow boiling correlation based on an explicit nucleate boiling term rather than on an empirical boiling number dependence for vertical and horizontal flows in tubes and annuli was proposed by Gungor and Winterton [43]. They modified the Chen's correlation to include the enhanced (E) and suppression factors (S). A new correlation from Liu and Winterton [44] introduced an asymptotic function to predict the heat transfer coefficient for vertical and horizontal flows in tubes and annuli. Moreover, Kandlikar [45] gave a general correlation for saturated flow boiling heat transfer inside horizontal and vertical tubes. The correlation was also based on a model utilizing the contributions due to nucleate boiling and convective mechanisms. It incorporated a fluid-dependent parameter in the nucleate boiling term. In a following study [46 ~ 48], he developed a new flow boiling map to depict the relationships among the heat transfer coefficient, vapor quality, heat flux and mass flux for subcooled and saturated flow boiling of different fluids inside circular tubes.

Chen et al. [49] proposed an empirical correlation for two-phase frictional performance in small diameter tubes. The Chisholm correlation was noted to have a

poor predictive ability for boiling in small diameter tubes. However, the homogeneous model gave good predictions for the refrigerant and air-water data. Selected correlations from the literature for the boiling heat transfer coefficient and pressure drops are given in Table 1.2.

1.4 Objective of This Study

The above literature review clearly indicates that the experimental data for the evaporation heat transfer and pressure drop of HFC refrigerants in small tubes are still rare. In this study we intend to measure the evaporation heat transfer coefficient and pressure drop of refrigerants R-134a and R-407C in horizontal small tubes. The effects of the vapor quality, refrigerant mass flux, imposed heat flux and system pressure on the evaporation heat transfer and pressure drop in the small tubes will be examined in detail.

Table 1.1 Comparison of Properties of three HFC refrigerants for air conditioning and refrigeration applications

Refrigerant	R-134a	R-410A	R-407C
Component	HFC-134a	HFC-32/125	HFC-32/125/134a
Wt %	100 %	50/50%	23/25/52%
Comparison with R-22	1. the lower working pressure. 2. the frication pressure drop is larger in the same capability of freezing.	1. near-azeotropic refrigerant. 2. the working pressure is five times than R-22. 3. the frication pressure drop is smaller.	1. zeotropic refrigerant, and the components charge easy. 2. the working pressure is same with R-22.
The energy efficiency ratio relative to R-22	72~90	94~100	90~97
Molecule quality	102.3	72.6	85.62
Remark	1. the volume of operating system becomes larger. 2. the air-out volume of compress is larger.	1. the design of system must to consider the strong and optimum elements.	1. the solutions of variation of R-407C components.
Green-house effect (100 years)	1300	1725	1526
Toxicity limit (kg/m^3)	0.25	0.44	0.31
Boiling point (℃)	-26.2	-52.7 R32 (-51.8℃) / R125 (-48.5℃)	-43.6 R32 (-51.8℃) / R125 (-48.5℃) / R134a (-26.2℃)
Temperature glides	—	＜1 °F	10 °F

Table 1.2 Classification of Two-phase heat transfer coefficient and friction factor correlations

Reference	Fluid	Heat Transfer Coefficient Correlations	Pressure Drop Correlations	Conditions
W. Yu et al. [10]	water	–	$X_{tt}=18.65(\frac{\rho_g}{\rho_l})^{0.5}(\frac{1-x}{x})\frac{\mathrm{Re}_g^{0.1}}{\mathrm{Re}_l^{0.5}}$ $\phi_{lo}^{2}=X_{tt}^{-1.9}$	$D=2.98mm$ $G=50\sim200kg/m^2s$ $P=2\mathrm{bar}$
B. Sumith et al. [11]	water	$h_z=2.83\cdot(1/X_{tt}+0.213)^{0.736}h_{LO}$	–	$D_{in}=1.45mm$ $G=23.4\sim152.7kg/m^2s$ $q=10\sim715kW/m^2$ $x_m=0\sim0.8$
Yan and Lin [12, 13]	R-134a	*For* $X_m\le0.7$ $h_{tp}=4.36\frac{k_l}{D_i}\mathrm{Pr}_l^{1/3}(1-X_m)^{-0.5}(C_1\cdot\mathrm{Re}_{eq}+C_2)\cdot(C_3\cdot Bo+C_4)$ *For* $X_m>0.7$ $h_{tp}=4.36\frac{k_l}{D_i}\mathrm{Pr}_l^{1/3}(1-X_m)^{-0.5}(C_1\cdot\mathrm{Re}_{eq}+C_2)$ $C_1=-0.0124G^{-0.368}$ $C_2=1.49G^{0.514}$ $C_3=-1166X_m+1028$ $C_4=0.53e^{0.931X_m}$	$f_{tp}=0.127\,\mathrm{Re}_{eq}^{-0.1925}$ $\mathrm{Re}_{eq}=\frac{GD}{\mu_l}((1-x)+x(\frac{\rho_l}{\rho_g})^{0.5})$	$D=2mm$ $T_{sat}=5\sim31^oC$ $G=50\sim200kg/m^2s$ $x=0.2\sim0.8$

Table 1.2 Continued (1)

Reference	Fluid	Heat Transfer Coefficient Correlations	Pressure Drop Correlations	Conditions
Y. Fujita et al. [15]	R-123	$h_{tp} = 0.884 G^{0.143} q^{0.714}$	$\Delta P_f = f_{tp} \frac{L}{D} \frac{G^2}{2\rho}$ $\quad \frac{1}{\rho} = \frac{x}{\rho_g} + \frac{1-x}{\rho_l}$ $\mathrm{Re}_{tp} = \frac{GD}{\mu}$ $\quad \frac{1}{\mu} = \frac{x}{\mu_g} + \frac{1-x}{\mu_l}$	$D: 1.12mm$ $\quad G: 50-400 kg/m^2 s$ $q: 5-20 kW/m^2$ $\quad \mathrm{Re}: 135-1070$ $P: 1.1-1.2 bar$ $\quad x: -0.2-0.9$ $Bo: 3\times10^{-4} - 8.9\times10^{-4}$
Lazarek and Black [16]	R-113	$h_{tp} = 30 \mathrm{Re}_l^{0.857} Bo^{0.714} (k_l / D)$	$\frac{\Delta P_{tp}}{\Delta P} = 1 + \frac{30}{X_{tt}} + \frac{1}{X_{tt}^2}$ $\quad X_{tt} = [\frac{1-x}{x}]^{0.9} [\frac{\rho_g}{\rho_l}]^{0.5} [\frac{\mu_l}{\mu_g}]^{0.1}$ $\Delta P = f \frac{L}{D} \frac{G^2}{2\rho_l} (1-x)^2$ $\quad f = 0.316 [\frac{G(1-x)D}{\mu_l}]^{-1/4}$	$D: 3.1mm$ $\quad G: 125-750 kg/m^2 s$ $q: 14-380 kW/m^2$ $\quad \mathrm{Re}: 860-5500$ $Bo: 2.3\times10^{-4} - 76\times10^{-4}$ $\quad P: 1.3-4.1 bar$
K. Cornwell and P. A. Kew [19]	R-113	*Isolated Bubble Regime*: $Nu = C_1 \cdot Bo^{0.7} \cdot Nu_{lo}$ *Confined Bubble Regime*: $Nu = C_2 \cdot Bo^m \cdot Co^n \cdot Nu_{lo}$ *Annular – Slug Flow*: $Nu = C_3 \cdot F \cdot Nu_{lo}$	–	$D_H = 1.03mm,\ G = 124 \sim 627\ kg/m^2 s$ $1.64\ mm,\ G = 211 \sim 317\ kg/m^2 s$ $L = 320\ mm$ $q = 4.3 \sim 20\ kW/m^2$
T. N. Tran et al. [21]	R-12, R113	$h = (8.4\times10^{-5})(Bo^2 We_l)^{0.3} (\frac{\rho_l}{\rho_g})^{-0.4}$ *for* $\quad \Delta T > 2.75\ ^oC$	–	$D: 2.46mm, 2.92mm; D_h = 2.4mm$ $G: 44-832 kg/m^2 s$ $\quad q: 7.5-129 kW/m^2$ $P_r: 0.045-0.2$ $\quad Bo: 2\times10^{-4} - 23\times10^{-4}$ $\Delta T_{sat}: 2.8-18.2^oC$
Z. Y. Bao et al. [22]	R-11, R-123	$h_{tp}/h_l = 1 + 3000 Bo^{0.86} +$ $1.12(x/(1-x))^{0.75} (\rho_l/\rho_g)^{0.41}$	–	$D: 1.95mm$ $\quad G: 50-1800 kg/m^2 s$ $q: 50-200 kW/m^2$ $\quad \mathrm{Re}: 860-5500$ $P: 2-5 bar$ $\quad x: -0.3-0.9$ $\Delta T_{sat}: 5-15^oC$

Table 1.2 Continued (2)

Reference	Fluid	Heat Transfer Coefficient Correlations	Pressure Drop Correlations	Conditions
G. R. Warrier et al. [24]	FC-84	$\frac{h_{tp}}{h_l} = 1 + 6Bo^{1/16} + f_2(Bo)(x)^{0.65}$ $f_2(Bo) = -5.3 \cdot [1 - 855Bo]$	$\Delta P_f = \Delta P_{flo}\{1 + (4.3\Gamma^{-2} - 1)$ $\cdot [N_{conf} x^{0.875}(1-x)^{0.875} + x^{1.75}]\}$ $\phi_{lo}^{\ 2} = \frac{\Delta P_f}{\Delta P_{flo}} \quad \alpha = [1 + 0.28 X_{tt}^{\ 0.71}]^{-1}$	$D: 0.75mm \quad G: 557 - 1600 kg/m^2 s$ $q: 0 - 59.9 kW/m^2 \quad \mathrm{Re}: 418 - 2015$
H. K. Oh et al. [25]	R-134a	$\frac{h_{TP}}{h_{LZ}} = \frac{240}{X_{tt}}\left(\frac{1}{\mathrm{Re}_{TP}}\right)^{0.6}$	–	$D_H = 2,\ 1$ and $0.75mm$ $L = 500mm$ $G = 240 \sim 720\ kg/m^2 s$ $q = 10 \sim 20\ kW/m^2$ $x = 0.1 \sim 1$
C. C. Wang and C. S. Chiang [33]	R-22 R-407C	–	$f_{tp} = -2.714 \times 10^{-3} + 2.3 \times 10^{-5} \cdot \mathrm{Re}^{0.5}$ $- 4.6 \times 10^{-14}\ \mathrm{Re}^2$	$D_{in} = 6.5mm$ $G = 100\ and\ 400 \mathrm{kg/m^2 s}$ $\mathrm{G}=100 \sim 700 \mathrm{kg/m^2 s}$ $\mathrm{q}=2.5 \sim 10 \mathrm{kW/m^2}$ $\mathrm{x}=0.11 \sim 0.93$
T. N. Tran et al. [38]	R-134a R-12 R-113	–	$\Delta P_f = \Delta P_{fLo}\{1 + (4.3\Gamma^2 - 1)$ $\cdot [N_{conf} x^{0.875}(1-x)^{0.875} + x^{1.75}]\}$ $N_{conf} = \frac{[\sigma / g(\rho_l - \rho_g)]^{0.5}}{D}$ $\Gamma^2 = \frac{(dP/dz)_{fgo}}{(dP/dz)_{flo}}$	$D = 2.46$ and $2.92mm$ $G = 33 \sim 832 kg/m^2 s$ $q = 2.2 \sim 129 kW/m^2$ $x_{out} = 0.02 \sim 0.95$ $P_r = 0.04 \sim 0.23$

Table 1.2 Continued (3)

Reference	Fluid	Heat Transfer Coefficient Correlations	Pressure Drop Correlations	Conditions
W. Qu and I. Mudawar [39]	water	–	$\Delta P_{tp,f} = \frac{L_{tp}}{x_{e,out}} \int_0^{x_{e,out}} \frac{2 f_f G^2 (1-x_e)^2 v_f}{d_h} \phi_f^2 dx_e$ $\phi_f^2 = 1 + \frac{C}{X_{tt}} + \frac{1}{X_{vv}^2}$ $C = 21[1-\exp(-0.319\times10^3 d_h)] \cdot (0.00418G + 0.0613)$ $X_{vv} = \left(\frac{\mu_f}{\mu_g}\right)\left(\frac{1-x_e}{x_e}\right)\left(\frac{v_f}{v_g}\right)^{0.5}$	$D_h = 0.348mm$ $T_{in} = 30 \sim 60^oC$ $G = 134.9 \sim 400.1 kg/m^2 s$ $P_{out} = 1.17bar$
Chen [40]		$h_{tp} = h_{conv} + h_{nb} \Leftrightarrow \quad h_{tp} = Fh_l + Sh_{pool}$ $h_{pool} = 0.00122 \cdot ((k_l^{0.79} c_{p,l}^{0.45} \rho_l^{0.49}) / (\sigma^{0.5} \mu_l^{0.29} i_{fg}^{0.24} \rho_g^{0.24})) \cdot \Delta T_{sat}^{0.24} \Delta P_{sat}^{0.75}$; $F = 2.35(1/X_{tt} + 0.213)^{0.736}$, $for X_{tt} > 0.1$ $S = (1 + 0.12\,\mathrm{Re}_{tp}^{1.14})^{-1}$, $for\ \mathrm{Re}_{tp} < 32.5$ $\mathrm{Re}_{tp} = G(1-x)D/\mu_l (F^{1.25})(10^{-4})$	–	–
K. E. Gungor et al. [43]		$h_{tp} = h_l \cdot E + h_{pool} \cdot S$ $h_l = 0.023 \cdot \mathrm{Re}_l^{0.8} \cdot \mathrm{Pr}_l^{0.4} (k_l / D)$ $h_{pool} = 55 \cdot \mathrm{Pr}^{0.12} \cdot (-\log_{10}^{\mathrm{Pr}})^{-0.55} \cdot M^{-0.5} \cdot q^{0.67}$ $E = 1 + 24000 \cdot Bo^{1.16} + 1.34 \cdot (1/X_{tt})^{0.86}$ $S = (1 + 1.15\times10^{-6} \cdot E^2 \cdot \mathrm{Re}_l^{1.17})^{-1}$	–	$D = 2.95 \sim 32mm$ $G = 12.4 \sim 61518 kg/m^2 s$ $q = 0.35 \sim 91534 kW/m^2$ $x = 0 \sim 1.46$

Table 1.2 Continued (4)

Reference	Fluid	Heat Transfer Coefficient Correlations	Pressure Drop Correlations	Conditions
T. Y. Choi et al. [35]	R-32 R-134a R-32/134a R-407C	For pure refrigerants $h_{tp} = E \cdot h_{DB} + S \cdot h_{SA}$ For mixture refrigerants $h_{tp} = E \cdot h_{DB} + F_M S \cdot h_{SA}$ $h_{DB} = 0.023\,\mathrm{Re}_l^{0.8}\,\mathrm{Pr}_l^{0.4}$ $h_{SA} = 207\frac{k_l}{bd}\left(\frac{q''bd}{k_l T_s}\right)^{0.674}\left(\frac{\rho_v}{\rho_l}\right)^{0.581}\mathrm{Pr}_l^{0.533}$ $F_M = \frac{1}{1+c_M\left\{[C_{pl}(T_{dew}-T_{bub})]/h_{fg}\right\}}$ $bd = 0.0146\beta[2\sigma/g(\rho_l-\rho_v)]$ *with* β=35° $E = c_1 Bo^{c_2} X_{tt}^{c_3}$ $S = c_4 Co^{c_5}$ $c_1 = 49.971 \quad c_2 = 0.383 \quad c_3 = -0.758$ $c_4 = 0.909 \quad c_5 = 0.039$	–	$D_{in} = 7.75mm$ $T_{sat} = -12 \sim 17^oC$ $G = 240 \sim 1060 kg/m^2 s$ $q'' = 4.1 \sim 28.6 kW/m^2$
Z. Liu et al. [44]		$h_{tp}^{\ 2} = (Fh_l)^2 + (Sh_{pool})^2$ $h_l = 0.023(k_l/D)\,\mathrm{Re}_l^{0.8}\,\mathrm{Pr}_l^{0.4}$ $h_{pool} = 55P_r^{0.12}(-\ln P_r)^{-0.55}M^{-0.5}q^{0.67}$ $F = (1 + x\,\mathrm{Pr}_l(\rho_l/\rho_g - 1))^{0.35}$ $S = (1 + 0.55F^{0.1}\,\mathrm{Re}_l^{0.16})^{-1}$	–	$D: 2.95 - 32mm \quad G: 12.4 - 8179.3 kg/m^2 s$ $q: 0.35 - 2620 kW/m^2 \quad \mathrm{Re}: 568.9 - 87500$ $P_r: 0.0023 - 0.895 \quad x: 0 - 0.948$ $Fr: 2.66\times10^{-4} - 2240 \quad \mathrm{Pr}_l = 0.83 - 9.1$

CHAPTER 2

EXPERIMENTAL APPARATUS AND PROCEDURES

The experimental system which is modified slightly from that used in the previous study [12] is employed here to investigate the evaporation heat transfer and pressure drop of the HFC refrigerants in small tubes. It is schematically depicted in Fig. 2.1. The modified test section along with the entry and exit sections are schematically shown in Fig 2.2. The experimental apparatus consists of three main loops, namely, a refrigerant loop, a water-glycol loop, and a hot-water loop.

2.1 Refrigerant Loop

The refrigerant loop consists of an oil-free variable–speed refrigerant pump, an accumulator (low pressure), a receiver (high pressure), a mass flow meter, the test section and the inlet and exit sections, a condenser, a sub-cooler, a filter/dryer and four sight glasses. The refrigerant mass flow rate is mainly controlled by an AC motor through the change of its inverter frequency. In addition, the refrigerant flow rate can also be further adjusted by regulating the bypass valve in the flow path from the refrigerant pump.

The refrigerant R-134a or R-407C at the outlet of the refrigerant pump must be kept subcooled to avoid any vapor flow through the mass flow meter, which has an estimated measurement error of $\pm 1\%$. The preheater is used to heat the subcooled refrigerant R-134a or R-407C to a specified vapor quality at the test section inlet by receiving heat from the hot water in the hot-water loop. Then, a vapor-liquid refrigerant mixture is generated and moves through the small tubes in the test section. The vapor flow leaving the test section is re-liquefied in an oversized

condenser/subcooler in the cold water-glycol loop.

After leaving the subcooler, the liquid R-134a or R-407C flows back to the receiver at the bottom of the system. An accumulator is connected to a high-pressure nitrogen tank to dampen the fluctuations of the refrigerant flow rate and pressure. The filter/dryer is used to filter the impurities and noncondensable gas possibly existing in the loop. Varying the temperature and flow rate of the water-glycol mixture flowing through the condenser and subcooler allows us to control the pressure of the refrigerant loop. Two absolute pressure transducers are installed at the inlet and exit of the test section with a resolution up to $\pm$ 2kPa. All the refrigerant and water temperatures are measured by copper-constantan thermocouples (T-type) with a calibrated accuracy of ± 0.2℃.

2.2 Test Section

Due to the tubes to be tested being relatively small, the refrigerant flow rates in them are very low and direct measurement of boiling heat transfer coefficient and pressure drop in the tubes is difficult and can be subject to large error. Thus 28 small tubes all made of copper, each having the same diameter and length, are put together to form the test section, as schematically shown in Fig. 2.2. Each small tube has the same diameter of 0.83 or 2.0 mm, outside diameter of 1.83 or 3.0 mm and length of 150 mm. Specifically, these 28 tubes are placed together side by side forming a plane tube bundle. In order to allow the refrigerant to flow smoothly into the small tubes, a section including divergent, convergent and straight portions is connected to the inlets of the tubes. Besides, another section including straight and convergent parts is attached to the exits of the tubes. Both the inlet and exit sections are formed by the stainless steel plates. At the middle axial location of the small tubes 14 thermocouples

are soldered onto the outer surface of the tubes. Specifically, these thermocouples are soldered onto 14 selected tubes at the circumferential position of 45° from the top of the tube or from the bottom of the tube, as shown in Fig. 2.3. Two copper plates of 5-mm thick are respectively soldered on the upper and lower sides of the tube bundle shown in Fig. 2.4. Obviously small crevices exist between the tube outside surface and copper plates. Due to the good thermal contact of the copper plates and the tubes, there is no need to fill the crevices with conducting grease. Instead, the crevices provide the space for the thermocouple wires leading to the data logger.

The copper plates are heated directly by an electric-resistance heater of 2.6-mm wide, 0.5-mm thick and 2.5-m long. The heater is connected to a 500W DC power supply. Mica sheet is placed in the narrow space between the heater and copper plates to prevent leak of electric current to the copper plates. The power input to the heater is measured by a power meter with an accuracy of ±0.5 %. In order to reduce the heat loss from the heaters, the whole test section is wrapped with a 10-cm thick polyethylene layer.

2.3 Water Loop for Pre-heater

In order to maintain the refrigerant R-134a or R-407C at the preset temperature at the test section inlet, a water loop is used to preheat the refrigerant before it arrives at the test section inlet. The water loop for the preheater includes a double-pipe heat exchanger having a heat transfer area of 0.12 m^2, a 125-liter hot water container with three 2.0 kW heaters in it, and a 0.5 hp water pump which can drive the hot water at a specified flow rate to the preheater. In the preheater the hot water passes through the outer pipe while the liquid refrigerant flows in the inner pipe. The water flow rate is controlled by an AC motor through the change of its inverter frequency and by the

by-pass valve. The connecting pipe between the preheater and test section is thermally insulated with a 5-cm think polyethylene layer to reduce the heat loss from the pipe.

2.4 Water-Glycol Loop

The water-glycol loop is designed for condensing the R-134a or R-407C vapor. The water-glycol loop is cooled by a water cooled R-22 refrigeration system. The cooling capacity is 3.5 kW for the water-glycol mixture at -20℃. The cold water-glycol mixture at a specified flow rate is driven by a 0.5 hp pump to the condenser as well as to the subcooler. A by-pass loop is provided to adjust the flow rate. By adjusting the mixture temperature and flow rate, the bulk temperature of the R-134a or R-407C in the subcooler can be controlled at a preset level.

2.5 DC Power Supply

As described above, the small tubes in the test section are heated by a resistance heater. A 50V-25A DC power supply delivers the required electric current to the heater. A Yokogawa DC meter is used to measure the DC current through the heater with an accuracy of ±1%. Then the voltage drop across the heater is measured by a Yokogawa multimeter. Thus the power input to the heater can be calculated.

2.6 Data Acquisition

The data acquisition system includes a recorder, a 24V-3A power supply and a controller. The recorder is used to record the temperature and voltage data. The water flowmeter and differential pressure transducer need the power supply as a driver to output an electric current of 4 to 20 mA. The IEEE488 interface is used to connect the controller and the recorder, allowing the measured data to be transmitted from the

recorder to the controller and the data are analyzed by the computer immediately. The system automatically monitors 22 copper-constantan thermocouples, two pressure transducers, and three mass flowmeters. The thermodynamic and transport properties of the refrigerants R-134a and R-407C are obtained by the manual from AlliedSignal Co. Ltd. and by the ASHRAE handbook.

2.7 Experimental Procedures

Before a test is started, the system temperature is compared with the saturation temperature of refrigerant R-134a or R-407C corresponding to the measured saturation pressure of the refrigerant and the allowable difference is kept in the range of 0.2-0.3K. Otherwise, the system is re-evacuated and then re-charged to remove some noncondensible gases possibly existing in the refrigerant loop. In each test the liquid refrigerant leaving the subcooler is first maintained at a specified temperature by adjusting the water-glycol temperature and flow rate. In addition, we adjust the thermostat in the water loop to stabilize the refrigerant temperature at the test section inlet. Next, the temperature and flow rate of the hot water loop for the preheater are adjusted to keep the vapor quality of R-134a or R-407C at the test section inlet at the desired value. Then, we regulate the refrigerant pressure at the test section inlet by adjusting the gate valve locating right after the exit of the test section. Meanwhile, by changing the current of the DC motor connecting to the refrigerant pump, the refrigerant flow rate can be varied. The imposed heat flux from the heater to the refrigerant is adjusted by varying the electric current delivered from the DC power supply. By measuring the current delivered to and voltage drop across the heater, we can calculate the heat transfer rate to the refrigerant. All tests are run when the experimental system has reached statistically steady state. Finally, all the data

channels are scanned every 5 seconds for a period of 50 seconds.

The thermophysical properties of the refrigerants R-134a and R-407C are given in Table 2.1.

Table 2.1 Comparison of thermophysical properties of R-134a and R-407C

Thermal properties		**R-407C**			**R-134a**		
Temperature (℃) (Saturated Pressure)		4.895 (665 kPa)	10.04 (776 kPa)	15.05 (900 kPa)	5 (349.8 kPa)	10 (414.6 kPa)	15 (488.6 kPa)
Viscosity ($\mu N \cdot s/m^2$)	Liquid	196.9	184.6	173.4	254.4	238.8	224.3
	μ_l - μ_g	**184.96**	**172.4**	**160.95**	**243.46**	**227.65**	**212.94**
	Vapor	11.94	12.2	12.45	10.94	11.15	11.36
Kinematic Viscosity ($\mu m^2/s$)	Liquid	0.1616	0.1539	0.147	0.199	0.1893	0.1803
	ν_l - ν_g	**0.1554**	**0.1478**	**0.1411**	**0.193**	**0.1834**	**0.1745**
	Vapor	0.4219	0.3689	0.3236	0.6382	0.5511	0.478
Density (kg/m^3)	Liquid	1218	1199	1179	1278	1261	1243.5
	ρ_l - ρ_g	**1189.7**	**1165.93**	**1140.53**	**1260.86**	**1240.77**	**1219.735**
	Vapor	28.3	33.07	38.47	17.14	20.23	23.765
Enthalpy (kJ/kg)	Liquid	206.9	214.3	221.7	206.75	213.6	220.5
	Latent heat of vaporization	**207.1**	**201.7**	**196.3**	**194.75**	**190.7**	**186.55**
	Vapor	414	416	418	401.5	404.3	407.05
Conductivity (W/m·K)	Liquid	**0.0983**	**0.09588**	**0.09585**	**0.0898**	**0.0876**	**0.08545**
	Vapor	0.0122	0.01264	0.013113	0.01195	0.0124	0.01286
Surface Tension (N/m)	Liquid	0.0099	0.00914	0.00839	0.010705	0.01014	0.00944

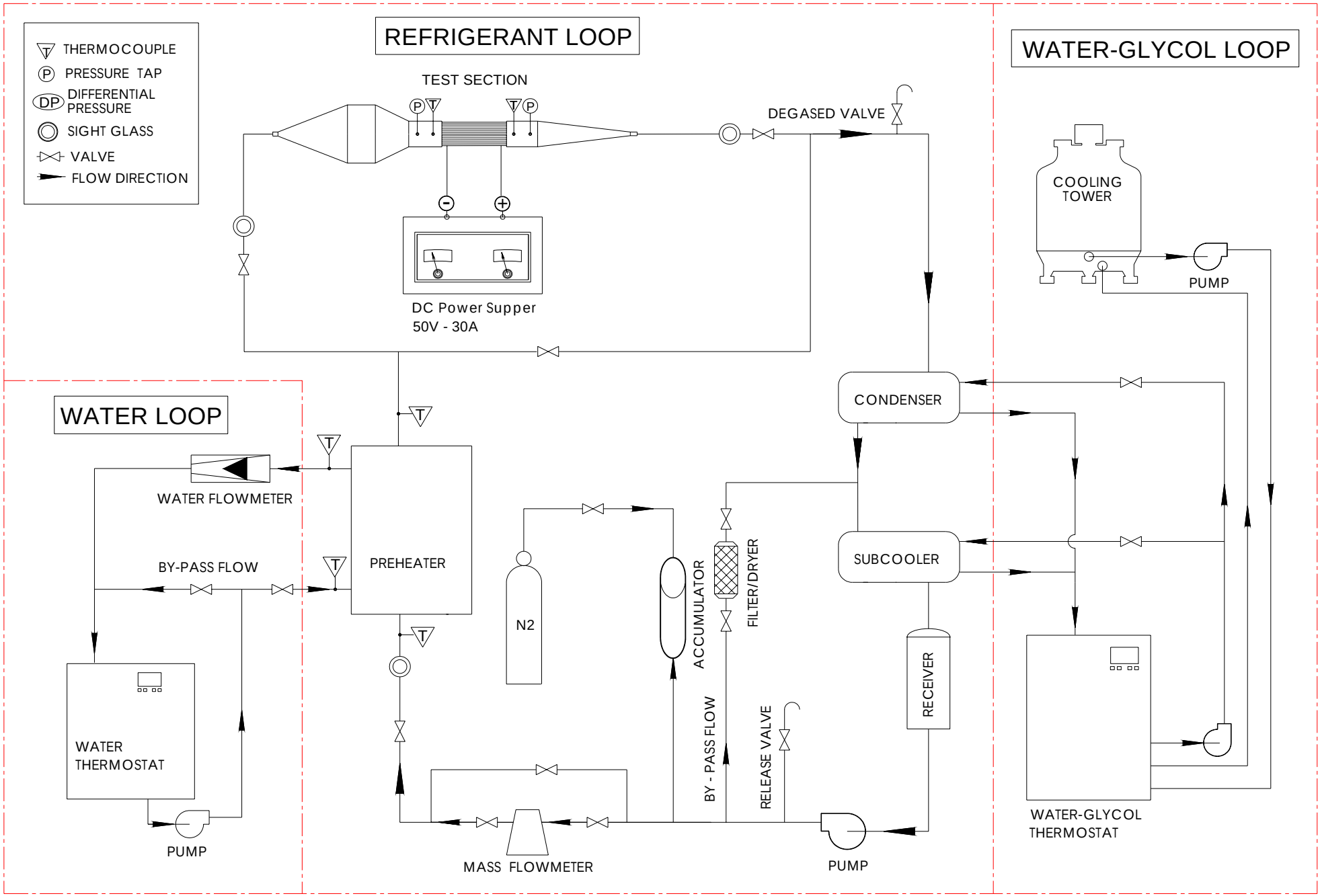

Fig. 2.1 Schematic layout of the experimental system.

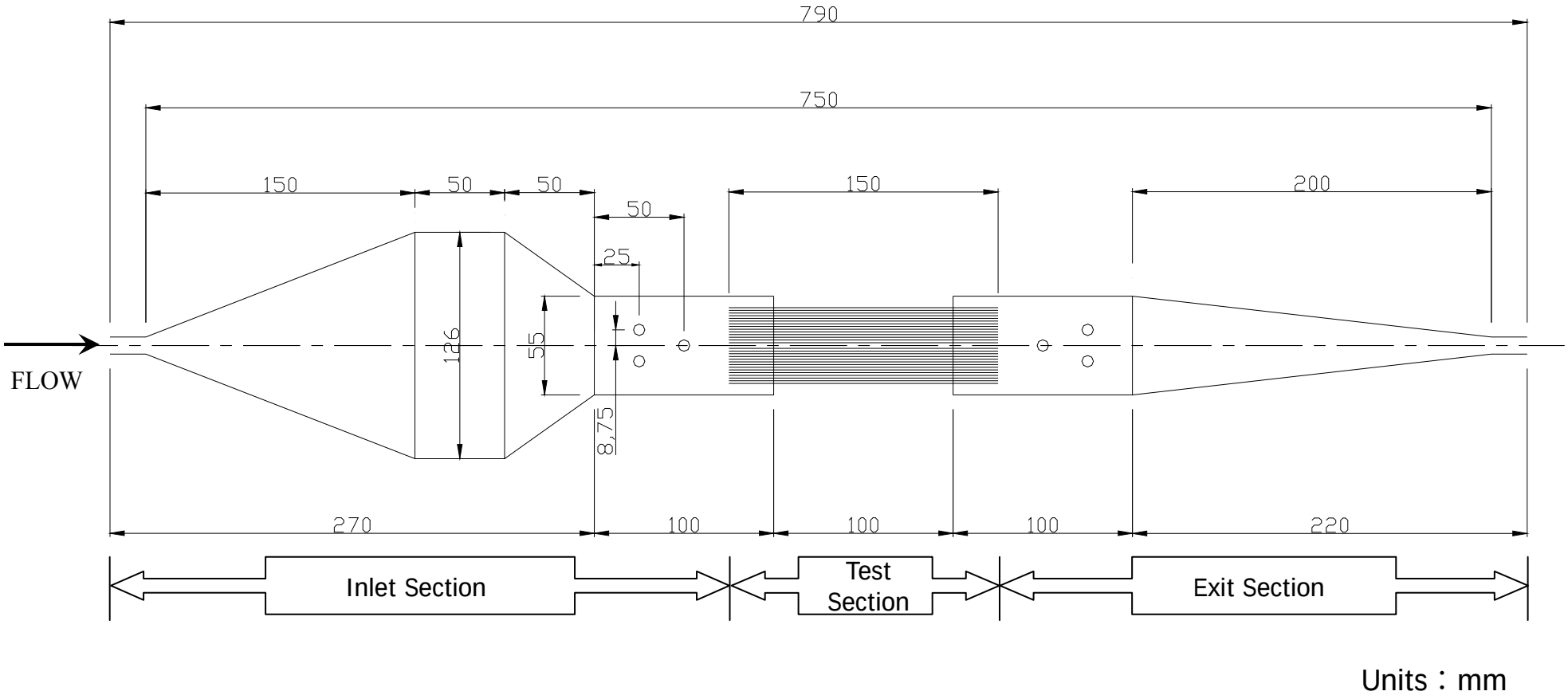

Fig. 2.2 Schematic diagram of test section along with the inlet and exit sections.

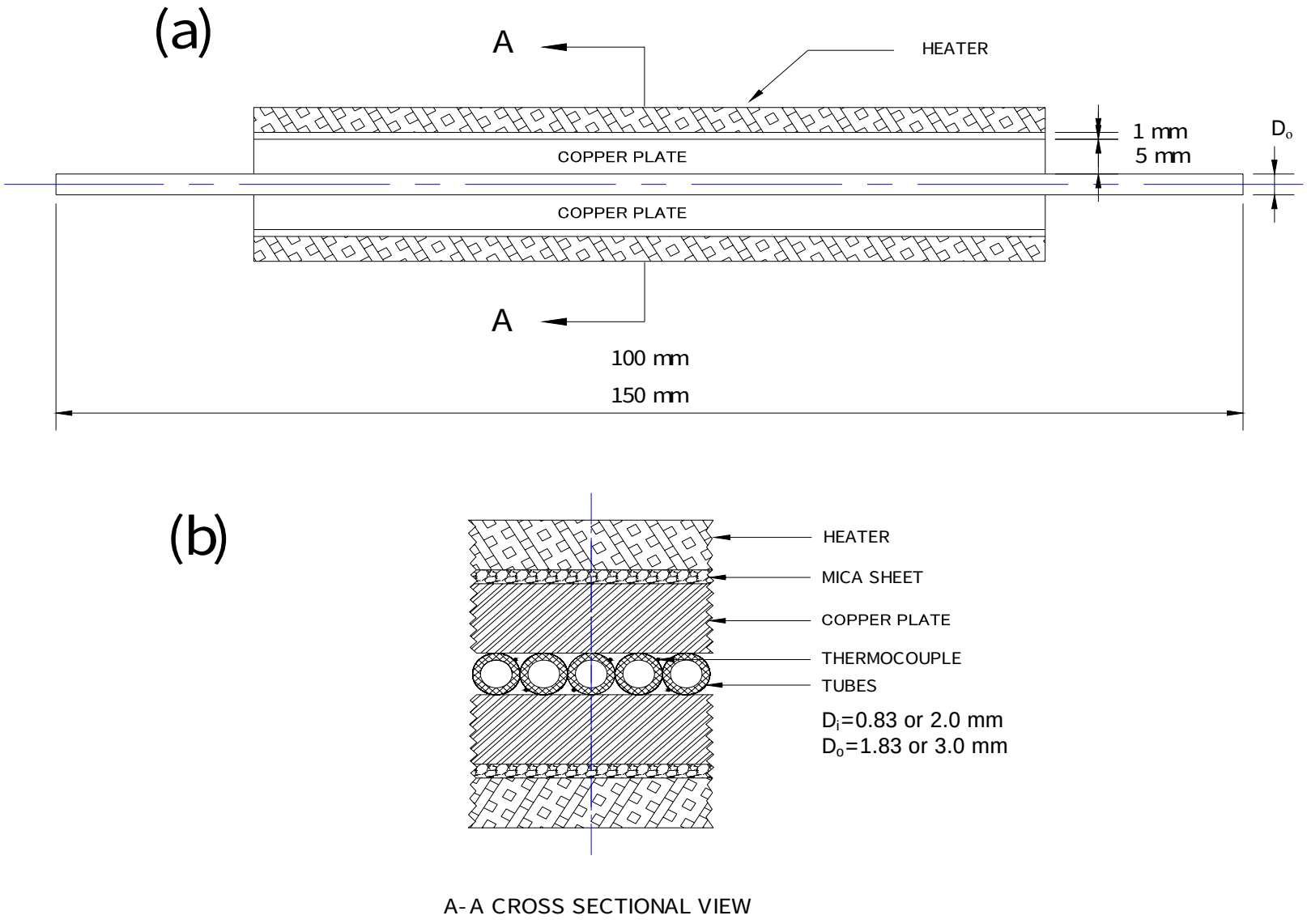

Fig. 2.3 (a) Test section of the small tubes and (b) locations of the thermocouples.

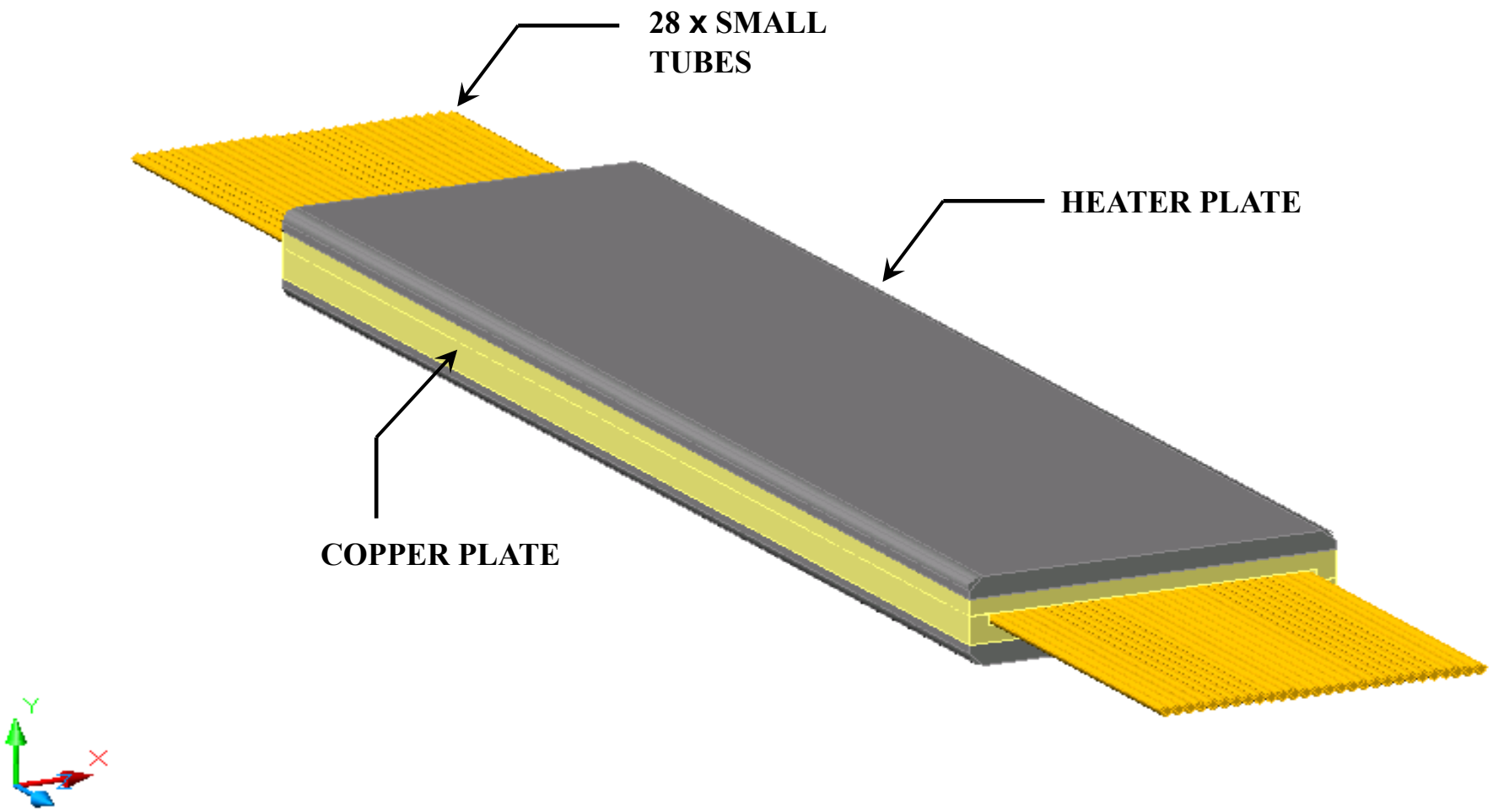

Fig. 2.4 The detail of test section.

CHAPTER 3

DATA REDUCTION

In the present measurement of the evaporation heat transfer coefficient and pressure drop of the refrigerant flow in the horizontal small tubes, a data reduction analysis is needed to calculate the heat transfer coefficient and friction factor from the measured raw data. The data reduction process is described in the following.

3.1 Single Phase Heat Transfer

Before the two-phase experiments, the total heat loss from the test section is evaluated by comparing the total power input from the power supply Q_t with that calculated from the energy balance in the single phase refrigerant flow, which can be expressed as

$$Q_s = G \cdot A_{cs} \cdot C_{p,r} \cdot \Delta T_{i,o} \tag{3.1}$$

where A_{cs} is the total cross-sectional area of the small tubes and $\Delta T_{i,o}$ is the difference in the refrigerant temperature at the exit and inlet of the test section. The total power input is computed from the product of the measured voltage drop across the resistance heater and the electric current passing through it, $Q_t = VI$. The imposed heat flux at the inside surface of the small tubes is then evaluated from the relation

$$q = \frac{Q_t}{A_s} \tag{3.2}$$

where V and I respectively represent the measured voltage drop and current, and A_s denotes the total inside surface area of the small tubes. The relative heat loss from the test section is defined as

$$\varepsilon = (Q_t - Q_s)/Q_t \tag{3.3}$$

The measured results indicated that for all runs in the energy balance test ε was within 2%. The average single phase convection heat transfer coefficient in the small tubes is defined as

$$h_l = \frac{Q_n}{A_s \cdot (T_{wall} - T_{r,ave})} \tag{3.4}$$

Here $Q_n = Q_t - \varepsilon \cdot Q_t = Q_s$ is the net power input to the liquid refrigerant R134a and R-407C refrigerants, T_{wall} is the average of the measured tube wall temperature at all detected locations, and $T_{r,ave}$ is the average refrigerant temperature in the tubes which in turn is estimated from the measured refrigerant temperatures at the inlet and exit of the test section as $(T_{r,i}+T_{r,o})/2$.

3.2 Two Phase Heat Transfer

The vapor quality of the R-134a and R-407C refrigerants entering the test section inlet is evaluated from the energy balance for the preheater. Based on the temperature drop on the water side the heat transfer in the preheater is calculated from the relation,

$$Q_{w,p} = W_{w,p} c_{p,w} (T_{w,p,i} - T_{w,p,o}) \tag{3.5}$$

While the heat transfer to the refrigerant in the preheater is the summation of the sensible heat transfer (for the temperature rise of the refrigerant to the saturated value) and latent heat transfer (for the evaporation of the refrigerant),

$$Q_{w,p} = Q_{sens} + Q_{lat} \tag{3.6}$$

here

$$Q_{sens} = W_r c_{p,r} (T_{r,sat} - T_{r,p,i}) \tag{3.7}$$

$$Q_{lat} = W_r \cdot i_{fg} \cdot x_{p,o} \tag{3.8}$$

The above equations can be combined to evaluate the refrigerant quality at the exit of the preheater that is considered to be the same as the vapor quality of the refrigerant

entering the test section. Specifically,

$$x_{in} = x_{p,o} = \frac{1}{i_{fg}}\left[\frac{Q_{w,p}}{W_r} - c_{p,r}(T_{r,sat} - T_{r,p,i})\right] \tag{3.9}$$

The total change of the refrigerant vapor quality in the test section is then deduced from the net heat transfer rate from the heater to the refrigerant in the test section, Q_n. Thus

$$\Delta x = \frac{Q_n}{W_r i_{fg}} \tag{3.10}$$

Finally, the average heat transfer coefficient for the evaporation of R-134a or R-407C refrigerants in the test section is determined from the definition

$$h_r \equiv \frac{Q_n}{A_s(T_{wall} - T_{r,sat})} \tag{3.11}$$

3.3 Friction Factor

Note that in the evaporation of R-134a or R-407C refrigerant in the tubes the flow accelerates, causing the pressure to drop, as it moves downstream. Besides, the refrigerant pressure also drops due to the contraction at the test section inlet and rises due to the expansion at the exits of the small tubes. Thus, in the refrigerant flow the two phase frictional pressure drop ΔP_f associated with the refrigerant evaporation in the small tubes is calculated by subtracting the pressure drop due to flow acceleration ΔP_a and the pressure drop at the test section inlet ΔP_i and by adding the pressure rise at the test section exit ΔP_o from the measured total pressure drop ΔP_{exp}. The frictional pressure drop is hence given as

$$\Delta P_f = \Delta P_{exp} - \Delta P_a - \Delta P_i + \Delta P_o \tag{3.12}$$

Note that the acceleration pressure drop is estimated by the homogeneous model for two phase flow [50] as

$$\Delta P_a = G^2 \nu_{fg} \Delta x \tag{3.13}$$

Moreover, the pressure drops associated with the sudden contraction and the pressure rises associated with the sudden expansion ΔP_o and ΔP_i for two phase flow moving through the inlet and exit ports estimated by Collier [50] based on a separated flow model are chosen here. They can be expressed as

$$\Delta P_i=(\frac{G}{C_c})^2(1-C_c)\{\frac{(1+C_c)[x_{in}^3\nu_g^2/\alpha^2+(1-x_{in})^3\nu_l^2/(1-\alpha)^2]}{2[x_{in}\nu_g+(1-x_{in})\nu_l]}-C_c[\frac{x_{in}^2\nu_g}{\alpha}+\frac{(1-x_{in})^2\nu_g}{(1-\alpha)}]\} \tag{3.14}$$

and

$$\Delta P_o=G^2\sigma(1-\sigma)\nu_l[\frac{(1-x_{in})^2}{(1-\alpha)}+(\frac{\nu_g}{\nu_l})\frac{x_{in}^2}{\alpha}] \tag{3.15}$$

where C_c in equation (3.14) is the coefficient of contraction and it is a function of the contraction ratio σ. The void fraction α in the above equations is calculated from the correlation given by Zivi [51] as

$$\alpha=\frac{1}{1+(\frac{1-x_{in}}{x_{in}})(\frac{\rho_g}{\rho_l})^{2/3}} \tag{3.16}$$

Finally, for the evaporation of R-134a or R-407C in the small tubes the two phase friction factor is expressed as

$$f_{tp} = \frac{\Delta P_f D_i}{2G^2\nu_m L} \tag{3.17}$$

where L is the length of the small tubes and ν_m is the mean specific volume of the vapor-liquid mixture in the small tubes when they are homogeneously mixed and can be expressed as

$$\nu_m=[x_m\nu_g+(1-x_m)\nu_l]=(\nu_l+x_m\nu_{fg}) \tag{3.18}$$

3.4 Uncertainty Analysis

As the tubes are miniaturized, it becomes harder to maintain the geometric precision of the tube cross section and to insure the smooth transition from the inlet section to the heat transfer section [52]. Uncertainty of a similar nature arises from the micro-roughness of the heat transfer surface and the presence of dust particles in the flow. Besides, the heat conduction from the test heater to the unheated part of the tubes increases as the test section is miniaturized. These factors result in higher uncertainties of the measured data.

Uncertainties of the heat transfer coefficients are estimated according to the procedures proposed by Kline et al. [53]. The detailed results from this uncertainty analysis are summarized in Table 3.1.

Table 3.1 Summary of the uncertainty analysis

Parameter	Uncertainty
Small tubes geometry	
Length, width and thickness	±0.5 %
Area	±1.0 %
Parameter measurement	
Temperature, T	±0.2 ℃
Temperature difference, ΔT	0.28 ℃
System pressure, P	±2 kPa
Pressure drop, ΔP	±200 Pa
Mass flux of refrigerant, G	±2 %
Single-phase heat transfer in small tubes	
Imposed heat flux, q	±4.5 %
Heat transfer coefficient, $h_{r,l}$	±10.5 %
Evaporation heat transfer in small tubes	
Imposed heat flux, q	±4.5 %
Inlet vapor quality, x_{in}	9.5 %
Heat transfer coefficient, h_r	±14.5 %
Friction pressure drop, ΔP_f	±16.5 %

CHAPTER 4

EVAPORATION HEAT TRANSFER

In this chapter selected data obtained here are presented to illustrate the evaporation heat transfer of R-134a or R-407C in the horizontal small circular tubes. The present experiments are performed for refrigerant R-134a or R-407C in a tube bank forming by 2.0-mm diameter tubes with the refrigerant mass flux G varied from 200 to 400 kg/m^{2}s, imposed heat flux q from 5 to 15 kW/m^2, inlet vapor quality x_{in} from 0.2 to 0.8, and refrigerant saturated temperature T_{sat} from 5 to 15℃. While for another tube tank forming by the 0.83-mm diameter tubes, G is varied from 800 to 1500 kg/m^{2}s with the other parameters varied in the same ranges as those for D_i=2.0 mm. The corresponding ranges of the associated dimensionless groups including the Reynolds, convection, confinement and boiling numbers are listed in Table 4.1. Note that the different ranges of the refrigerant mass flux are tested for the different sizes of the tubes, since at the low mass flow rate the refrigerant flow in the smaller tubes for D_i=0.83 mm is somewhat unsteady, leading to the unstable intermittent flow in the system.

In what follows the effects of the vapor quality, imposed heat flux and refrigerant mass flux and saturated temperature on the R-134a and R-407C average evaporation heat transfer coefficients are examined in detail.

4.1 Single Phase Heat Transfer

Before measuring the R-134a and R-407C evaporation heat transfer coefficients, single phase liquid R-134a and R-407C convection heat transfer coefficients in the

small tubes were obtained for the refrigerant inlet temperature fixed at 15℃ and imposed heat flux of 5 kW/m^2 with the refrigerant mass flux respectively varied from 200 to 800 kg/m^{2}s and from 400 to 3000 kg/m^{2}s in the 2.0-mm and 0.83-mm diameter tubes. Note that the single phase heat transfer test is conducted here to check the energy balance in the test section and the suitability of the experimental system for the present measurement. The measured single phase liquid of R-134a and R-407C heat transfer coefficients are compared with the Dittus-Boelter [9] and Gnielinski [10] correlations in Figs. 4.1 and 4.2.

The Dittus-Boelter correlation is

$$\mathrm{Nu} = 0.023 \cdot \mathrm{Re}^{0.8} \cdot \mathrm{Pr}^{0.4} \tag{4.1}$$

for $\mathrm{Re} > 10^5$ and $0.7 < \mathrm{Pr} < 16{,}700$

and the Gnielinski correlation is

$$\mathrm{Nu} = \frac{(f/2)(\mathrm{Re}-1000)\,\mathrm{Pr}}{1.07 + 12.7\sqrt{f/2}\,(\mathrm{Pr}^{2/3}-1)} \tag{4.2}$$

for $2300 < \mathrm{Re} < 10^6$ and $0.6 < \mathrm{Pr} < 10^5$,where

$$f = (1.58 \ln \mathrm{Re} - 3.28)^{-2} \tag{4.3}$$

The single phase heat transfer results indicate that in the energy balance test the relative heat loss defined in Eq.(3.3) is within 2% for all run. Thus the heat loss from the test section is small. The measured single phase heat transfer data are compared in Figs. 4.1 and 4.2 with those calculated form the two correlations given in Equs.(4.1) & (4.2). The results show that for the 2.0-mm tubes the data are close to the Dittus-Boelter correlation. While for the 0.83-mm tubes the data are well fitted with Gnielinski correlation.

4.2 Evaporation Heat Transfer in 2.0-mm Tubes

The heat transfer data for the R-134a and R-407C evaporation in the 2.0-mm tubes are examined first. The data set illustrating how the refrigerant saturated temperature T_{sat}, mass flux G and imposed heat flux q affect the heat transfer coefficients for R-134a evaporation in the 2.0-mm tubes is showed in Figs. 4.3 ~ 4.11. The measured heat transfer coefficients are examined by checking their variations with the inlet vapor quality at the test section inlet x_{in}. Since the tubes are short, the inlet and outlet quality change Δx in the small tubes is relatively small, ranging from 0.01 to 0.03 in the present study. Note that for given q, T_{sat} and G the evaporation heat transfer coefficients increase almost linearly with the inlet quality. At higher T_{sat}, q and G the increase in h_r is significant. The significant increase of the evaporation heat transfer coefficients with the inlet vapor quality is considered to result from the fact that at a higher quality the liquid film thickness of the refrigerant on the inside surface of the tubes becomes thinner. Hence the thermal resistance of the liquid film is reduced and heat transfer across the film is improved. Besides, at a higher vapor quality the mass flux of the vapor and the velocity of vapor flow are faster. This also improves the interfacial heat transfer. More specifically, for the case at T_{sat}=15℃, G=400 kg/m^{2}s and q=15 kW/m^2, the R-134a evaporation heat transfer coefficients at x_{in}=0.2 and 0.8 are respectively 4430 and 5820 W/m℃ (Fig. 4.5(c)). Hence an increase of 31% in h_r occurs for x_{in} raised from 0.2 to 0.8 for this case. The effects of each parameter on h_r are examined in detail in the following. At first, the effects of the saturated temperature T_{sat} are presented in Figs. 4.3 ~ 4.5 by showing the variations of the evaporation heat transfer coefficients with the inlet vapor quality at T_{sat}=5, 10 , 15℃ for different refrigerant mass fluxes and imposed heat flux. The results in Figs. 4.3 ~ 4.5 indicate that at fixed q and G the R-134a evaporation heat transfer coefficients rise with the saturated temperature of the refrigerant. This trend in h_r variation with T_{sat} is ascribed to the fact that at a higher T_{sat} the latent heat of

vaporization h_{fg} is lower, which in turn results in a higher evaporation rate of the liquid R-134a. Hence the R-134a vapor in the tubes flows at a higher speed, producing a higher convection effect and therefore a higher h_r. Moreover, we note that at the higher q of 10 & 15 kW/m^2 and G of 300 & 400 kg/m^{2}s the increase of h_r with T_{sat} is noticeably higher than that at the lower q (=5 kW/m^2) and G (=200 kg/m^{2}s). To be more quantitative on the effects of T_{sat} on the R-134a evaporation heat transfer coefficient, the quality-averaged evaporation heat transfer coefficients $\bar{h}_r$ at G=400 kg/m^{2}s and q=15 kW/m^2 are calculated from the data in Fig 4.5(c). The results show that $\bar{h}_r$ at T_{sat}=5℃ and 15℃ are about 4402 W/m℃ and 5244 W/m℃, respectively. Thus for T_{sat} raised from 5℃ to 15℃, $\bar{h}_r$ is increased by 19.1%. The above physical mechanisms for R-134a are similar to that for R-407C in 2.0-mm small tubes (Figs. 4.12 ~ 4.20).

Next, the effects of the refrigerant mass flux on the R-134a evaporation in the 2.0-mm tubes shown in Figs. 4.6 ~ 4.8 indicate that the increase of h_r with the R-134a mass flux is rather significant especially at a high q, suggesting that the interfacial evaporation is effectively enhanced by the rise in the refrigerant mass flux. Hence the convection mechanism is important in the flow. Quantitatively, according to the data in Fig. 4.8(c) for T_{sat}=15℃ and q=15 kW/m^2 the quality-averaged evaporation heat transfer coefficients for G=200 and 400 kg/m^{2}s are 4054.3 and 5129.2 W/m℃, respectively. Thus $\bar{h}_r$ is increased by 26.5% for G raised from 200 to 400 kg/m^{2}s.

Then, the results presented in Figs. 4.9 ~ 4.11 indicate that the R-134a evaporation heat transfer coefficient increases rather significantly with the imposed heat flux for various T_{sat} and G. This significant increase of h_r with q reflects that the evaporation at the liquid-vapor interface in the refrigerant flow is substantially augmented by the increase in the imposed heat flux. According to the data in Fig. 4.11(a) for T_{sat}=15℃ and G=200 kg/m^{2}s, the quality-averaged evaporation heat

transfer coefficients at q=5 and 15 kW/m^2 are 2656 and 4055 W/m°C, respectively. Thus for q raised from 5 to 15 kW/m^2, $\bar{h}_r$ is increased by 52.7%. Furthermore, we note that at the same T_{sat}, G and q the differences in the evaporation heat transfer coefficients between that for R-134a and R-407C in 2.0-mm tubes are less than 25% for all cases studied here.

4.3 Evaporation Heat Transfer in the Smaller Tubes (D_i=0.83 mm)

The measured heat transfer data for the smaller tubes with D_i=0.83 mm are presented in Figs. 4.21 ~ 4.29 for the R-134a evaporation and in Figs. 4.30 ~ 4.38 for the R-407C evaporation, covering the effects of various parameters on the evaporation heat transfer coefficients for these two refrigerants. First, it is noted from the results in Figs. 4.21 ~ 4.29 that for given T_{sat}, G and q the R-134a evaporation heat transfer coefficient also increases noticeably with the inlet vapor quality except at high vapor quality for some cases at high T_{sat}, G and q (Figs. 4.23(a) & (b), 4.26 & 4.29). A close inspection of data in Figs. 4.21 ~ 4.29 reveals that at low mass flux and high imposed heat flux, h_r even decreases with a rise in x_{in} at a high quality for x_{in}>0.6. This is conjectured to result from the partial dryout of the refrigerant on the tube wall at high x_{in} at these conditions. In fact, the data from Yan and Lin [12] for R-134a evaporation in the 2.0-mm tubes show the decline of h_r with a rise in x_{in} for many cases. These earlier pool data are the results of the significant refrigerant dryout in the tubes, as already mentioned here, apparently due to the bad refrigerant distribution at the inlet of the test section. This has been improved considerably in the present study by noting that the partial dryout only occurs in the smaller tubes with D_i=0.83 mm at high x_{in} & q and low G. Moreover, at an intermediate quality the increase of h_r with x_{in} is rather large for the cases at high T_{sat}, q and G. However, for these cases the increase is rather

mild at low quality. To be more quantitative on the effects of x_{in} on h_r, we compare the values of h_r at x_{in}=0.2 & 0.8 for two cases. First for R-134a at T_{sat}=5°C, G=800 kg/m^{2}s and q=5 kW/m^2, Fig. 4.21(a) shows that the evaporation heat transfer coefficients at x_{in}=0.2 & 0.8 are 2380 and 2850 W/m°C, respectively. This is a 19.7% increase for x_{in} raised from 0.2 to 0.8. While for the case with T_{sat}=15°C, G=1500 kg/m^{2}s and q=15 kW/m^2 the corresponding increase is 24% (Fig. 4.23(c)).

According to the results in Figs. 4.30 ~ 4.38, the R-407C evaporation heat transfer coefficients increase almost linearly with the inlet vapor quality for most cases except at the low saturated temperature of 5°C, low mass flux of 800 kg/m^{2}s and high heat flux of 15 kW/m^2 (Figs. 4.32(a) and 4.35(a)). The increase is rather substantial at high T_{sat}, q and G. For the special case with T_{sat}=5°C, q=15kW/m^2 and G=800 kg/m^{2}s the evaporation heat transfer levels off at increasing x_{in} for x_{in} >0.6 (Fig. 4.32(a)). Checking the numerical values for h_r in Figs. 4.30 ~ 4.38 reveals the quantitative increase of h_r with x_{in} for R-407C. For example, at T_{sat}=5°C, G=800 kg/m^{2}s and q=5 kW/m^2 h_r is increased from 2200 W/m^2°C to 2480 W/m^2°C for x_{in} raised from 0.2 to 0.8 (Fig. 4.30(a)). It is a 12.7% increase. But at T_{sat}=15°C, G=1500 kg/m^{2}s and q=15 kW/m^2 we have a much larger increase of 26.3% for the same rise in x_{in} (Fig. 4.32(c)).

An overall inspection of the data presented in Figs. 4.21 ~ 4.29 discloses that for R-134a evaporation in the smaller tubes with D_i=0.83 mm the heat transfer in the flow can be significantly increased by raising the refrigerant saturated temperature, mass flux and heat flux. These trends are similar to that for the large tubes with D_i=2.0-mm already examined in Sec. 4.2. A further inspection of the results in Figs. 4.21 ~ 4.29 reveals that the effects of the refrigerant saturated temperature and mass flux on h_r are more pronounced at a higher heat flux (Figs. 4.22, 4.23, 4.26). Finally, the heat flux variation is more important at high T_{sat} and G, as evident from the results in Fig. 4.29.

For R-407C evaporation in the smaller tubes a substantial increase in h_r with the refrigerant saturated temperature, mass flux and heat flux are also noted from the results in Figs. 4.30 ~ 4.38. It should be mentioned that for R-407C evaporation at high vapor quality h_r does not decline for a rise in x_{in}, unlike that for R-134a. This is attributed to the fact that R-407C has a high latent heat of vaporization and the partial dryout on the tube wall is less likely to occur in R-407C evaporation. Moreover, we also note that at the same T_{sat}, G and q the differences in the evaporation heat transfer coefficients between that for R-134a and R-407C in 0.83-mm tubes are less than 28% for all cases studied here.

To be more quantitative on the effects of various parameters on the heat transfer data in the smaller tubes, the quality-averaged evaporation heat transfer coefficients for various cases are evaluated. The results from this evaluation show that for R-134a at G=800 kg/m^{2}s and q=15 kW/m^2, $\bar{h}_r$ is increased from 3476 to 4272 W/m^2°C when T_{sat} is raised from 5°C to 15°C (Fig. 4.23(a)). It is a 22.8% increase. While for R-407C the corresponding increase is 32.2% with $\bar{h}_r$ enhanced from 4650 to 6150 W/m^2°C (Fig. 4.32(a)). Next, we note that for R-134a at T_{sat}=5°C and q=15 kW/m^2, $\bar{h}_r$ is increased from 3576 to 4771 W/m^2°C for G raised from 800 to 1500 kg/m^2°C. This is a 33.4% increase (Fig. 4.26(a)). The corresponding increase for R-407C is 36.1% with $\bar{h}_r$ increased from 4641 to 6320 W/m^2°C (Fig. 4.35(a)). Finally, $\bar{h}_r$ is increased from 4467 to 5291 W/m^2°C for q raised from 5 to 15 kW/m^2 for R-134a at T_{sat}=15°C and G=1500 kg/m^{2}s (Fig. 4.29(c)). It is a 18.4% increase. For R-407C the corresponding increase is 39.6% with $\bar{h}_r$ changed from 5903 to 8244 W/m^2°C (Fig. 4.38(c)).

4.4 Correlation Equation for Evaporation Heat Transfer Coefficients

For practical application the present data for the R-134a and R-407C evaporation in the 2.0-mm and 0.83-mm tubes need to be correlated empirically. The correlation is expressed as

$$h_{tp} = \frac{25}{X_{tt}^{0.5}} \mathrm{Re}_l^{0.83} Bo^{0.65} \left(\frac{k_l}{D_i} \right) \tag{4.4}$$

The Boiling number, Martinelli parameter and liquid Reynolds number are defined respectively as

$$\mathrm{X_{tt}} = \left(\frac{1-x}{x} \right)^{0.9} \left(\frac{\rho_g}{\rho_l} \right)^{0.5} \left(\frac{\mu_l}{\mu_g} \right)^{0.1} \tag{4.5}$$

$$\mathrm{Re}_l = \frac{G \cdot (1-x) \cdot D_i}{\mu_l} \tag{4.6}$$

$$\mathrm{Bo} = \frac{\mathrm{q}}{\mathrm{G} \cdot \mathrm{i_{fg}}} \tag{4.7}$$

Comparison of the above correlation with the present experimental data shown in Fig. 4.39 indicates that more than 85 % of the present data for h_r fall within ± 35 % of Eq. (4.4), and the mean deviation between the present data for h_r and the proposed correlation is 13.2 %.

4.5 Concluding Remarks

Experiments have been conducted here to investigate the evaporation heat transfer of R-134a and R-407C in the small tubes with D_i=0.83 & 2.0-mm. The effects of the refrigerant saturated temperature, mass flux, imposed heat flux, tube dimensions and vapor quality of R-134a and R-407C on the evaporation heat transfer coefficients have been examined in detail. The results show that the R-134a and R-407C evaporation heat transfer coefficient in the small tubes increases almost linearly with the vapor quality and the increases are significant except at low imposed

heat flux, refrigerant mass flux and saturated temperature. Moreover, the increases of the R-134a and R-407C evaporation heat transfer coefficient in both tubes with the imposed heat flux, refrigerant mass flux and saturated temperature are also substantial. Besides, the evaporation heat transfer coefficients for R-134a are lower than that for R-407C at the same T_{sat}, G and q, but are within 25% and 28% in 2.0-mm and 0.83-mm tubes, respectively.

Furthermore, for R-134a in the smaller tubes (D_i=0.83-mm) partial dryout may occur, resulting in the decline of h_r at increasing inlet vapor quality at high x_{in}. This is normally seen at high imposed heat flux and saturated temperature, lower mass flux. Finally, an empirical correlation is proposed to correlate the present data for R-134a and R-407C evaporation heat transfer in the small tubes.

Table 4.1 List of conditions of the experimental parameters for R-134a and R-407C refrigerants

D_i (mm)	Parameters		G (kg/m^2s)	q (kW/m^2)	T_{sat} (℃)	P_{sat} (kPa)	x_{in}	α	Re_l	Co	N_{conf}	Bo
2.0	R-134a & R-407C	Single Phase	200 ~ 800	5	15	488 & 900	—	—	1780 ~ 7130 & 2300 ~ 9230	—	—	—
		Two Phase	200, 300, 400	5, 10, 15	5, 10, 15	350, 415, 488 & 665, 776, 900	0.2 ~ 0.8	0.9289 ~ 0.9966 & 0.8845 ~ 0.9941	314 ~ 2853 & 406 ~ 3250	0.0382 ~ 0.419 & 0.05 ~ 0.547	0.44 ~ 0.46 & 0.43 ~ 0.46	6.4×10^{-5}~ 4×10^{-4} & 6×10^{-5}~ 3.8×10^{-4}
0.83	R-134a & R-407C	Single Phase	400 ~ 3000	5	15	488 & 900	—	—	1480 ~ 11101 & 1914 ~ 14360	—	—	—
		Two Phase	800, 1150, 1500	5, 10, 15	5, 10, 15	350, 415, 488 & 665, 776, 900	0.2 ~ 0.8	0.9289 ~ 0.9966 & 0.8845 ~ 0.9941	522 ~ 4440 & 674 ~ 5743	0.0382 ~ 0.419 & 0.05 ~ 0.547	1.07 ~ 1.12 & 1.04 ~ 1.10	1.7×10^{-5}~ 1×10^{-4} & 1.6×10^{-5}~ 3.8×10^{-4}

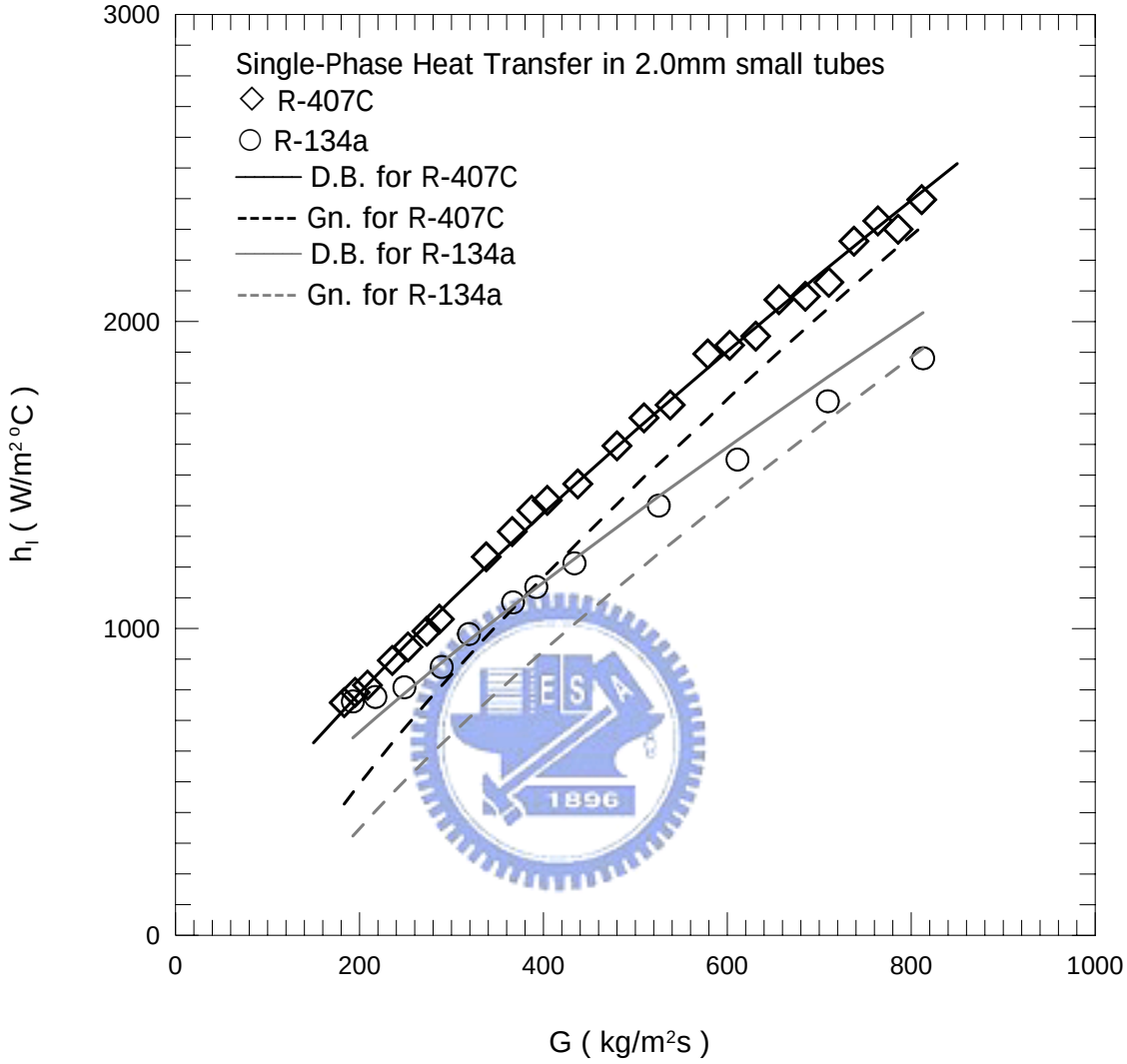

Fig. 4.1 Comparison of the present data for the liquid phase of R-134a and R-407C heat transfer coefficient in 2.0-mm small tubes with the Dittu-Boelter and Gnielinski correlations

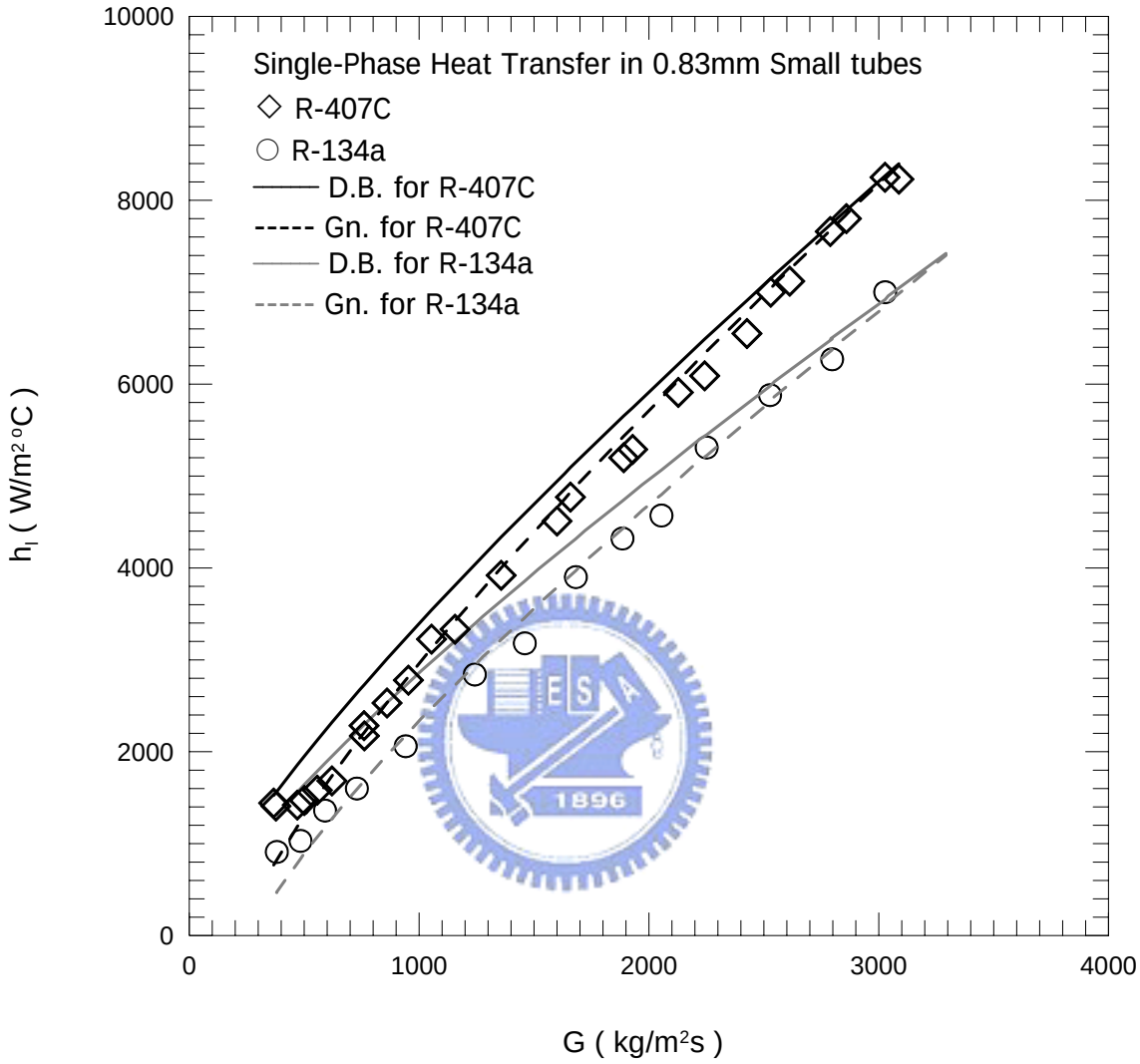

Fig. 4.2 Comparison of the present data for the liquid phase of R-134a and R-407C heat transfer coefficient in 0.83-mm small tubes with the Dittu-Boelter and Gnielinski correlations

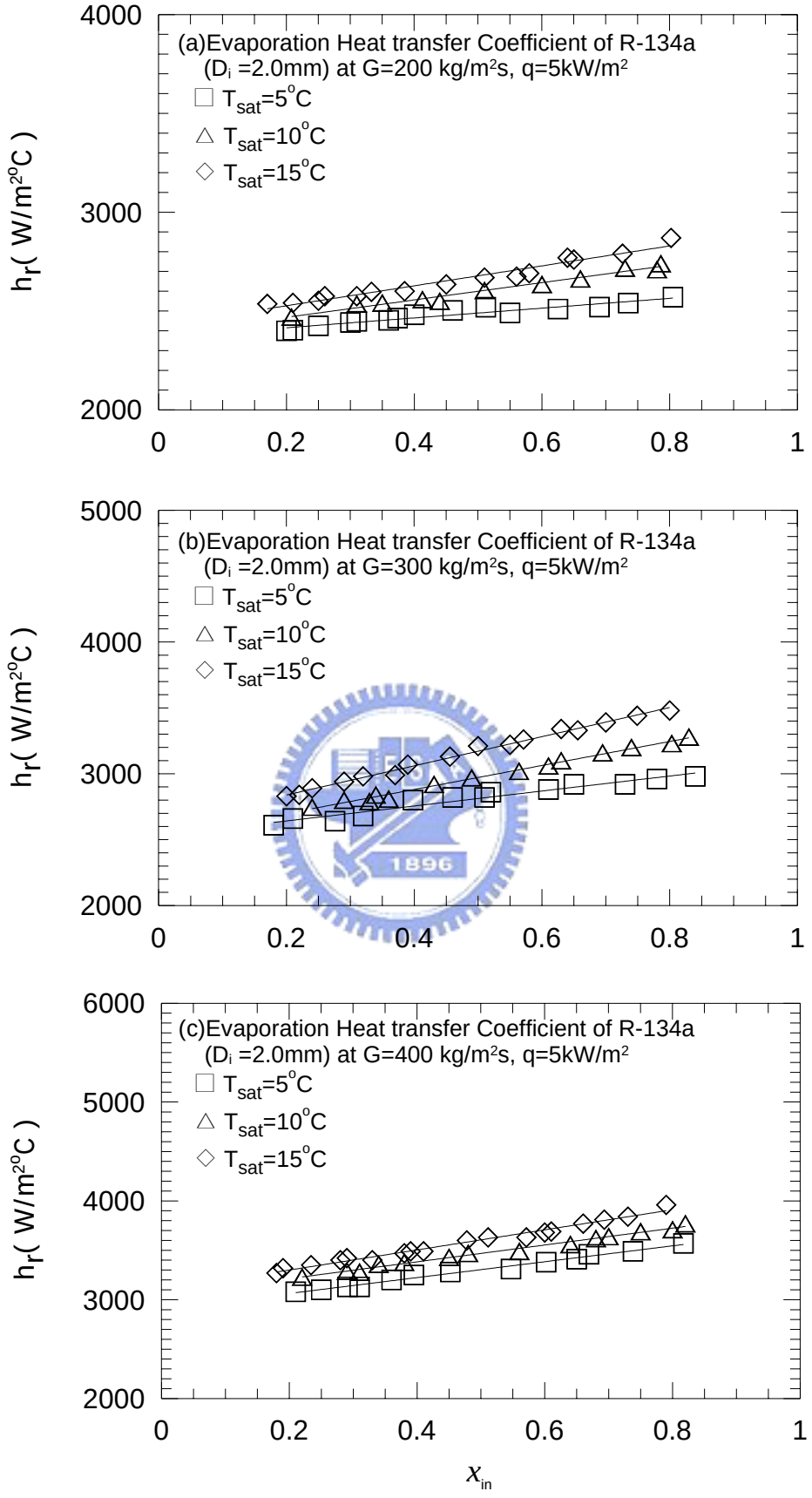

Fig. 4.3 Variations of R-134a evaporation heat transfer coefficient with inlet vapor quality in 2.0-mm small tubes at q=5 kW/m^2 for various T_{sat} for (a) G=200 kg/m^{2}s, (b) G=300 kg/m^{2}s, and (c) G=400 kg/m^{2}s.

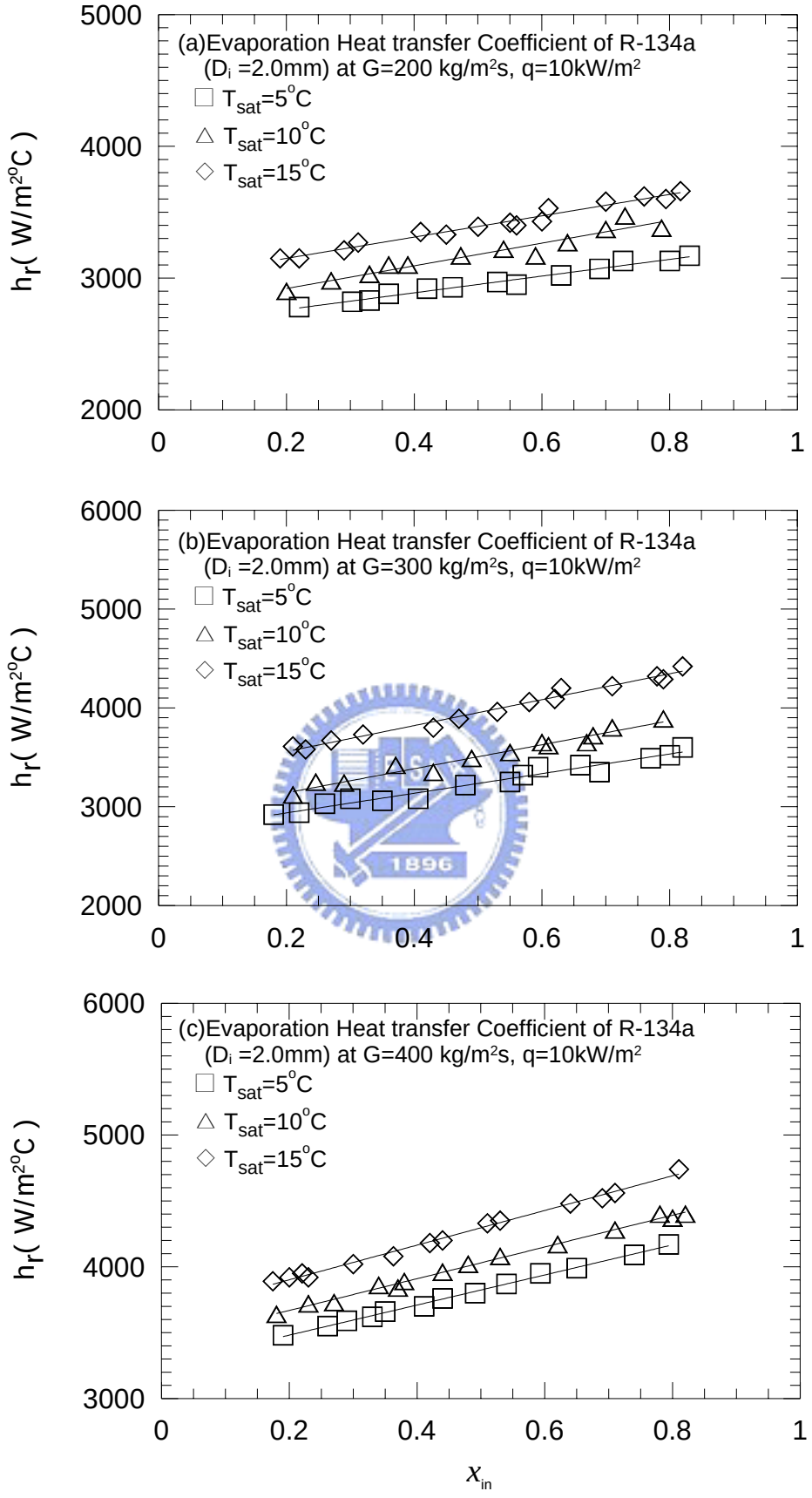

Fig. 4.4 Variations of R-134a evaporation heat transfer coefficient with inlet vapor quality in 2.0-mm small tubes at q=10 kW/m^2 for various T_{sat} for (a) G=200 kg/m^{2}s, (b) G=300 kg/m^{2}s, and (c) G=400 kg/m^{2}s.

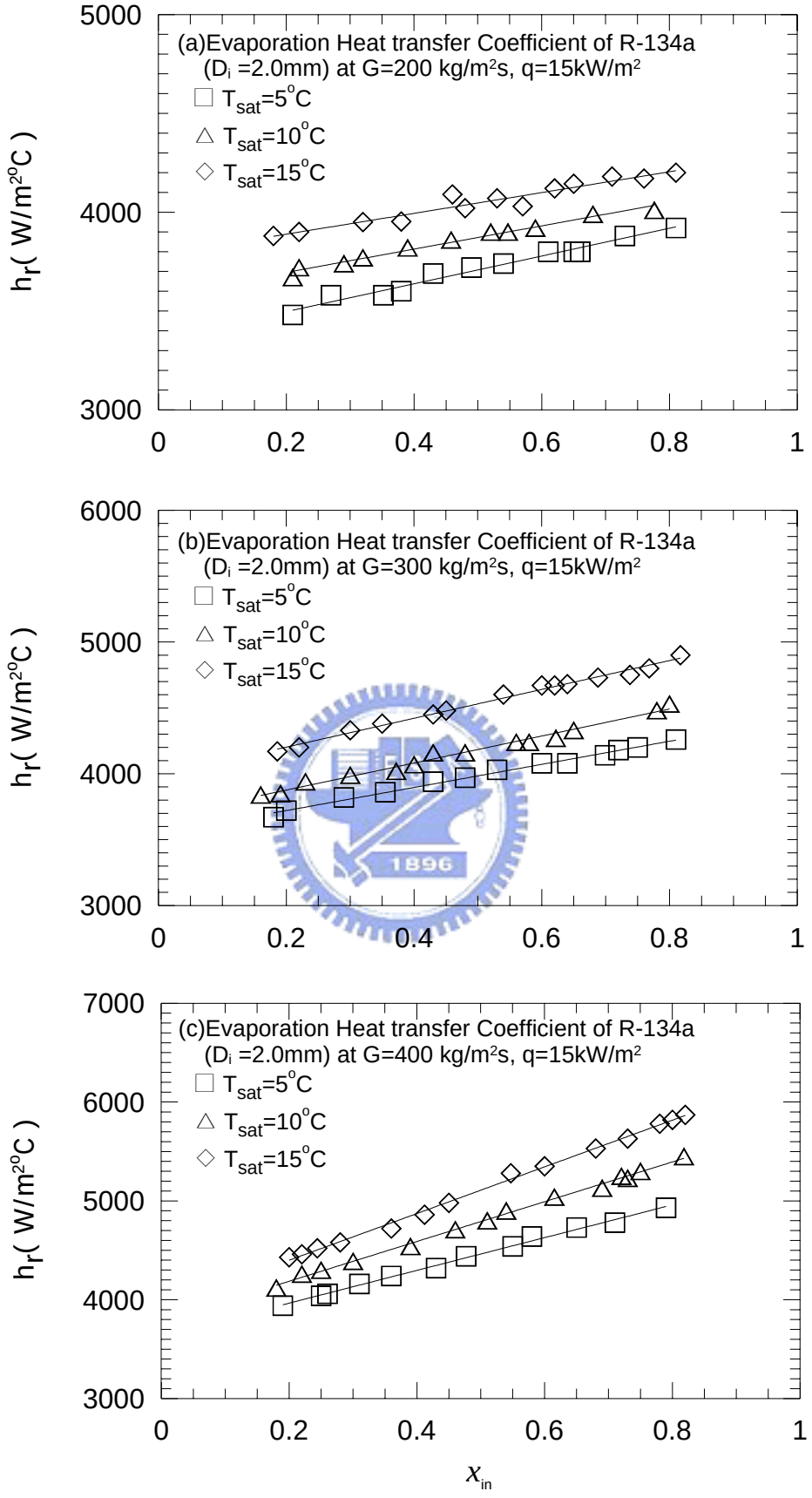

Fig. 4.5 Variations of R-134a evaporation heat transfer coefficient with inlet vapor quality in 2.0-mm small tubes at q=15 kW/m^2 for various T_{sat} for (a) G=200 kg/m^{2}s, (b) G=300 kg/m^{2}s, and (c) G=400 kg/m^{2}s.

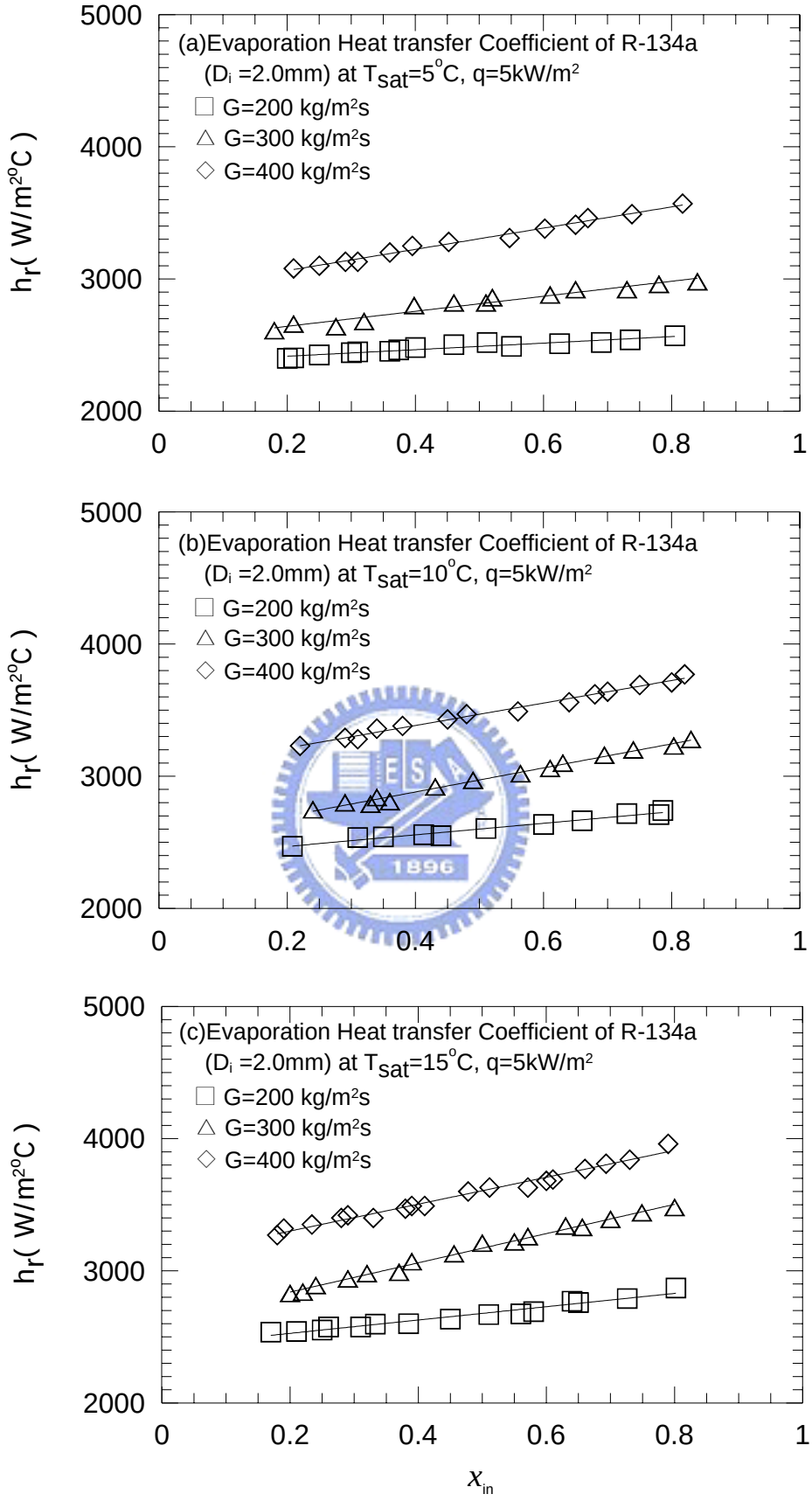

Fig. 4.6 Variations of R-134a evaporation heat transfer coefficient with inlet vapor quality in 2.0-mm small tubes at q=5 kW/m^2 for various G for (a) T_{sat}=5℃, (b) T_{sat}=10℃, and (c) T_{sat}=15℃.

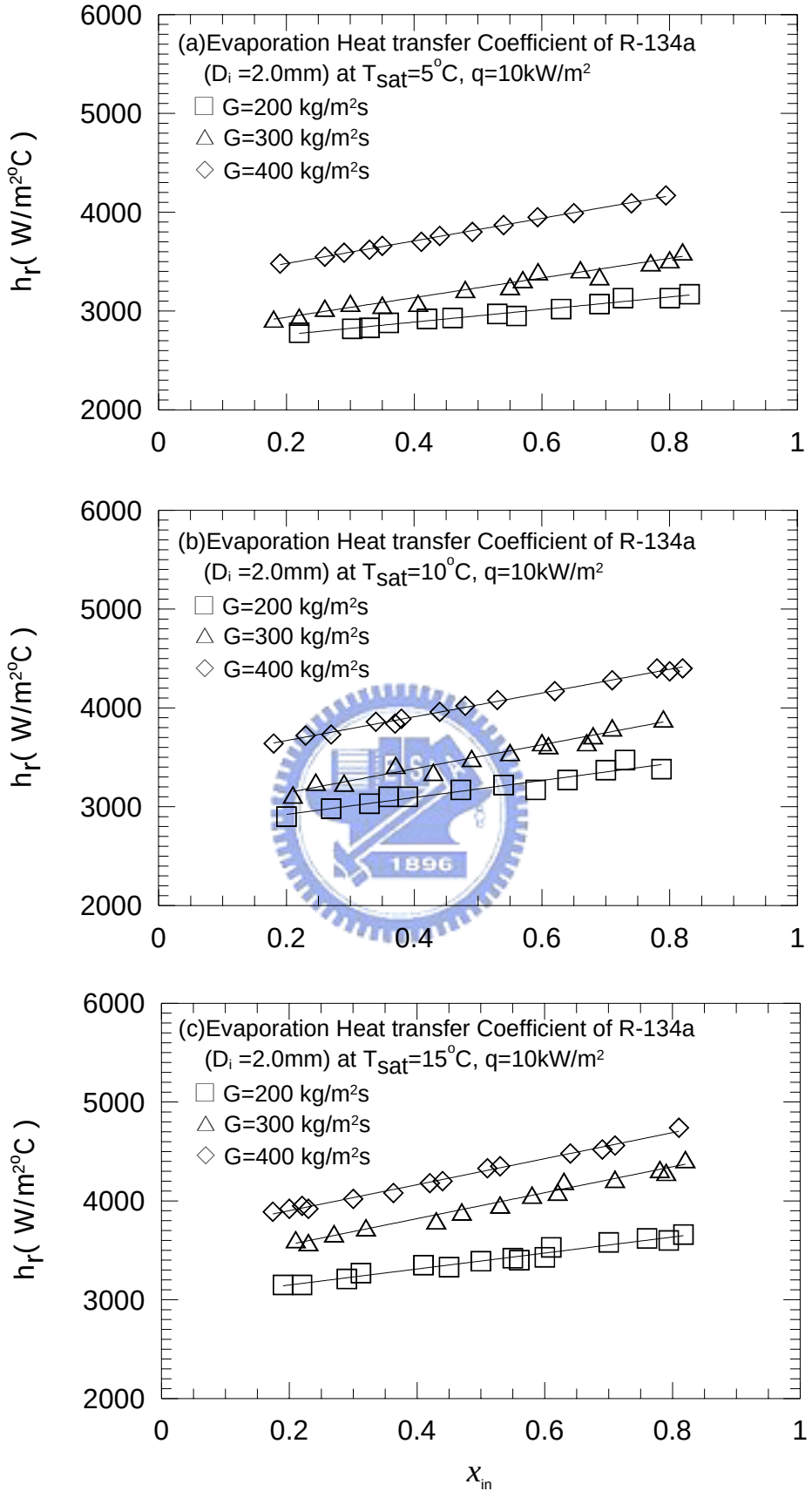

Fig. 4.7 Variations of R-134a evaporation heat transfer coefficient with inlet vapor quality in 2.0-mm small tubes at q=10 kW/m^2 for various G for (a) T_{sat}=5℃, (b) T_{sat}=10℃, and (c) T_{sat}=15℃.

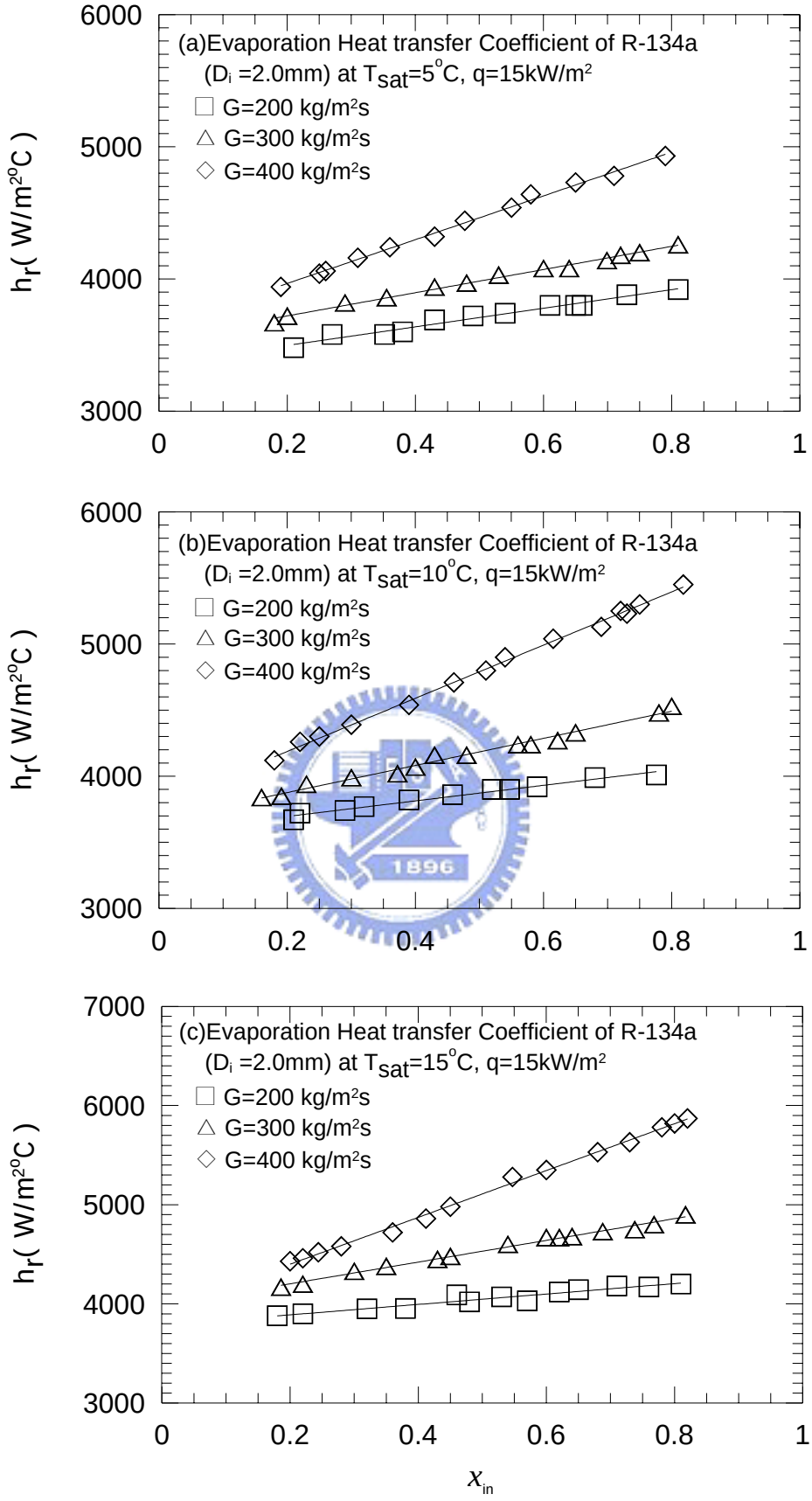

Fig. 4.8 Variations of R-134a evaporation heat transfer coefficient with inlet vapor quality in 2.0-mm small tubes at q=15 kW/m^2 for various G for (a) T_{sat}=5℃, (b) T_{sat}=10℃, and (c) T_{sat}=15℃.

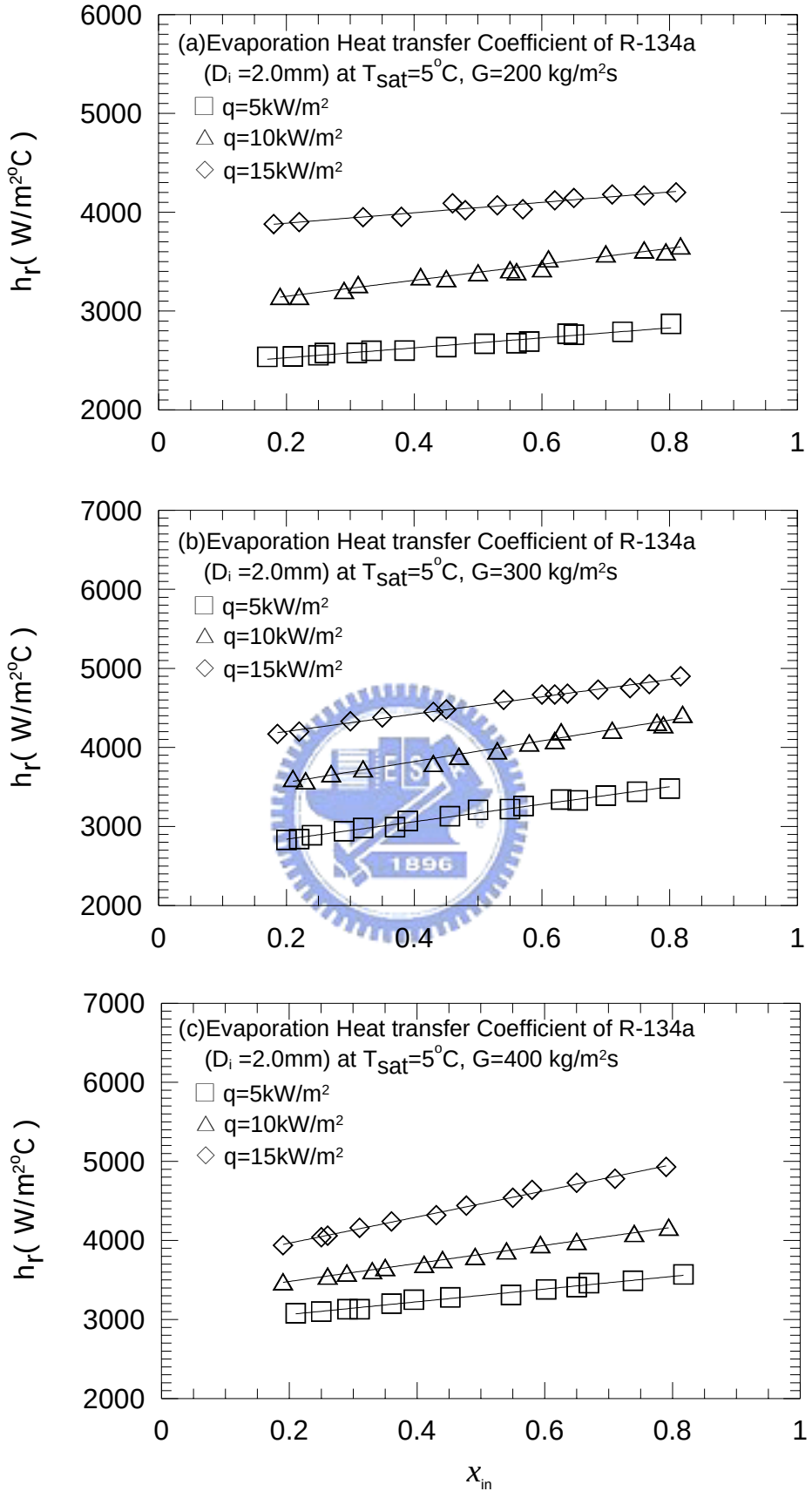

Fig. 4.9 Variations of R-134a evaporation heat transfer coefficient with inlet vapor quality in 2.0-mm small tubes at T_{sat}=5°C for various q for (a) G=200 kg/m^{2}s, (b) G=300 kg/m^{2}s, and (c) G=400 kg/m^{2}s.

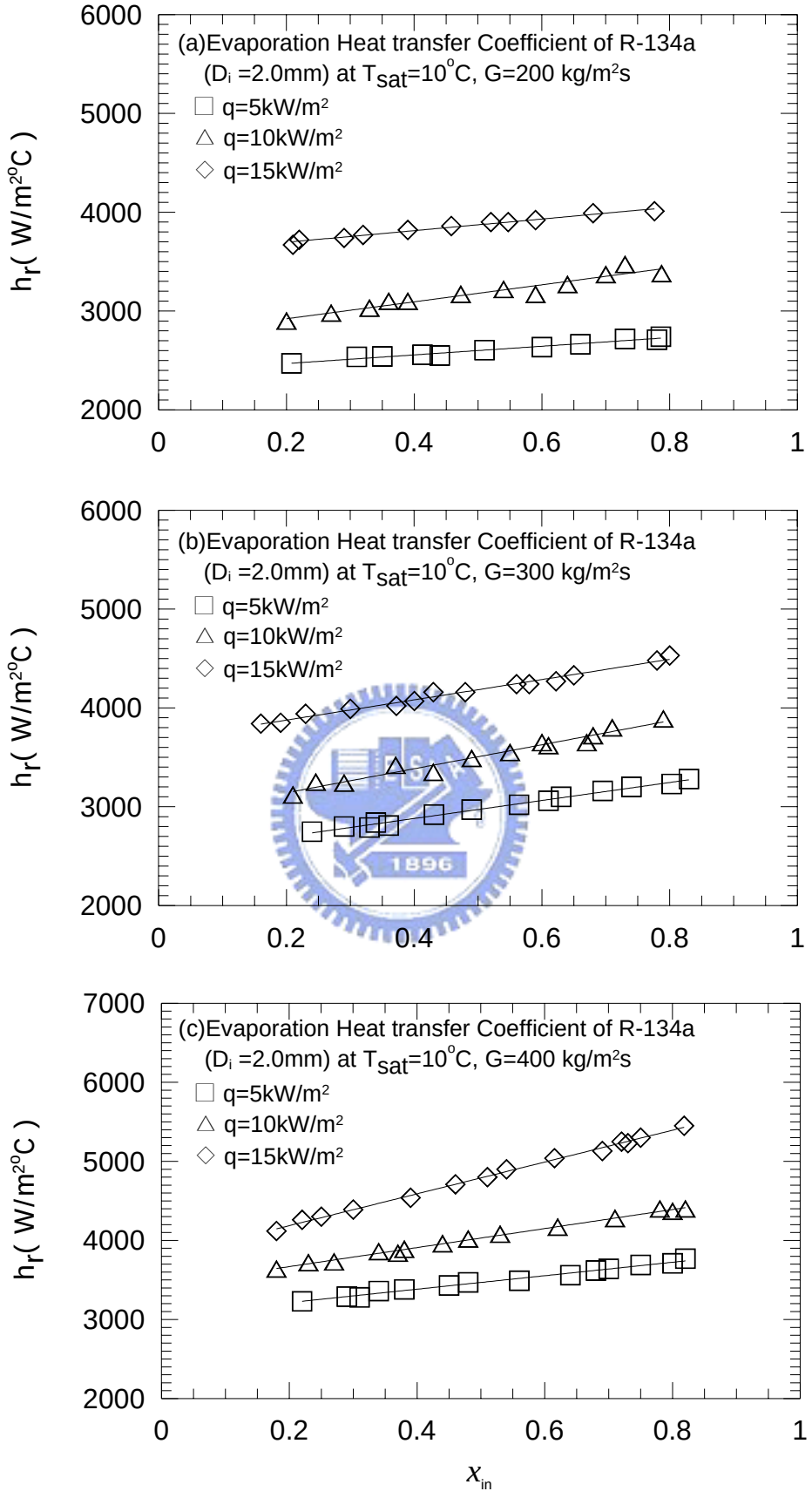

Fig. 4.10 Variations of R-134a evaporation heat transfer coefficient with inlet vapor quality in 2.0-mm small tubes at T_{sat}=10°C for various q for (a) G=200 kg/m^{2}s, (b) G=300 kg/m^{2}s, and (c) G=400 kg/m^{2}s.

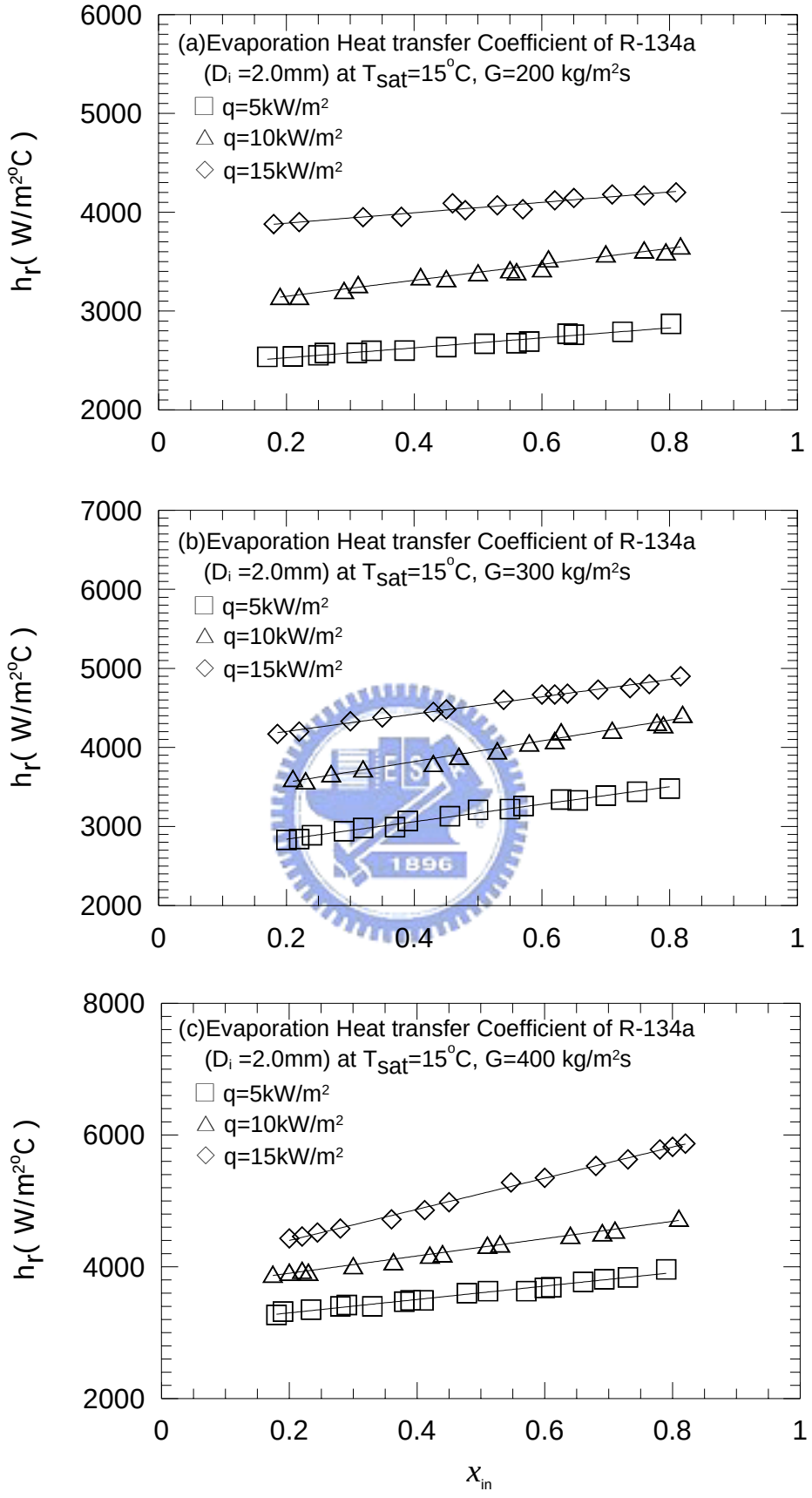

Fig. 4.11 Variations of R-134a evaporation heat transfer coefficient with inlet vapor quality in 2.0-mm small tubes at T_{sat}=15℃ for various q for (a) G=200 kg/m^{2}s, (b) G=300 kg/m^{2}s, and (c) G=400 kg/m^{2}s.

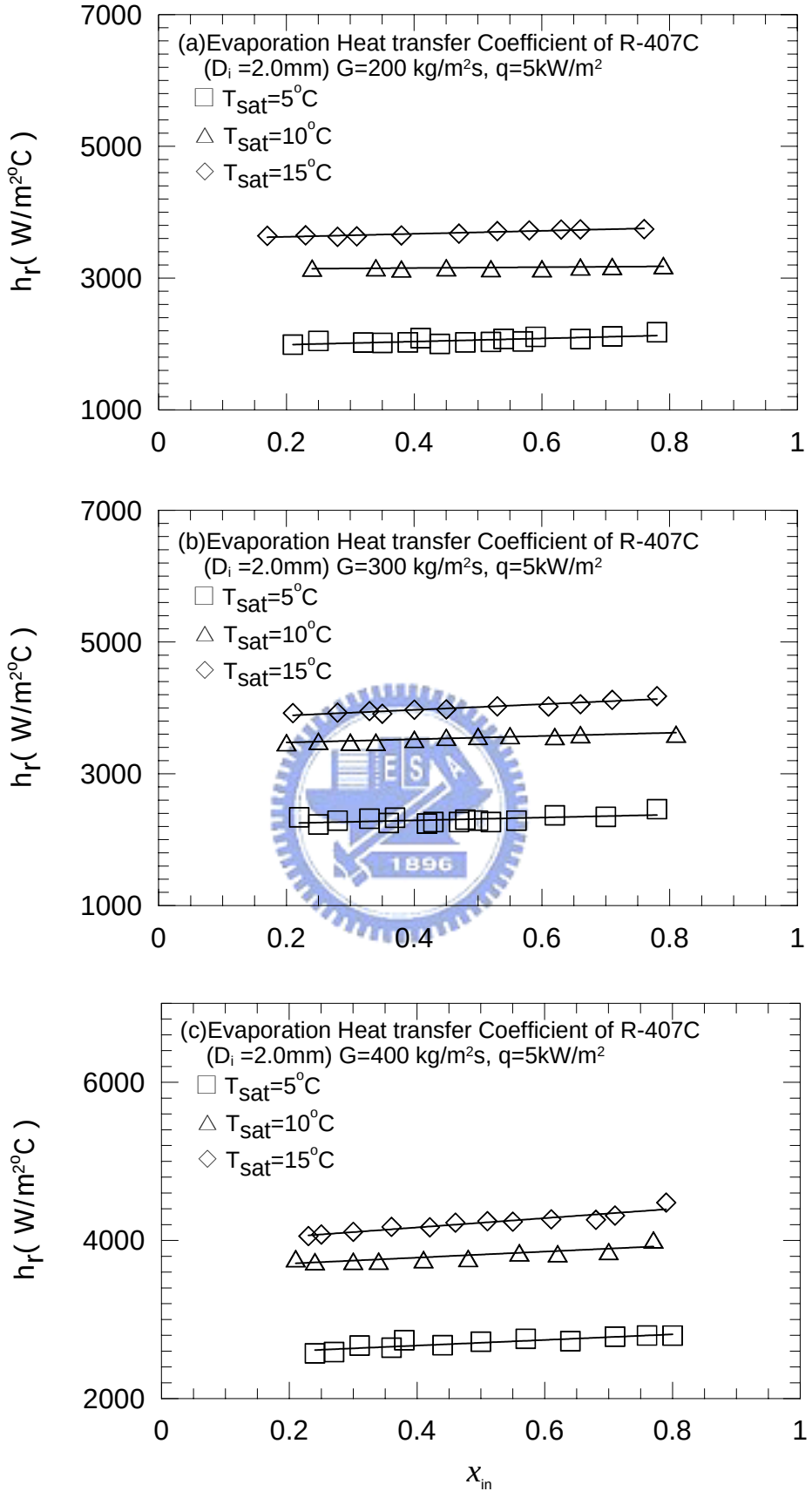

Fig. 4.12 Variations of R-407C evaporation heat transfer coefficient with inlet vapor quality in 2.0-mm small tubes at q=5 kW/m^2 for various T_{sat} for (a) G=200 kg/m^{2}s, (b) G=300 kg/m^{2}s, and (c) G=400 kg/m^{2}s.

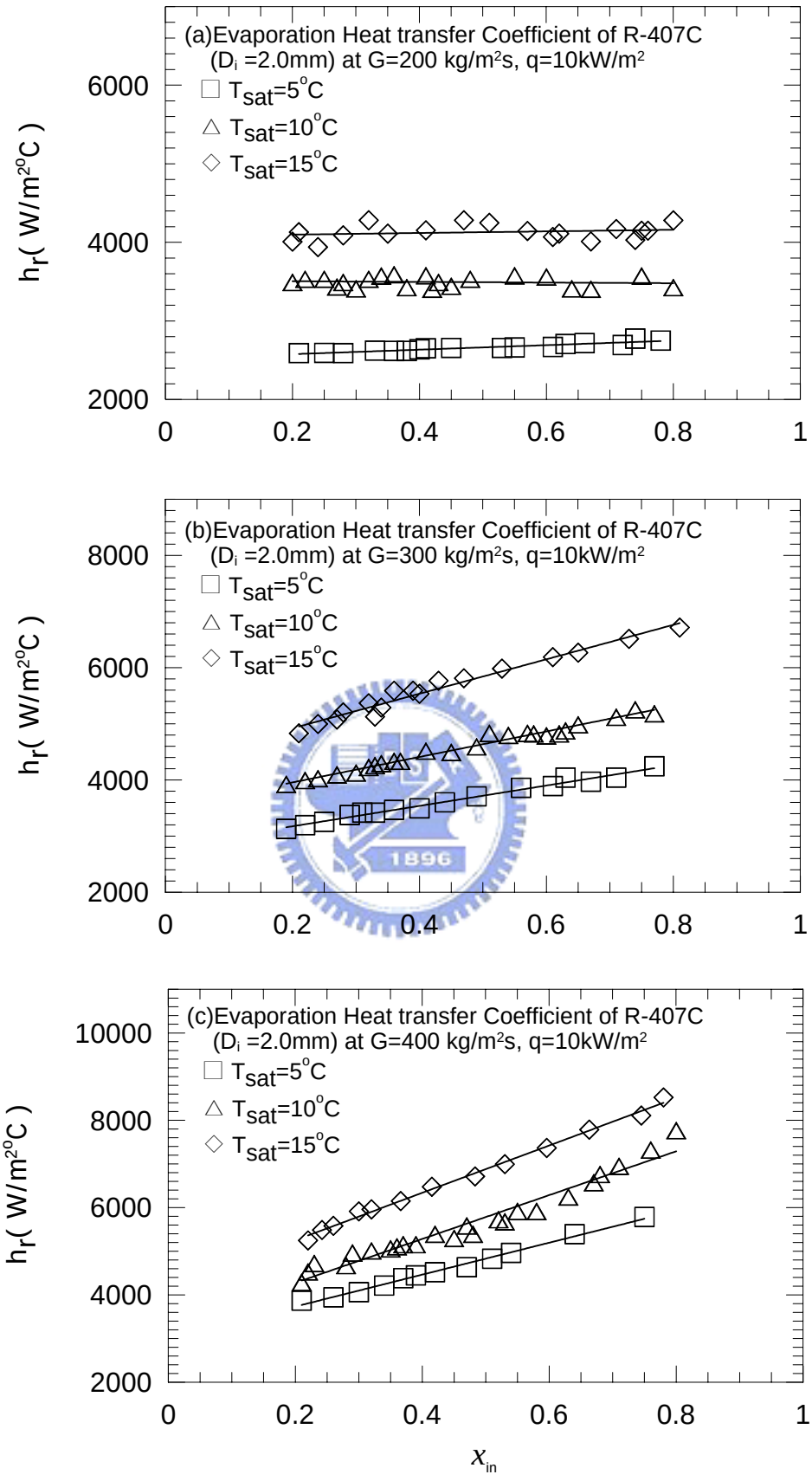

Fig. 4.13 Variations of R-407C evaporation heat transfer coefficient with inlet vapor quality in 2.0-mm small tubes at q=10 kW/m^2 for various T_{sat} for (a) G=200 kg/m^{2}s, (b) G=300 kg/m^{2}s, and (c) G=400 kg/m^{2}s.

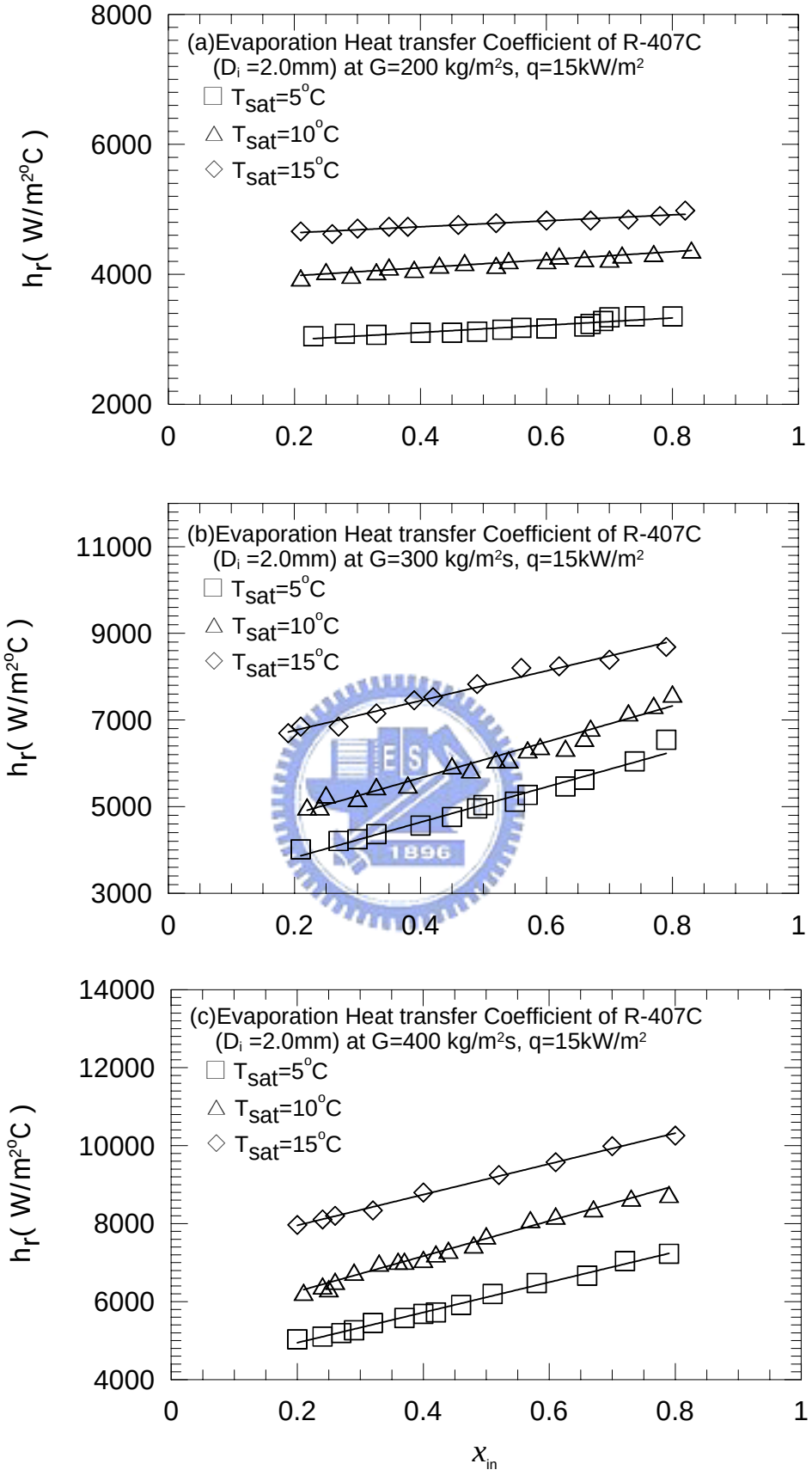

Fig. 4.14 Variations of R-407C evaporation heat transfer coefficient with inlet vapor quality in 2.0-mm small tubes at q=15 kW/m^2 for various T_{sat} for (a) G=200 kg/m^{2}s, (b) G=300 kg/m^{2}s, and (c) G=400 kg/m^{2}s.

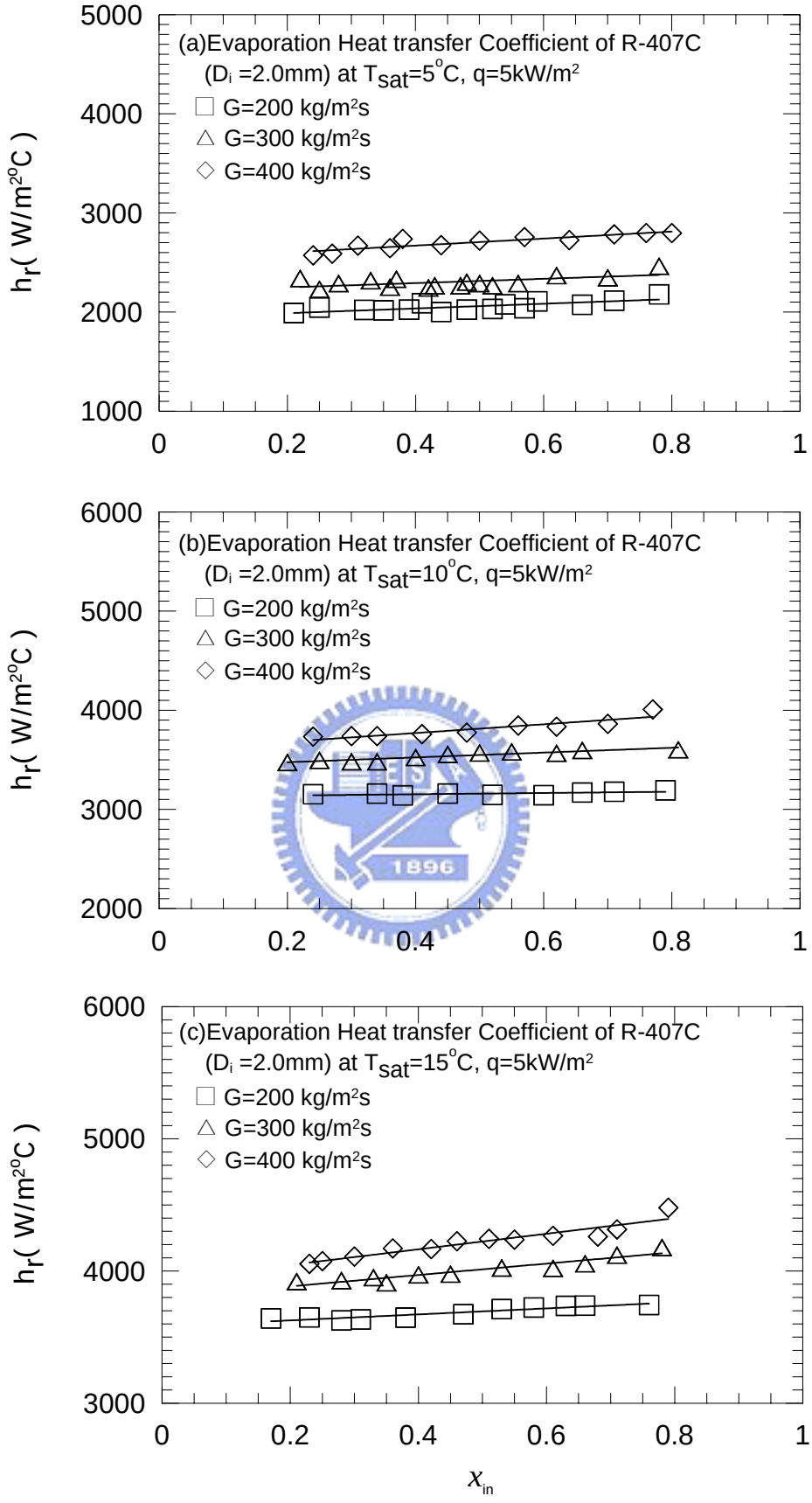

Fig. 4.15 Variations of R-407C evaporation heat transfer coefficient with inlet vapor quality in 2.0-mm small tubes at q=5 kW/m^2 for various G for (a) T_{sat}=5℃, (b) T_{sat}=10℃, and (c) T_{sat}=15℃.

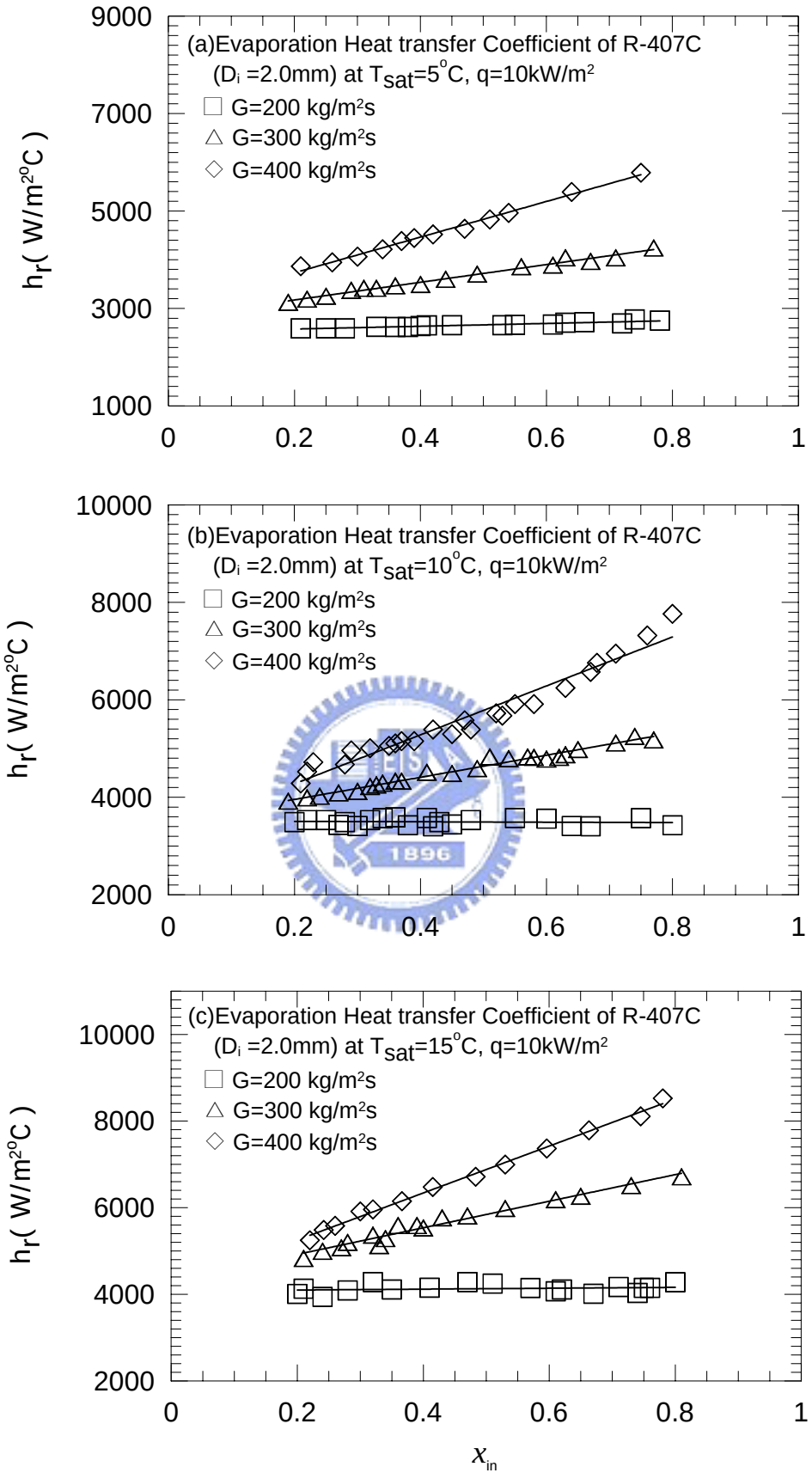

Fig. 4.16 Variations of R-407C evaporation heat transfer coefficient with inlet vapor quality in 2.0-mm small tubes at q=10 kW/m^2 for various G for (a) T_{sat}=5℃, (b) T_{sat}=10℃, and (c) T_{sat}=15℃.

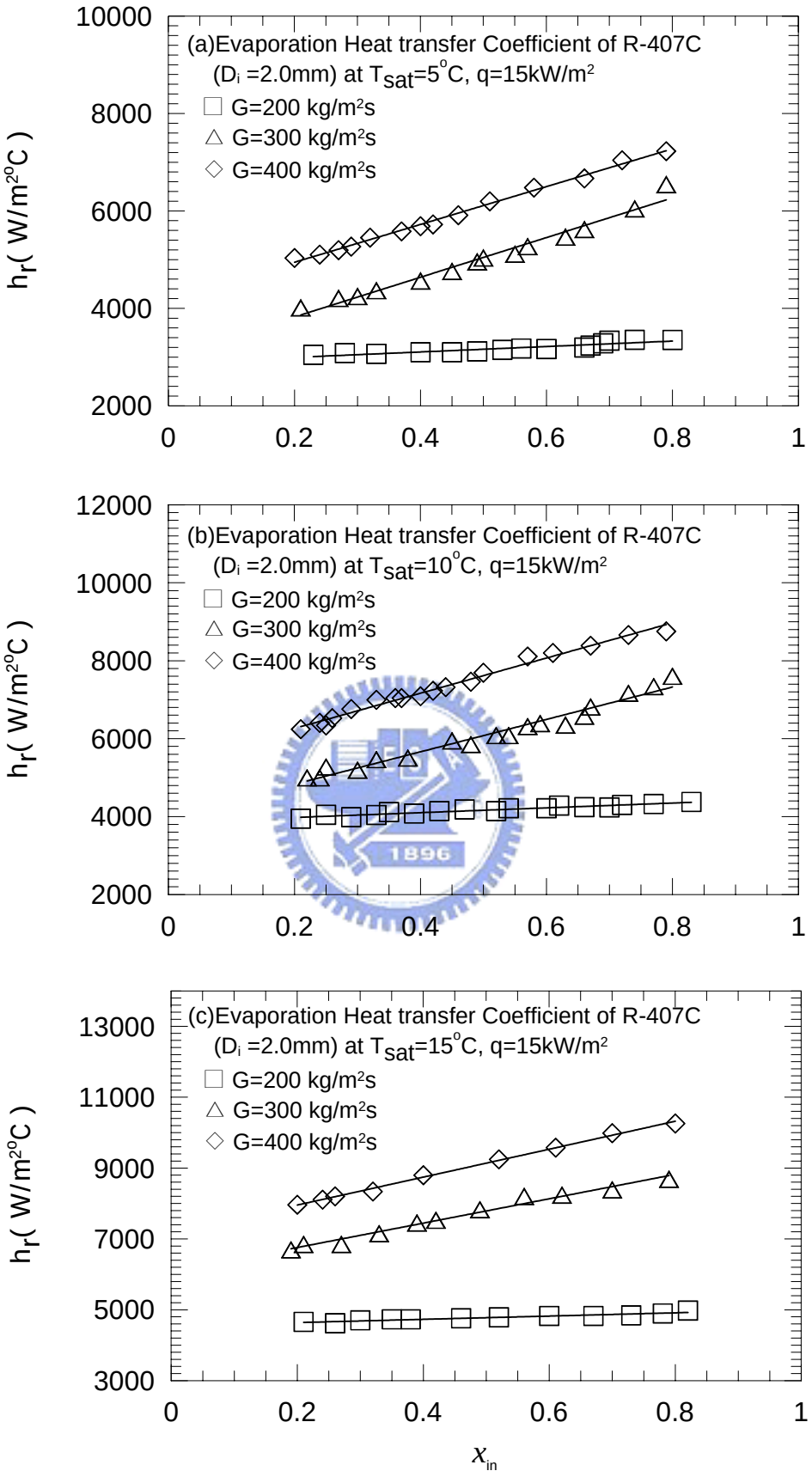

Fig. 4.17 Variations of R-407C evaporation heat transfer coefficient with inlet vapor quality in 2.0-mm small tubes at q=15 kW/m^2 for various G for (a) T_{sat}=5℃, (b) T_{sat}=10℃, and (c) T_{sat}=15℃.

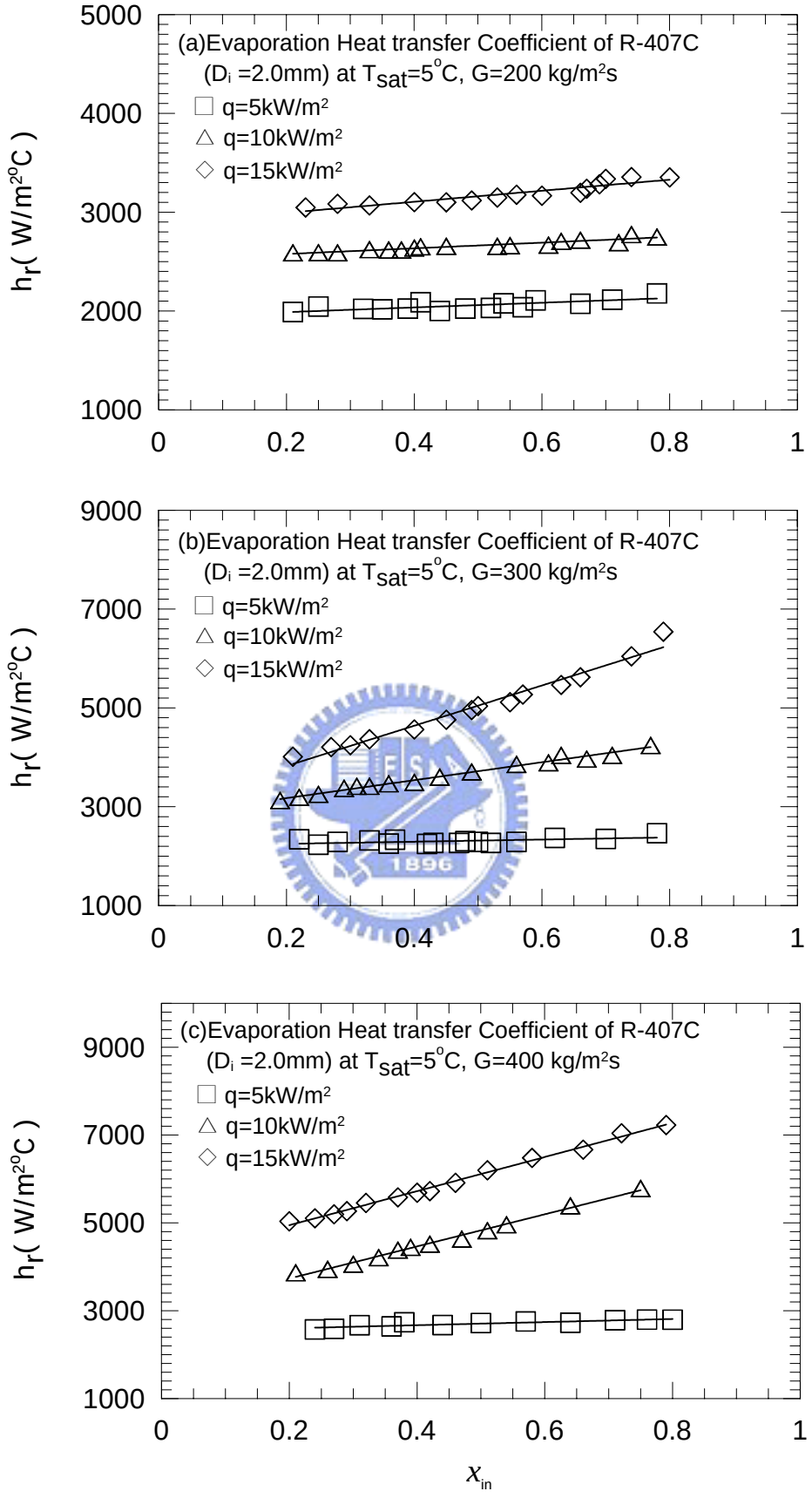

Fig. 4.18 Variations of R-407C evaporation heat transfer coefficient with inlet vapor quality in 2.0-mm small tubes at T_{sat}=5℃ for various q for (a) G=200 kg/m^{2}s, (b) G=300 kg/m^{2}s, and (c) G=400 kg/m^{2}s.

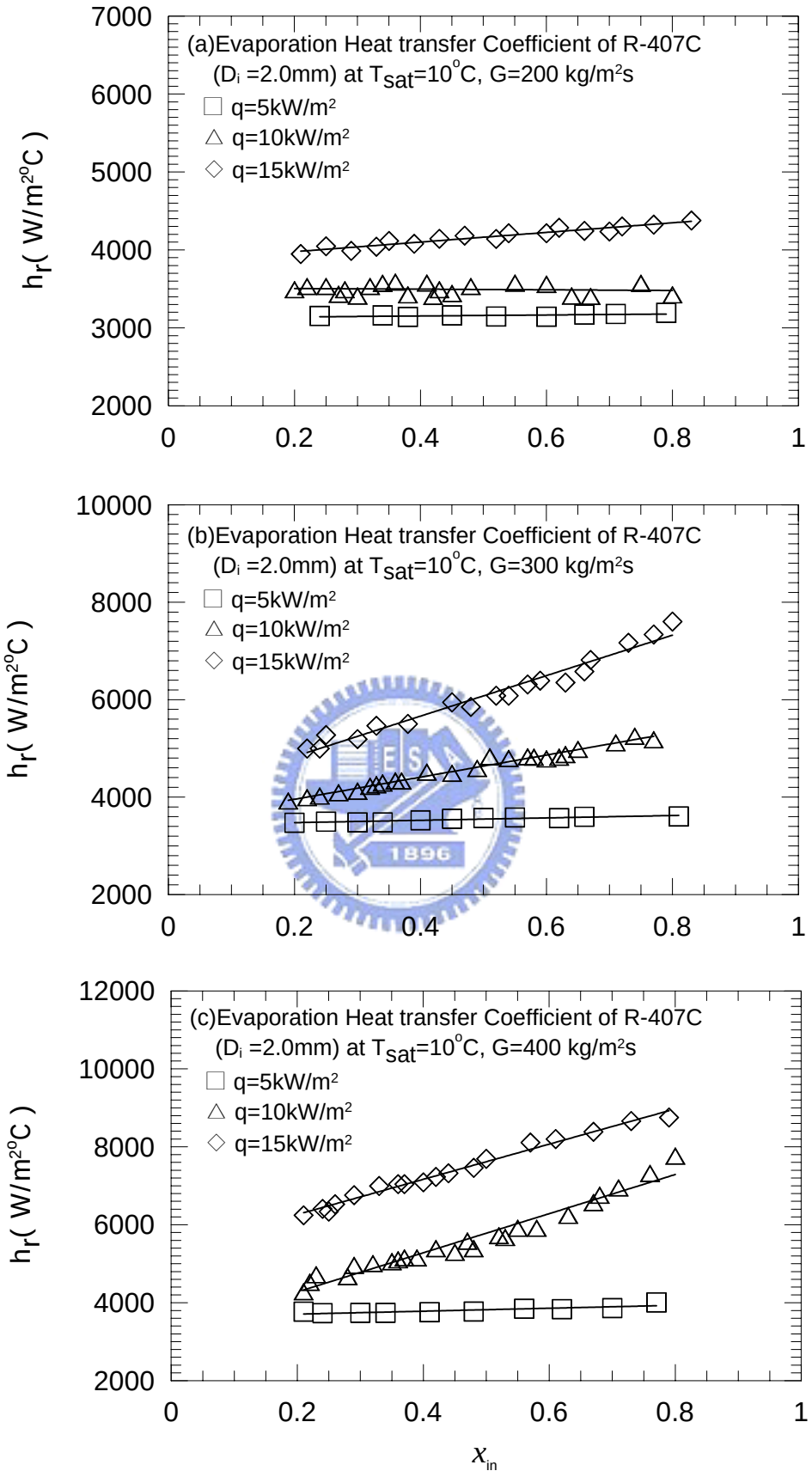

Fig. 4.19 Variations of R-407C evaporation heat transfer coefficient with inlet vapor quality in 2.0-mm small tubes at T_{sat}=10°C for various q for (a) G=200 kg/m^{2}s, (b) G=300 kg/m^{2}s, and (c) G=400 kg/m^{2}s.

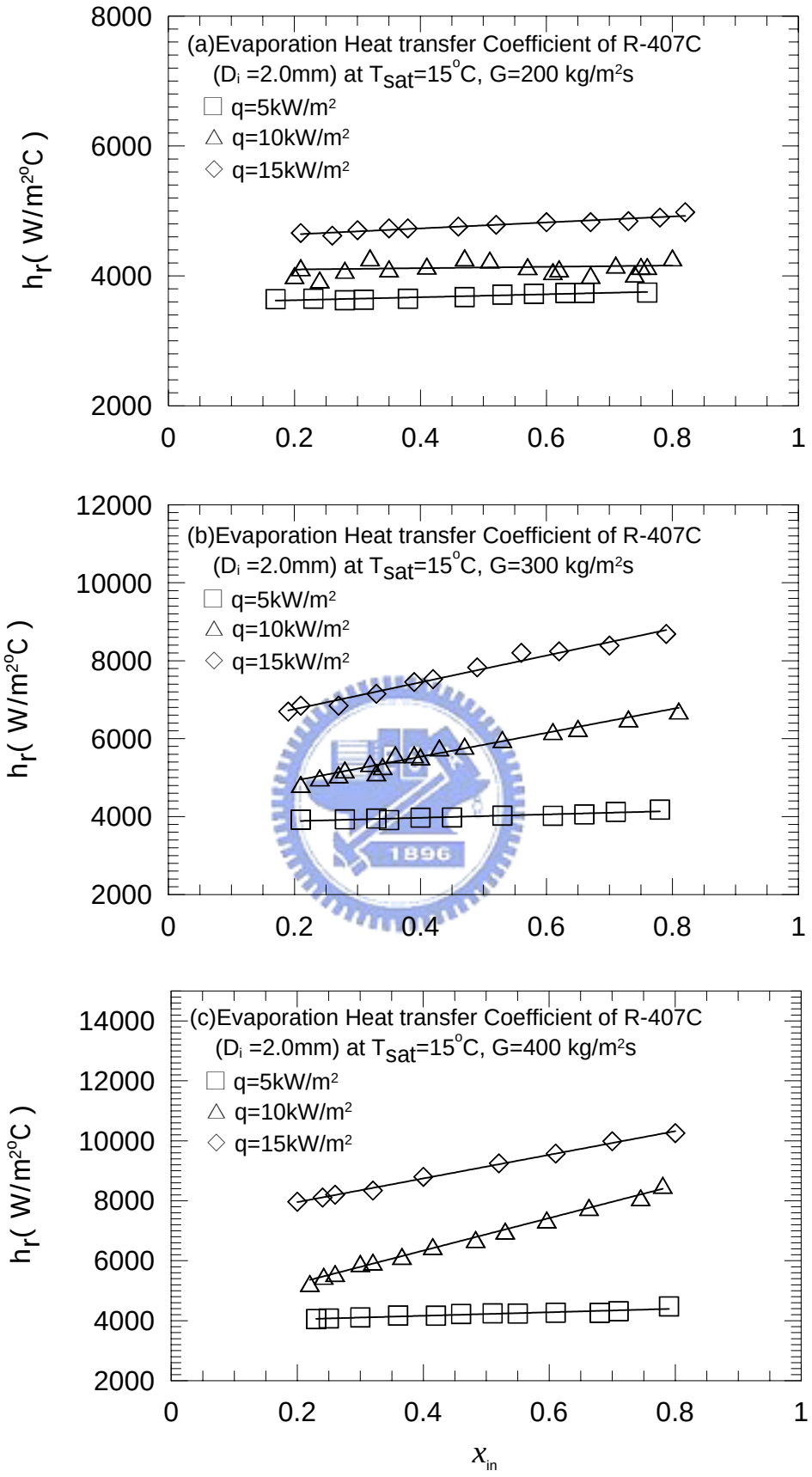

Fig. 4.20 Variations of R-407C evaporation heat transfer coefficient with inlet vapor quality in 2.0-mm small tubes at T_{sat}=15°C for various q for (a) G=200 kg/m^{2}s, (b) G=300 kg/m^{2}s, and (c) G=400 kg/m^{2}s.

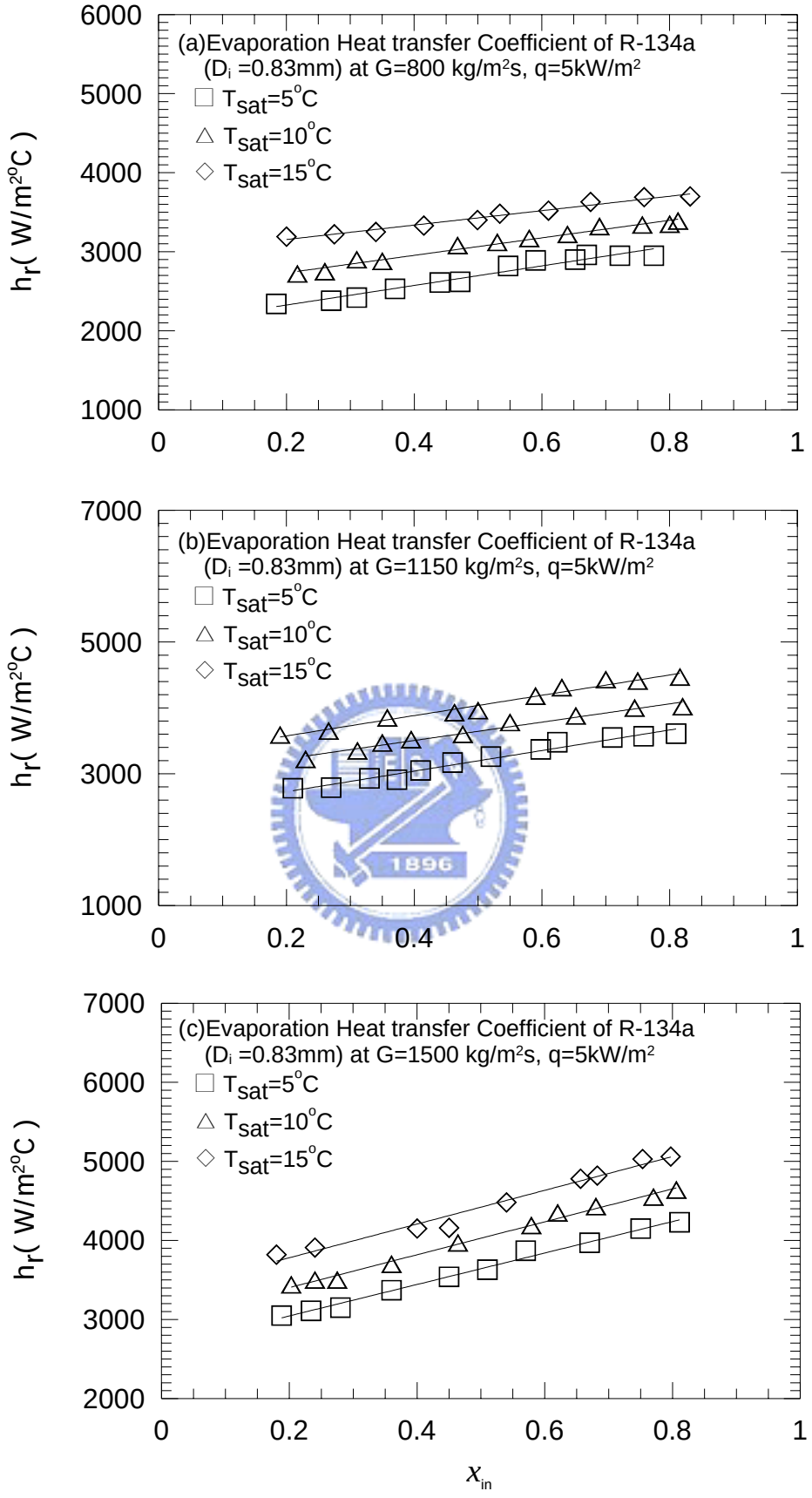

Fig. 4.21 Variations of R-134a evaporation heat transfer coefficient with inlet vapor quality in 0.83-mm small tubes at q=5 kW/m^2 for various T_{sat} for (a) G=800 kg/m^{2}s, (b) G=1150 kg/m^{2}s, and (c) G=1500 kg/m^{2}s.

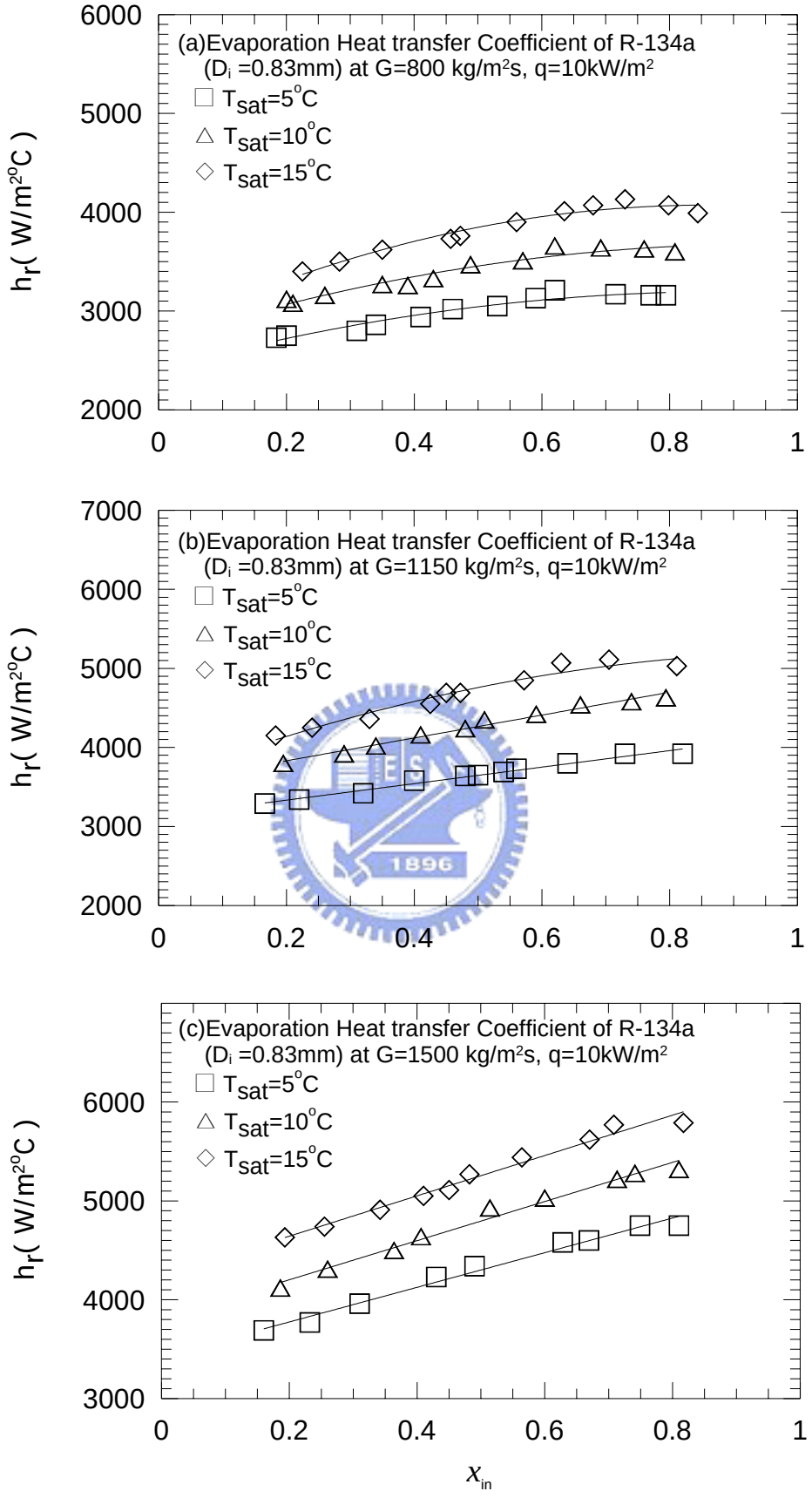

Fig. 4.22 Variations of R-134a evaporation heat transfer coefficient with inlet vapor quality in 0.83-mm small tubes at q=10 kW/m^2 for various T_{sat} for (a) G=800 kg/m^{2}s, (b) G=1150 kg/m^{2}s, and (c) G=1500 kg/m^{2}s.

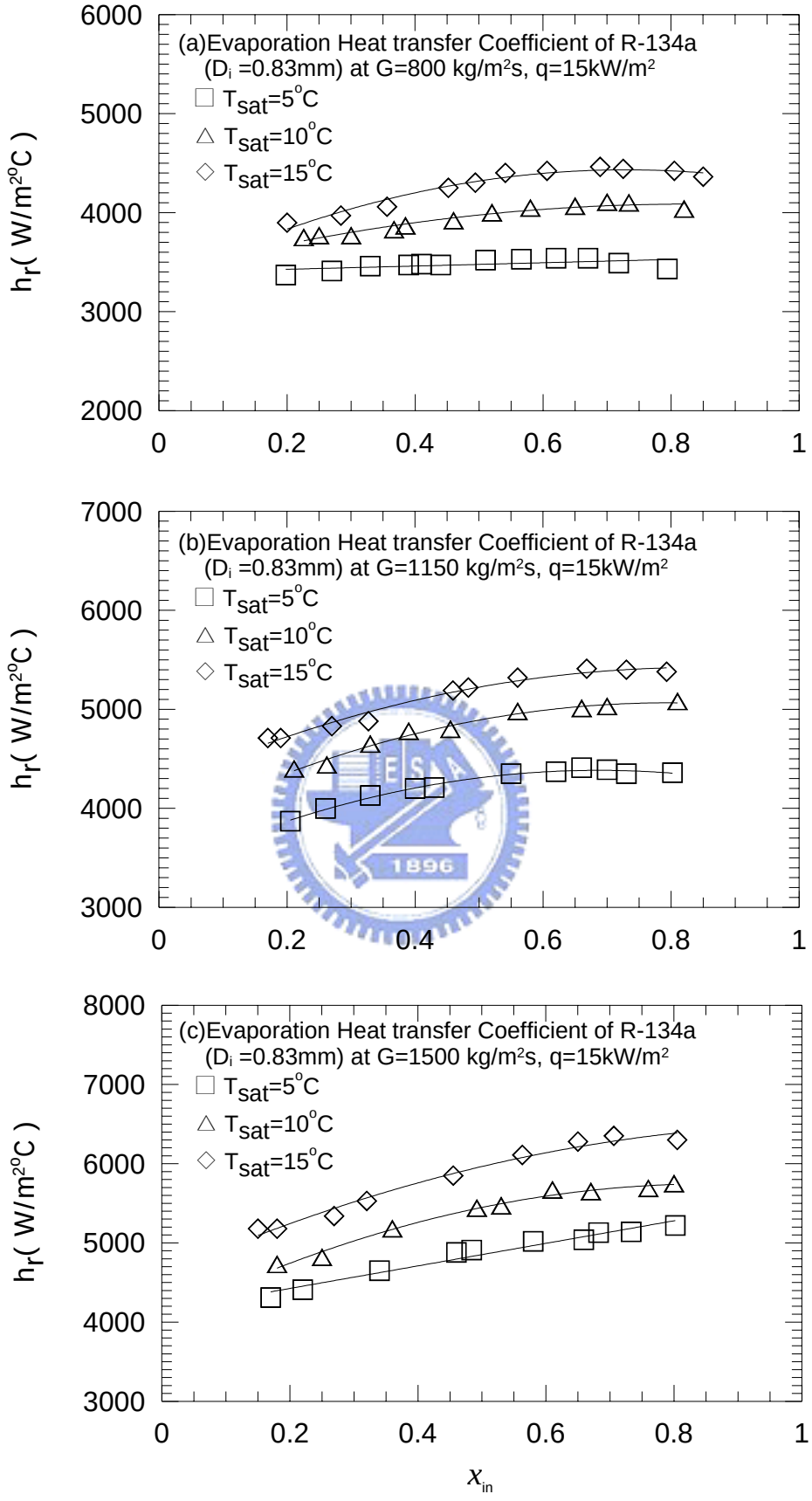

Fig. 4.23 Variations of R-134a evaporation heat transfer coefficient with inlet vapor quality in 0.83-mm small tubes at q=15 kW/m^2 for various T_{sat} for (a) G=800 kg/m^{2}s, (b) G=1150 kg/m^{2}s, and (c) G=1500 kg/m^{2}s.

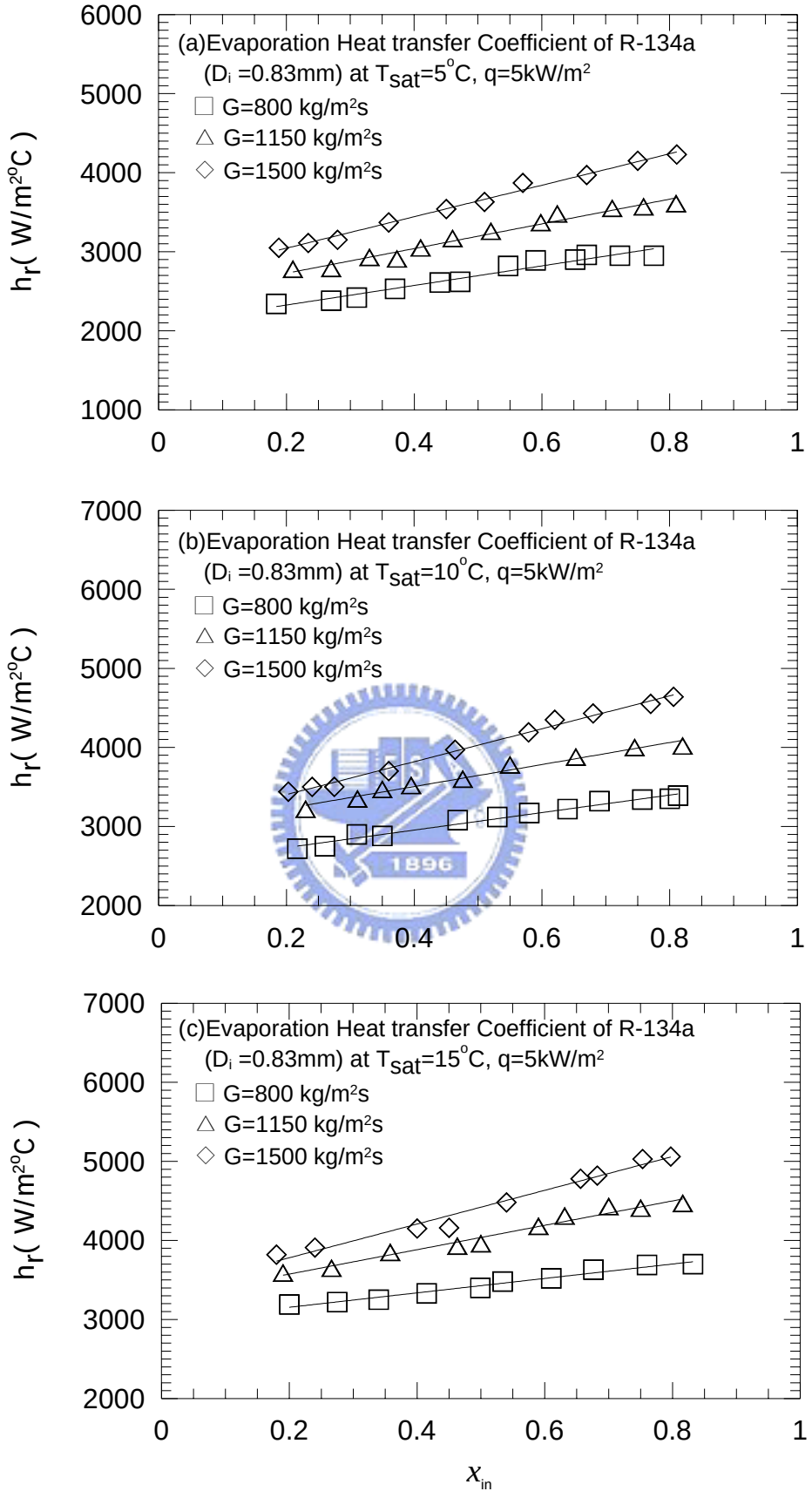

Fig. 4.24 Variations of R-134a evaporation heat transfer coefficient with inlet vapor quality in 0.83-mm small tubes at q=5 kW/m^2 for various G for (a) T_{sat}=5℃, (b) T_{sat}=10℃, and (c) T_{sat}=15℃.

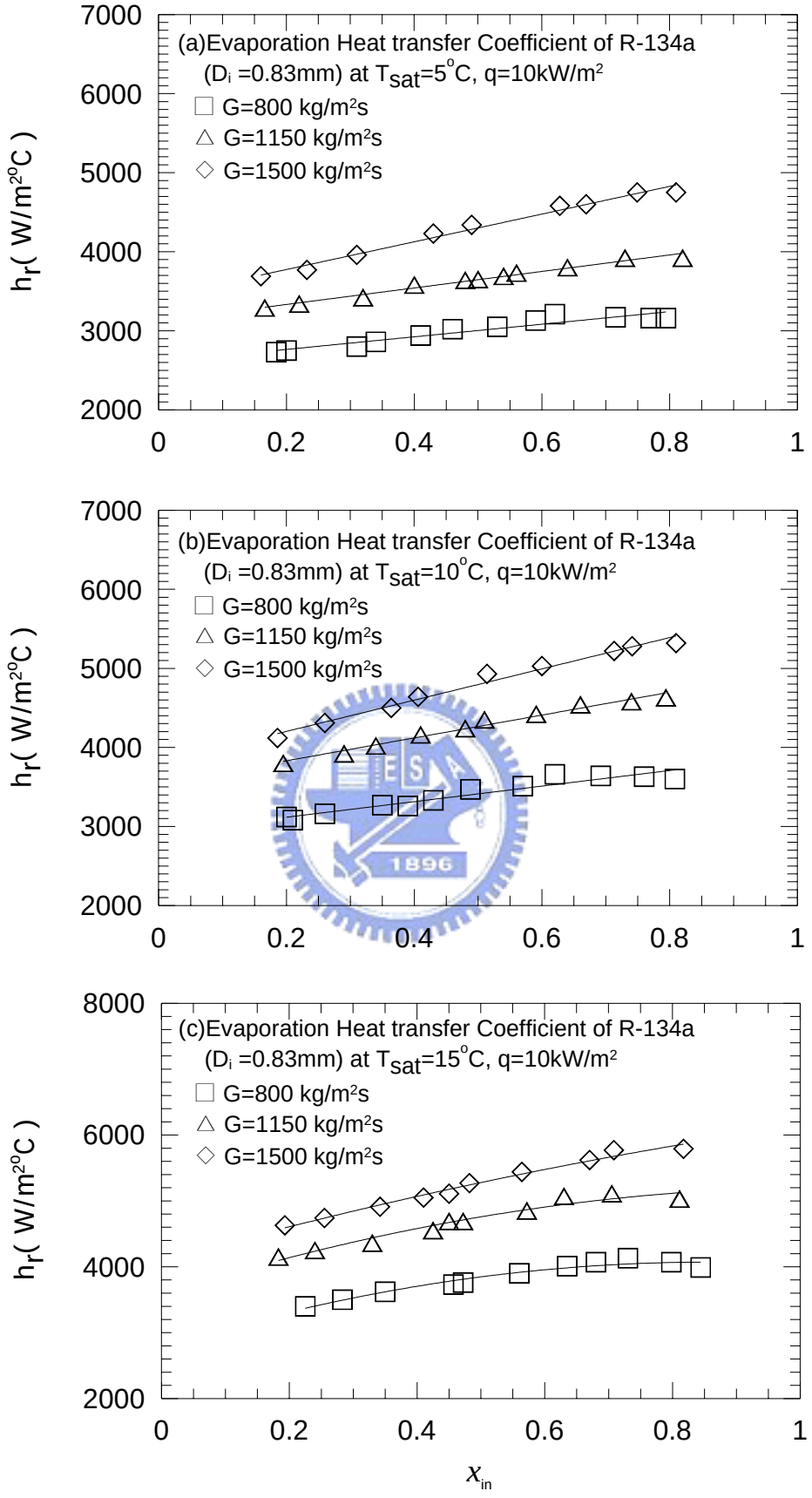

Fig. 4.25 Variations of R-134a evaporation heat transfer coefficient with inlet vapor quality in 0.83-mm small tubes at q=10 kW/m^2 for various G for (a) T_{sat}=5℃, (b) T_{sat}=10℃, and (c) T_{sat}=15℃.

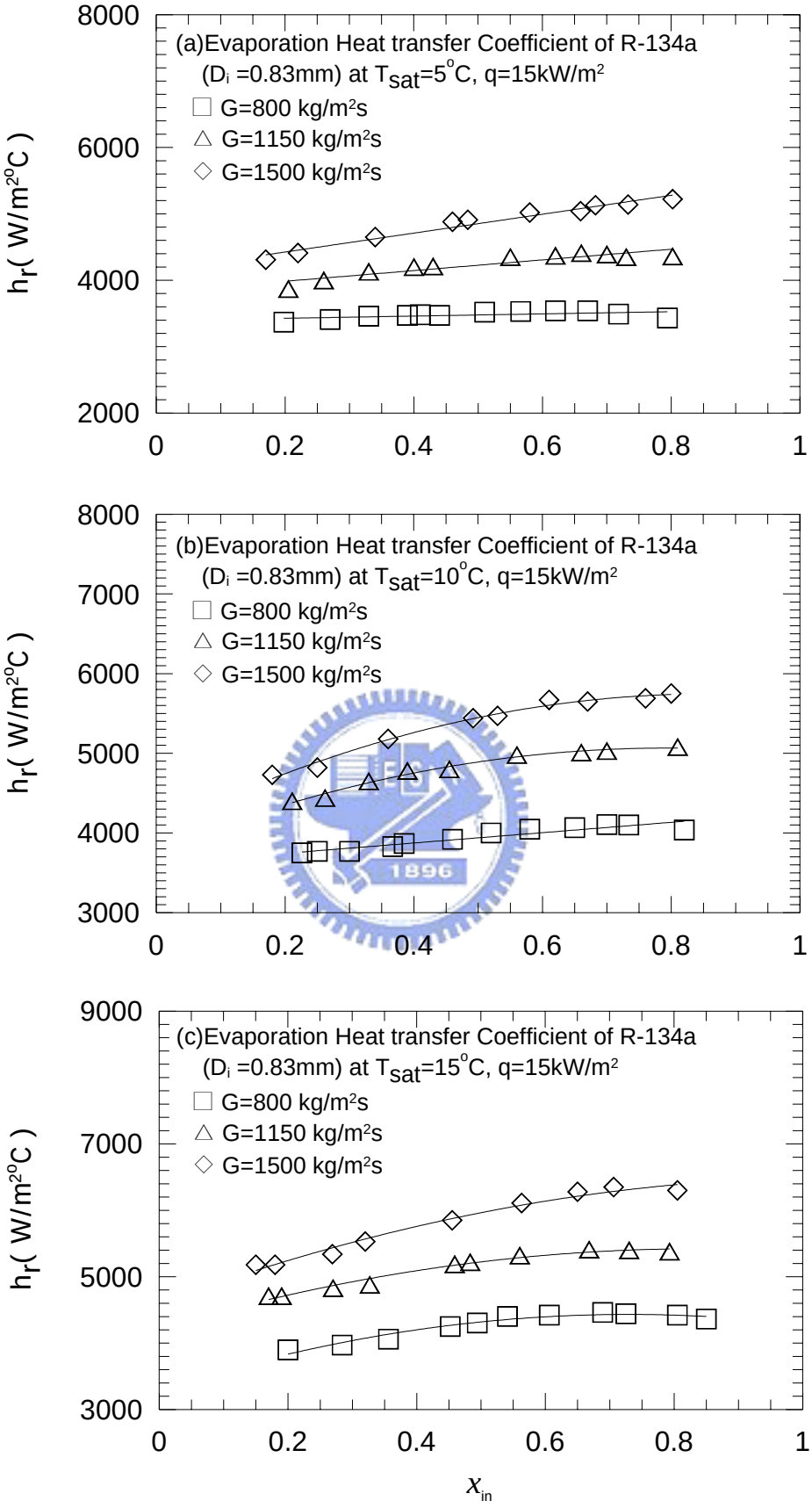

Fig. 4.26 Variations of R-134a evaporation heat transfer coefficient with inlet vapor quality in 0.83-mm small tubes at q=15 kW/m^2 for various G for (a) T_{sat}=5℃, (b) T_{sat}=10℃, and (c) T_{sat}=15℃.

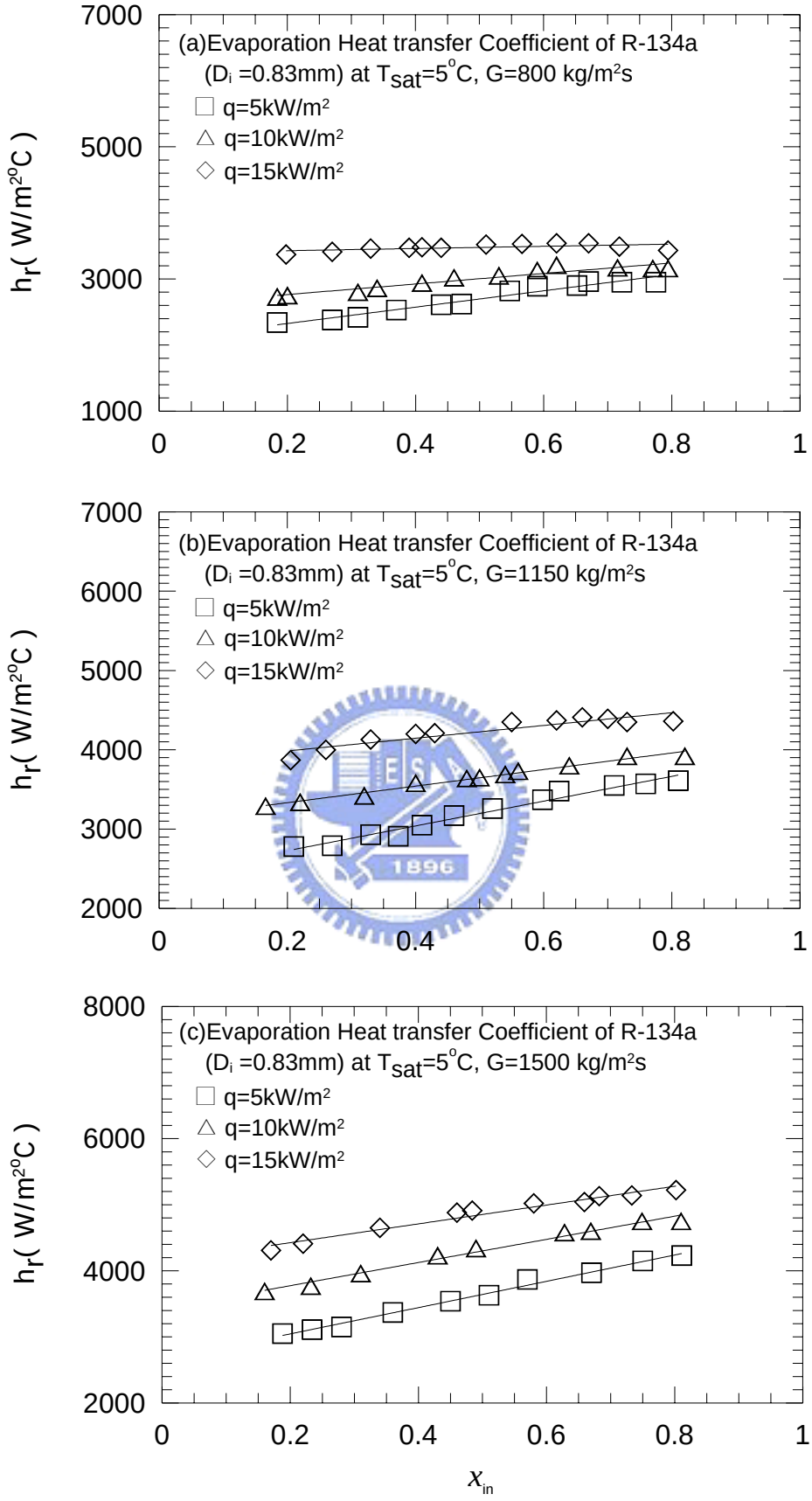

Fig. 4.27 Variations of R-134a evaporation heat transfer coefficient with inlet vapor quality in 0.83-mm small tubes at T_{sat}=5°C for various q for (a) G=800 kg/m^{2}s, (b) G=1150 kg/m^{2}s, and (c) G=1500 kg/m^{2}s.

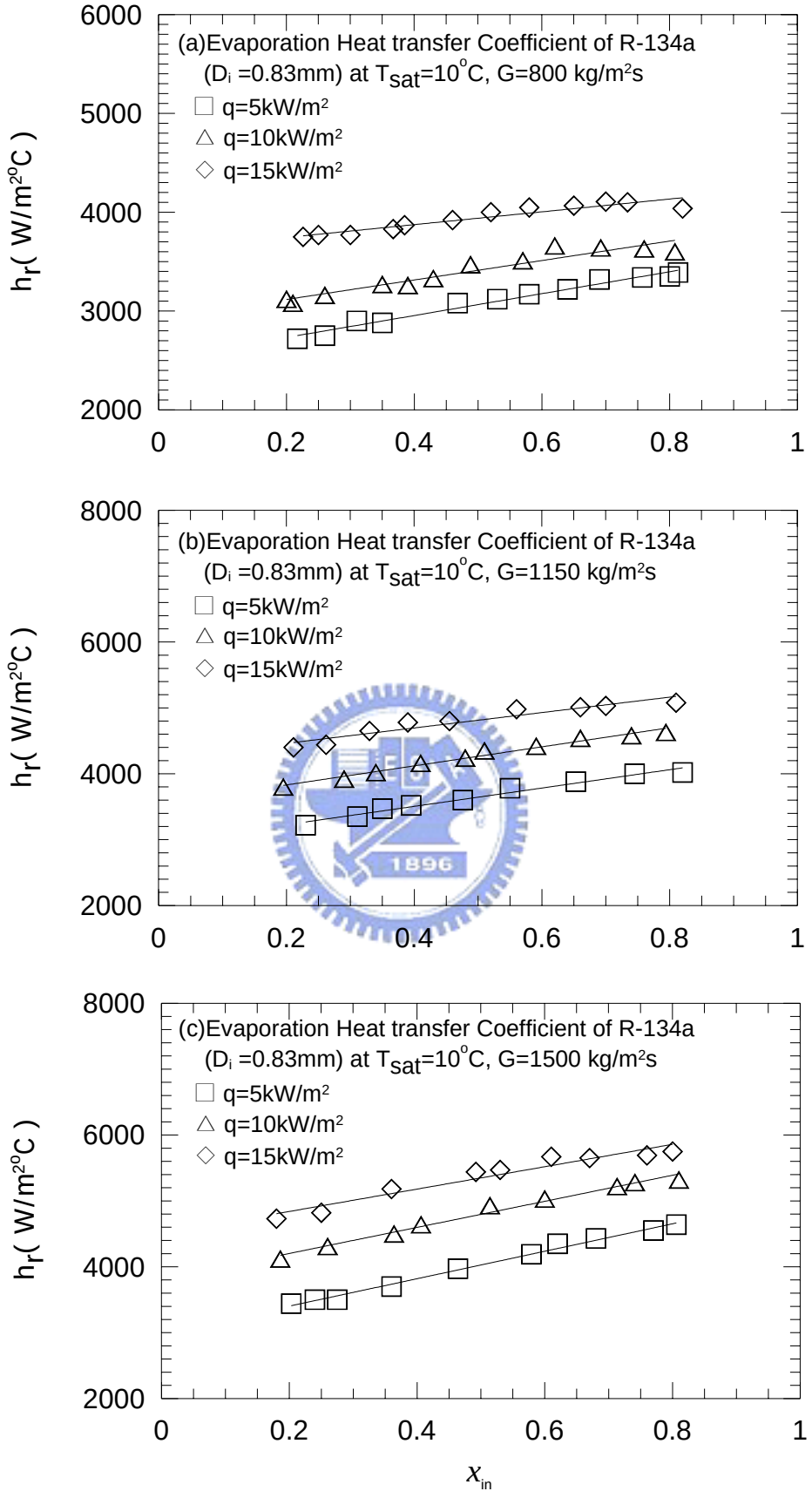

Fig. 4.28 Variations of R-134a evaporation heat transfer coefficient with inlet vapor quality in 0.83-mm small tubes at T_{sat}=10°C for various q for (a) G=800 kg/m^{2}s, (b) G=1150 kg/m^{2}s, and (c) G=1500 kg/m^{2}s.

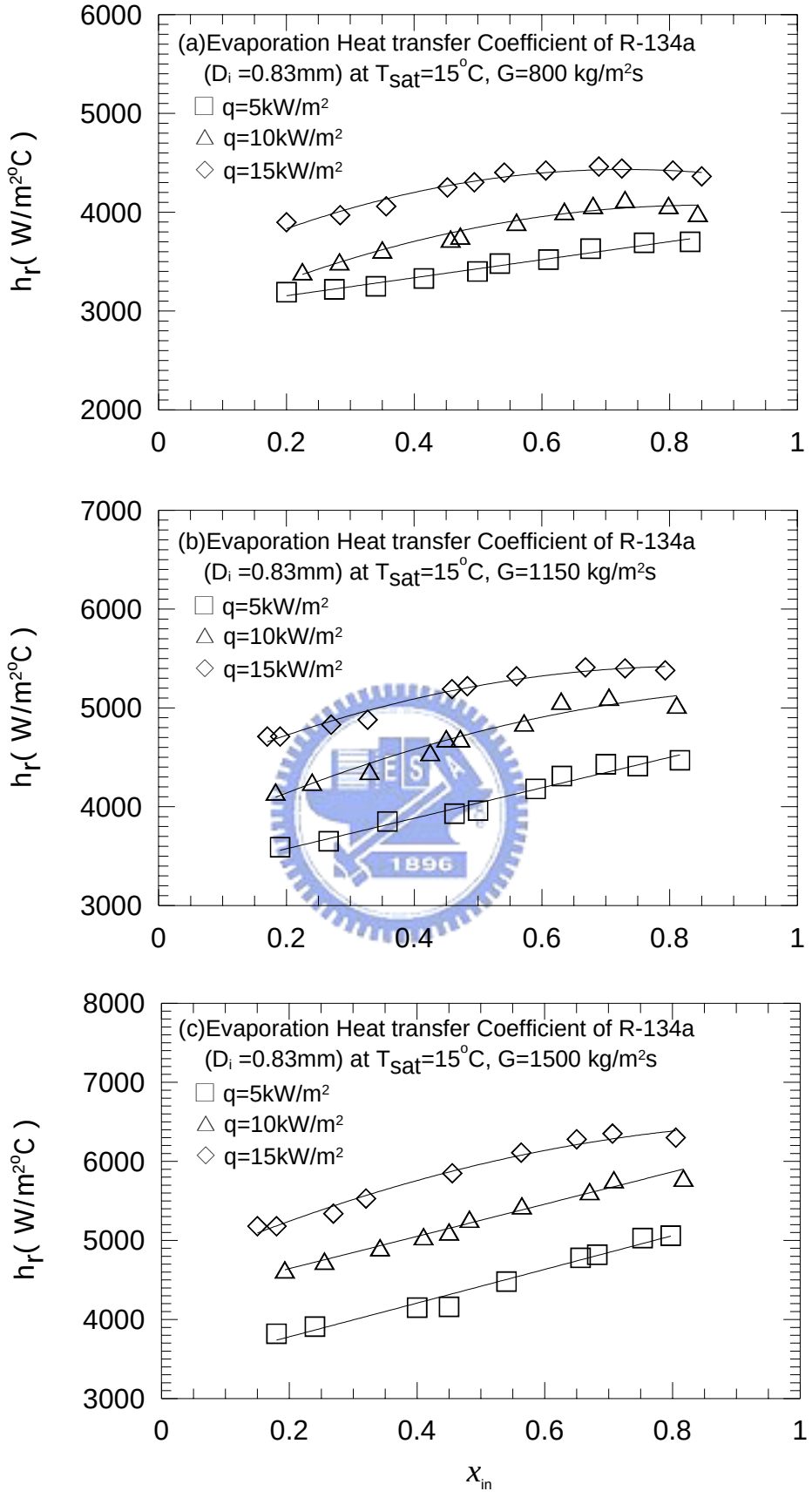

Fig. 4.29 Variations of R-134a evaporation heat transfer coefficient with inlet vapor quality in 0.83-mm small tubes at T_{sat}=15°C for various q for (a) G=800 kg/m^{2}s, (b) G=1150 kg/m^{2}s, and (c) G=1500 kg/m^{2}s.

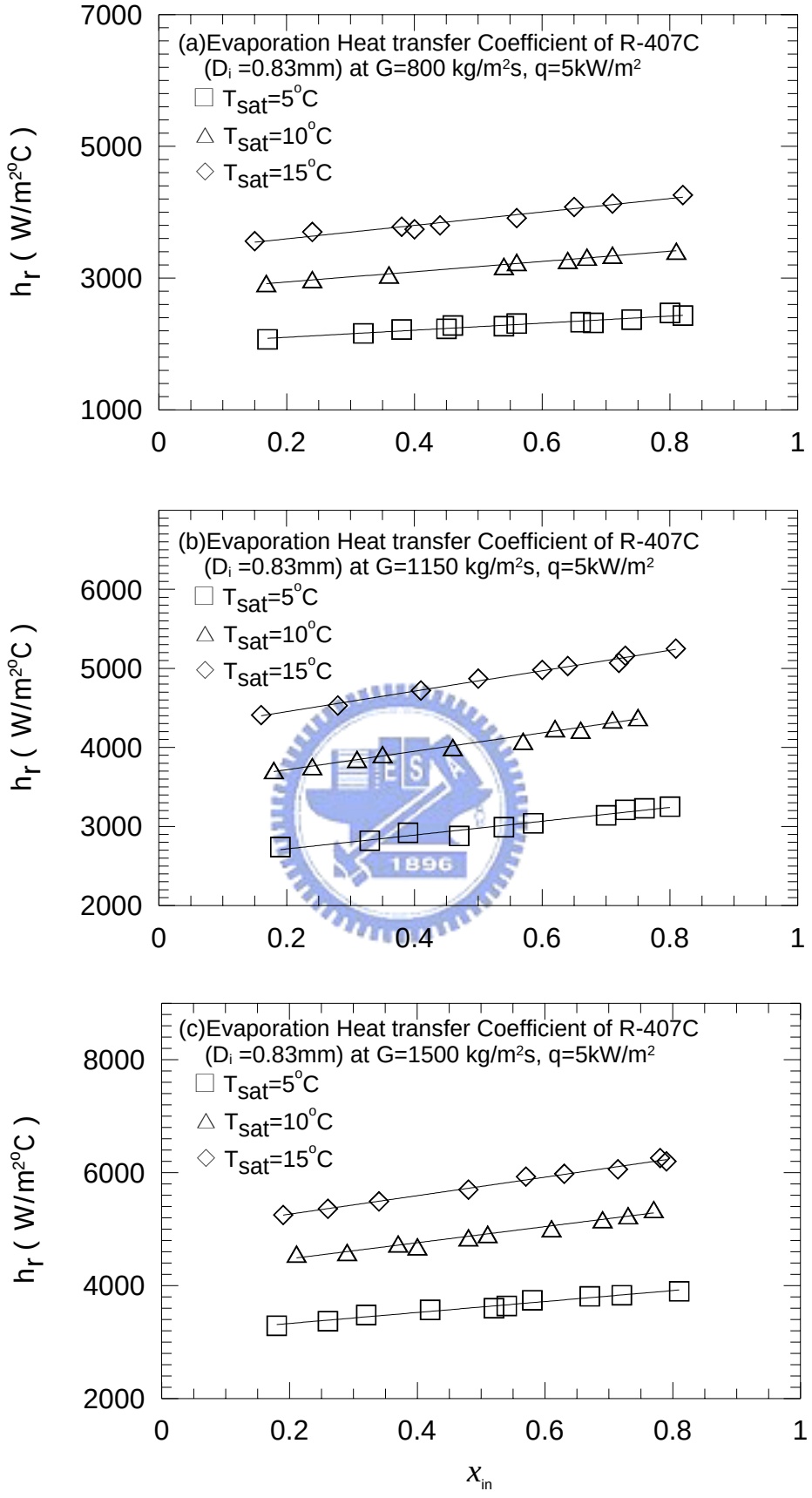

Fig. 4.30 Variations of R-407C evaporation heat transfer coefficient with inlet vapor quality in 0.83-mm small tubes at q=5 kW/m^2 for various T_{sat} for (a) G=800 kg/m^{2}s, (b) G=1150 kg/m^{2}s, and (c) G=1500 kg/m^{2}s.

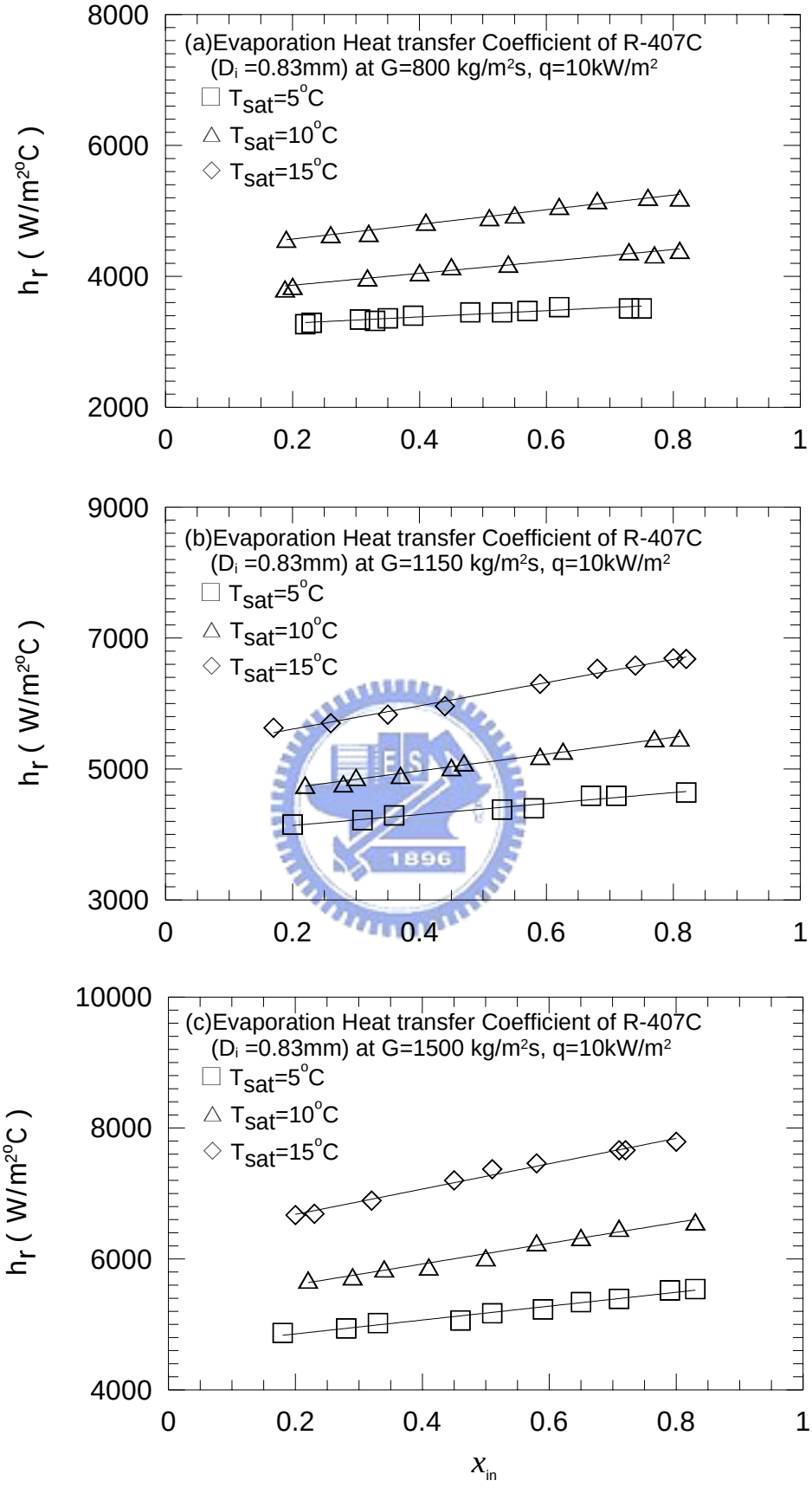

Fig. 4.31 Variations of R-407C evaporation heat transfer coefficient with inlet vapor quality in 0.83-mm small tubes at q=10 kW/m^2 for various T_{sat} for (a) G=800 kg/m^{2}s, (b) G=1150 kg/m^{2}s, and (c) G=1500 kg/m^{2}s.

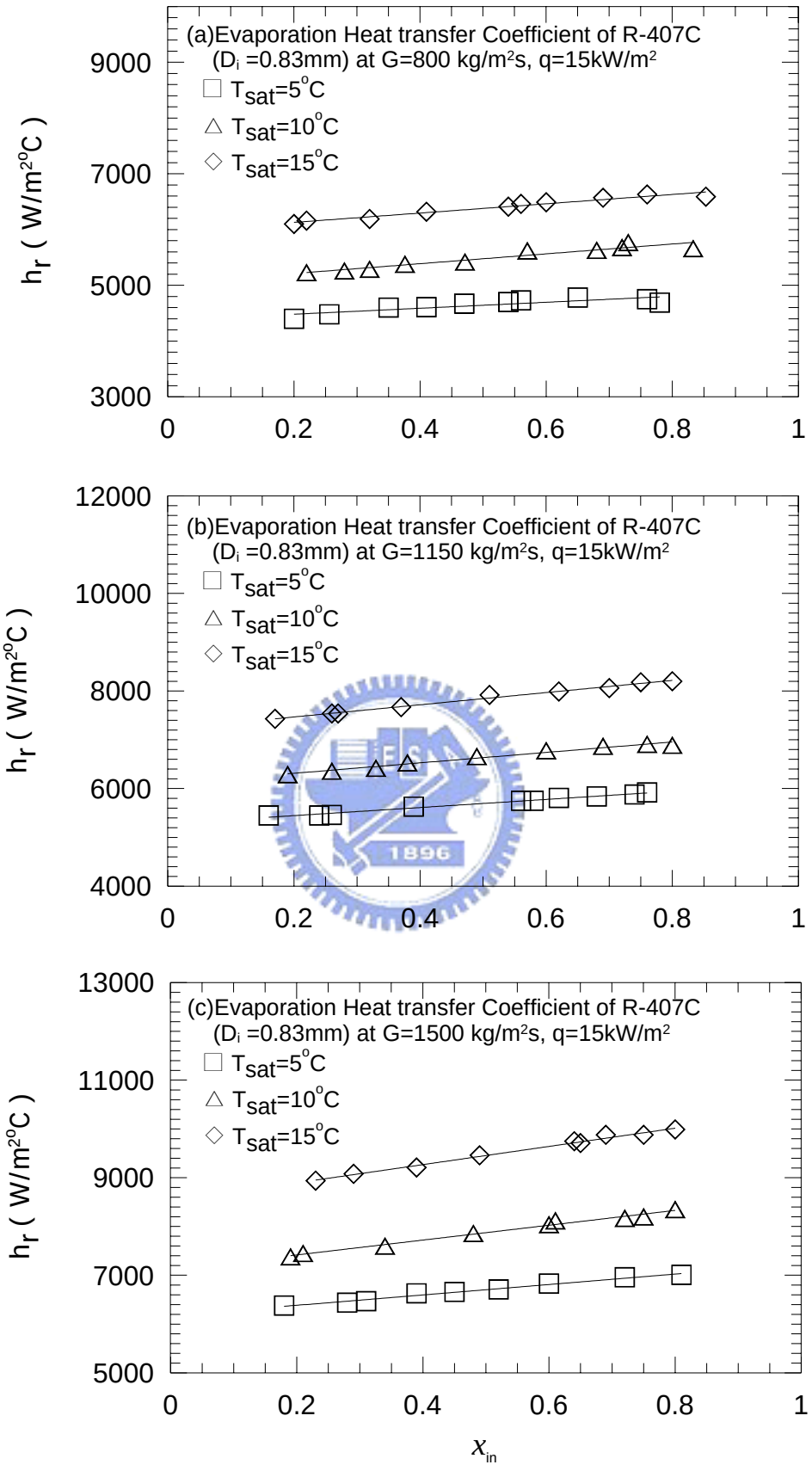

Fig. 4.32 Variations of R-407C evaporation heat transfer coefficient with inlet vapor quality in 0.83-mm small tubes at q=15 kW/m^2 for various T_{sat} for (a) G=800 kg/m^{2}s, (b) G=1150 kg/m^{2}s, and (c) G=1500 kg/m^{2}s.

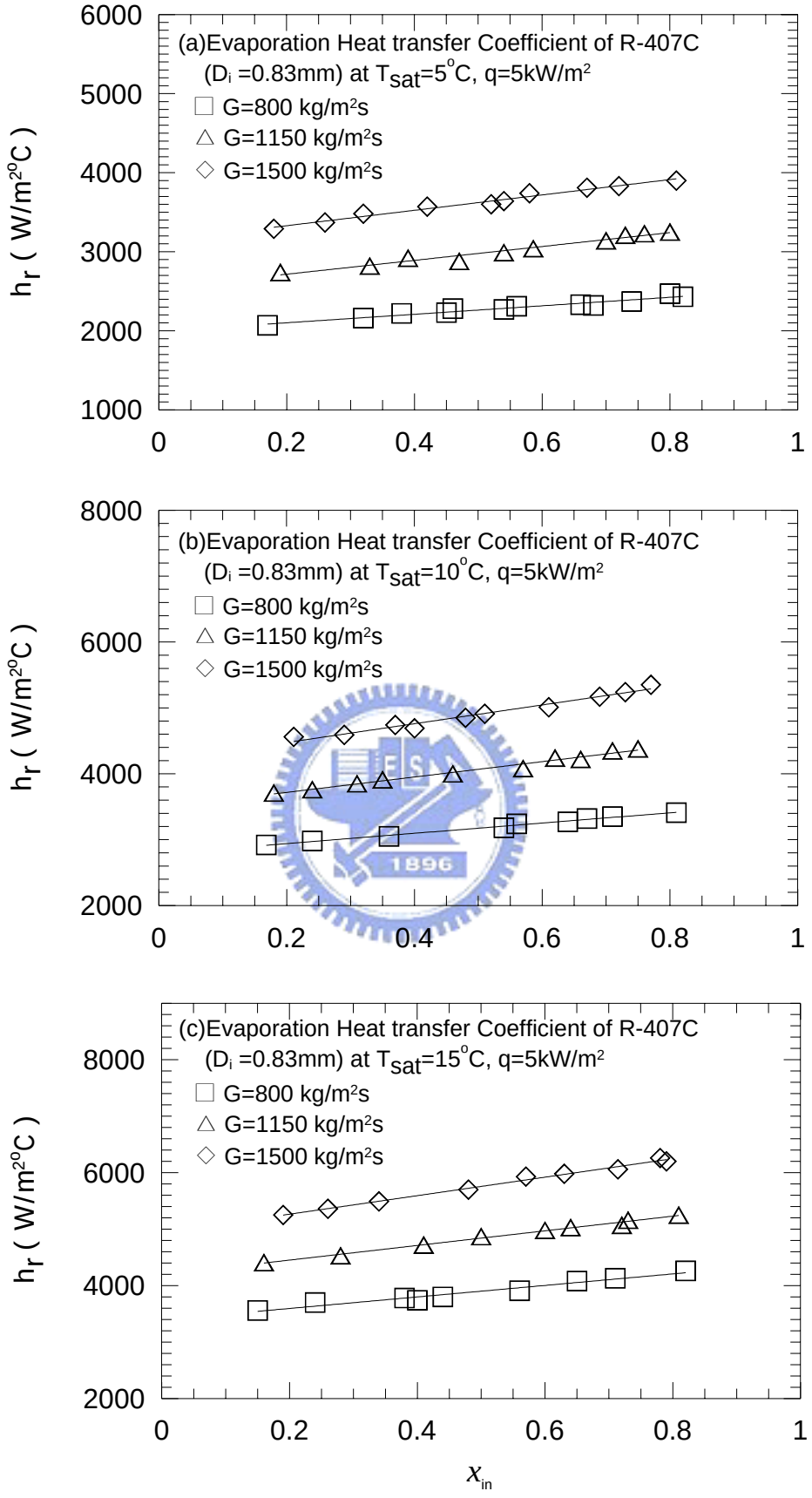

Fig. 4.33 Variations of R-407C evaporation heat transfer coefficient with inlet vapor quality in 0.83-mm small tubes at q=5 kW/m^2 for various G for (a) T_{sat}=5℃, (b) T_{sat}=10℃, and (c) T_{sat}=15℃.

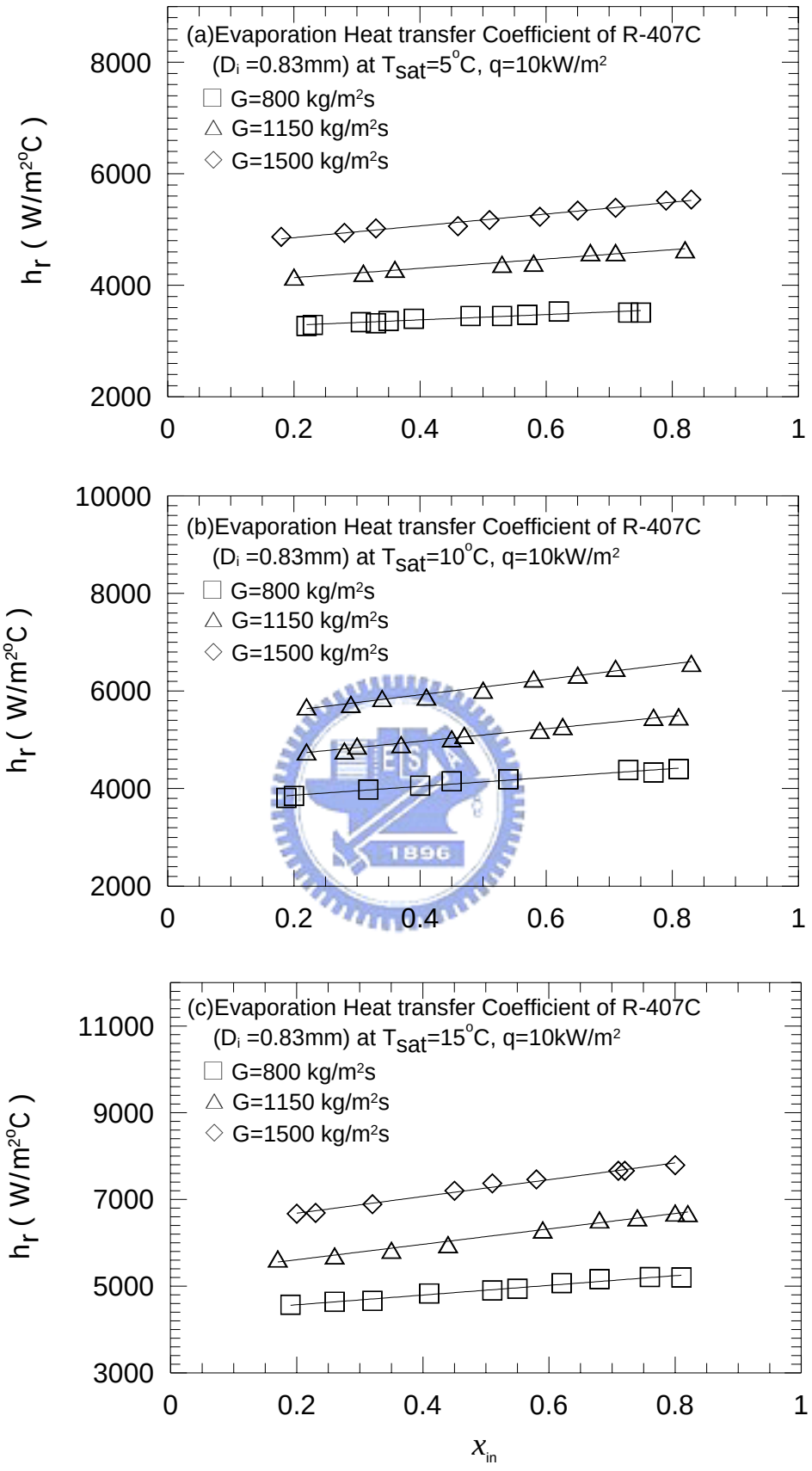

Fig. 4.34 Variations of R-407C evaporation heat transfer coefficient with inlet vapor quality in 0.83-mm small tubes at q=10 kW/m^2 for various G for (a) T_{sat}=5℃, (b) T_{sat}=10℃, and (c) T_{sat}=15℃.

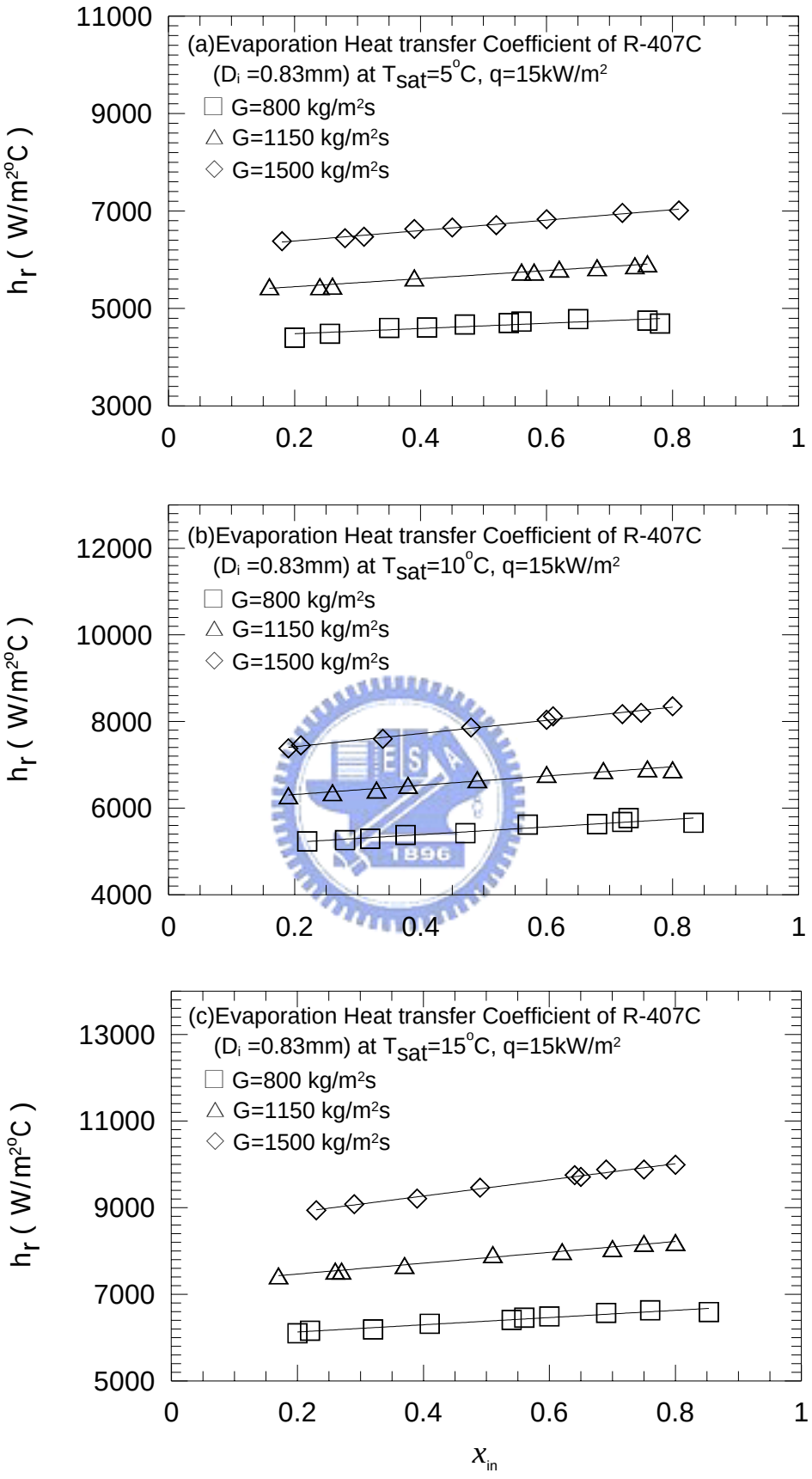

Fig. 4.35 Variations of R-407C evaporation heat transfer coefficient with inlet vapor quality in 0.83-mm small tubes at q=15 kW/m^2 for various G for (a) T_{sat}=5℃, (b) T_{sat}=10℃, and (c) T_{sat}=15℃.

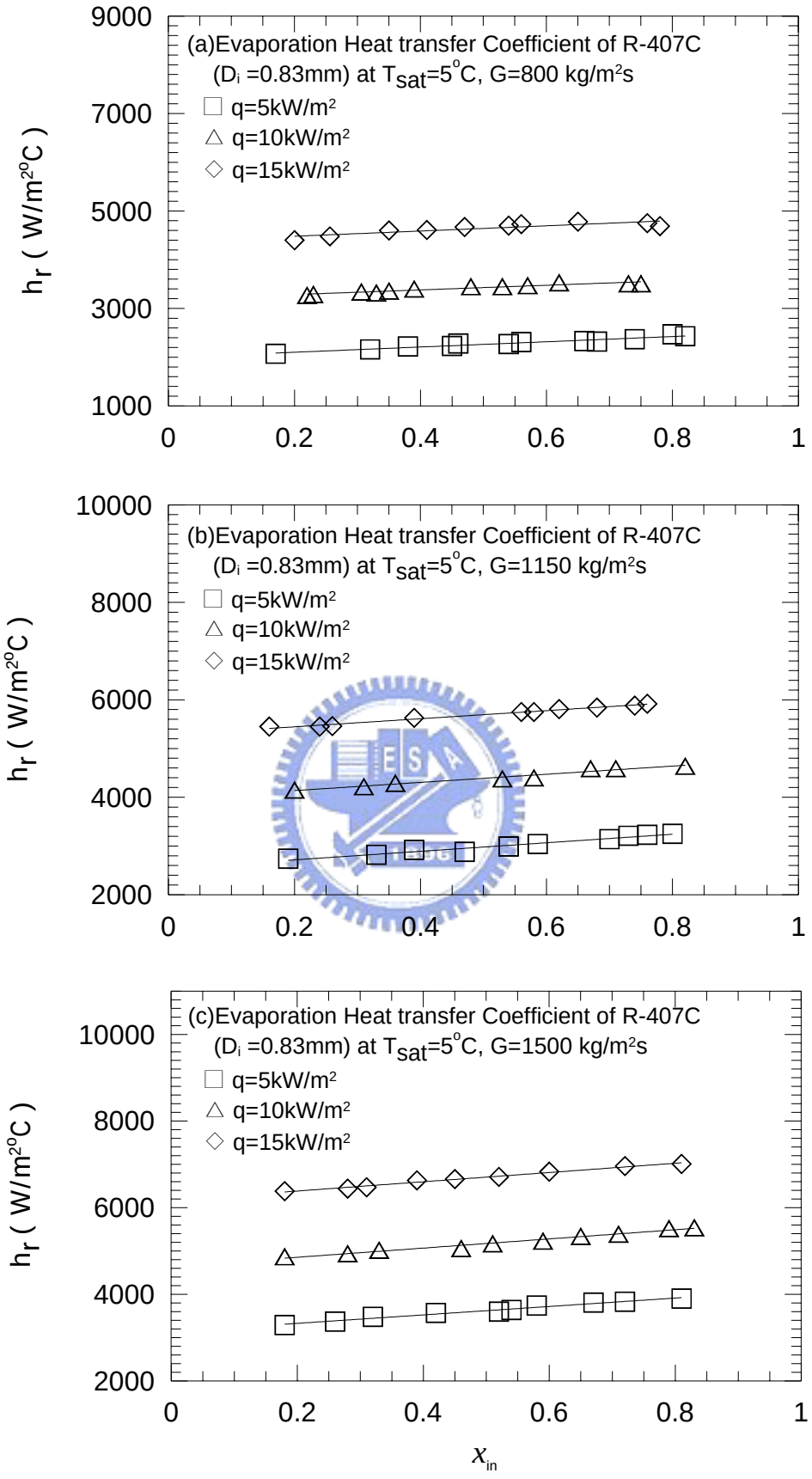

Fig. 4.36 Variations of R-407C evaporation heat transfer coefficient with inlet vapor quality in 0.83-mm small tubes at T_{sat}=5°C for various q for (a) G=800 kg/m^{2}s, (b) G=1150 kg/m^{2}s, and (c) G=1500 kg/m^{2}s.

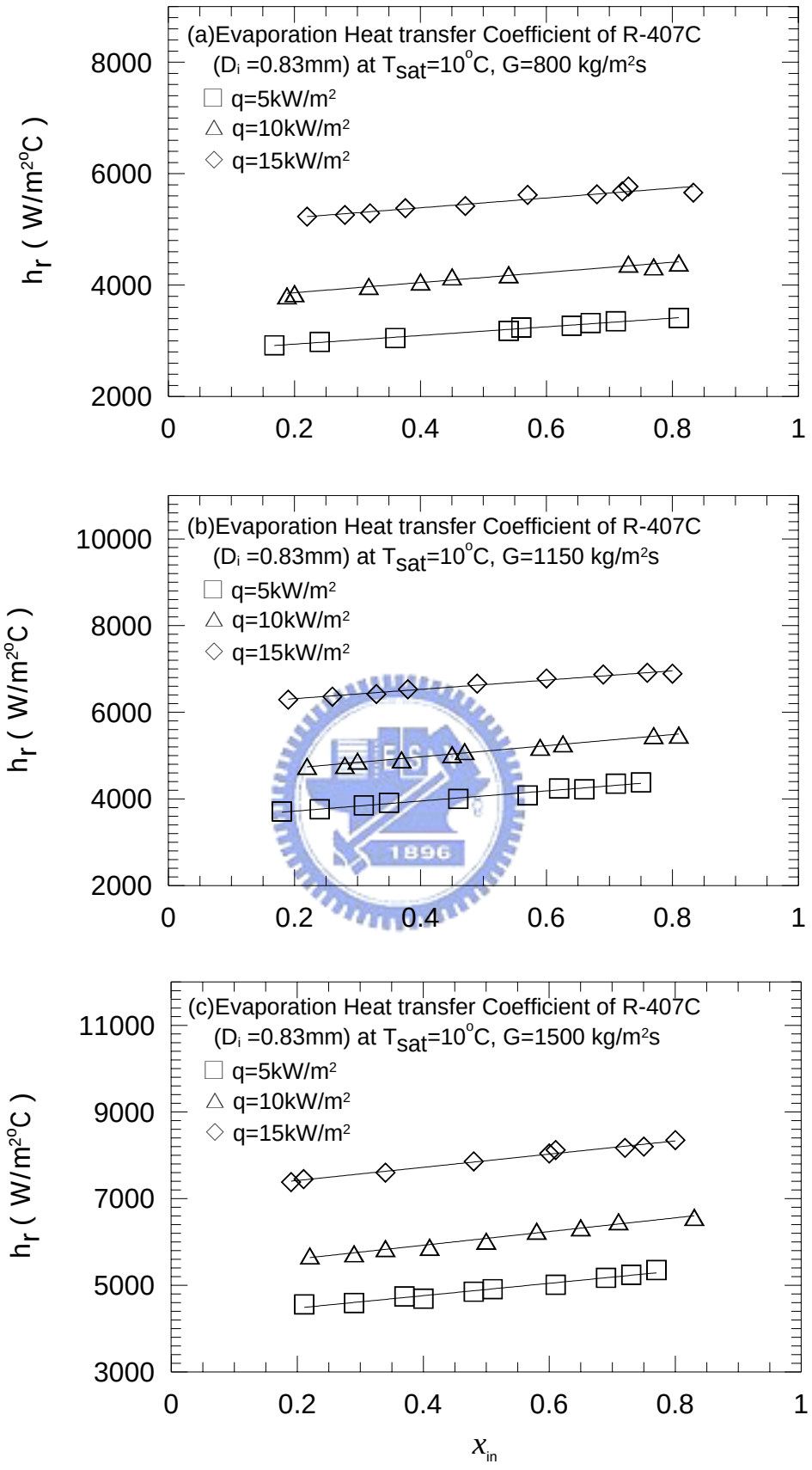

Fig. 4.37 Variations of R-407C evaporation heat transfer coefficient with inlet vapor quality in 0.83-mm small tubes at T_{sat}=10°C for various q for (a) G=800 kg/m^{2}s, (b) G=1150 kg/m^{2}s, and (c) G=1500 kg/m^{2}s.

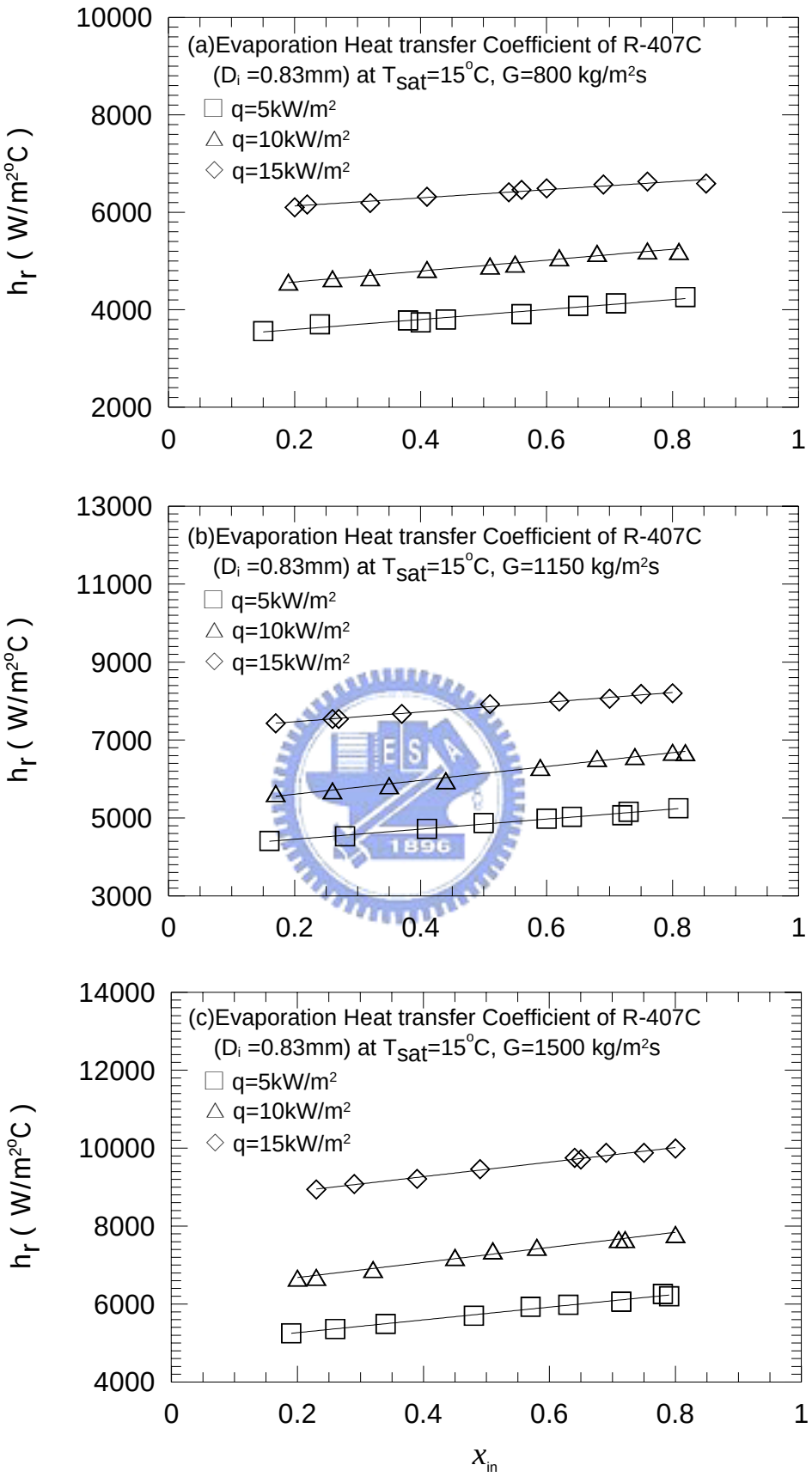

Fig. 4.38 Variations of R-407C evaporation heat transfer coefficient with inlet vapor quality in 0.83-mm small tubes at T_{sat}=15℃ for various q for (a) G=800 kg/m^{2}s, (b) G=1150 kg/m^{2}s, and (c) G=1500 kg/m^{2}s.

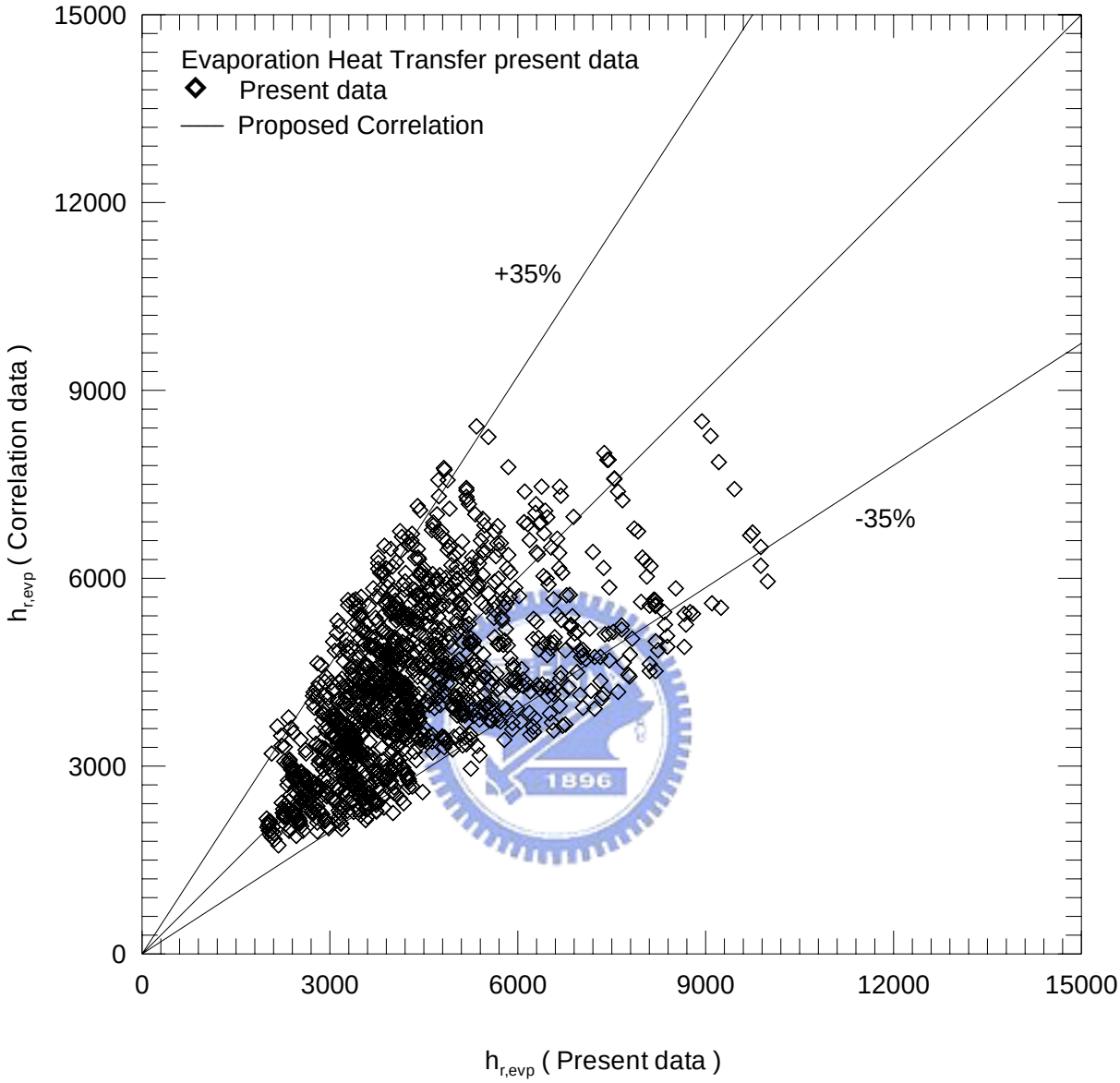

Fig. 4.39 Comparison of the measured data for heat transfer coefficient in the evaporation of R-134a and R-407 in 0.83-mm and 2.0-mm small tubes with the proposed correlation.

CHAPTER 5

TWO PHASE FRICTIONAL PRESSURE DROP

The frictional pressure drops for the R-134a and R-407C evaporation in the small tubes deduced from the measured raw data for ΔP_{exp} are presented in this chapter. In the following the effects of the refrigerant vapor quality, saturated temperature, mass flux and imposed heat flux on the frictional pressure drop will be examined in detail for both tubes.

5.1 Frictional Pressure Drops in 2.0-mm Tubes

The variations of the frictional pressure drops with the inlet vapor quality for R-134a evaporation in the 2.0-mm tubes are shown in Figs. 5.1 ~ 5.9 for various refrigerant saturated temperatures, mass fluxes and imposed heat fluxes. The results indicate that for all T_{sat}, G and q tested here the frictional pressure drop of R-134a in the tubes increases linearly with the inlet vapor quality. The increase is significant for a lower refrigerant saturated temperature and a higher mass flux. For instance, at T_{sat}=5°C, G=400 kg/m^{2}s and q=5 kW/m^2 the data in Fig. 5.1(c) show that the frictional pressure drop ΔP_f is increased from 15,100 Pa to 22,400 Pa when x_{in} is raised from 0.2 to 0.8. It is an increase of 48.3%. Figures 5.1 ~ 5.3 show that an increase in the R-134a saturated temperature causes a large reduction in the frictional pressure drop. For example, the quality-averaged frictional pressure drops at G=400 kg/m^{2}s and q=5 kW/m^2 are respectively 18,354 Pa and 11,532 Pa for T_{sat}=5 & 15°C (Fig. 5.1(c)). Thus ΔP_f is reduced by 37.2% for T_{sat} raised from 5 to 15°C. This mainly reflects the fact that the viscosity of the liquid R-134a is lower and the density

of the R-134a vapor is higher at a higher saturated temperature (Table 2.1). Thus the speed of the vapor flow in the duct core is lower. Hence the frictions at the liquid-vapor interface and at the wall are reduced at increasing T_{sat}, resulting in a significant reduction in ΔP_f. It is also noted from Figs. 5.4 ~ 5.6 that a substantial increase in ΔP_f results for the increase of the mass flux of R-134a. According to Fig. 5.4(c), at T_{sat}=15℃ and q=5 kW/m^2 the quality-averaged frictional pressure drops are respectively 6,298 Pa and 11,532 Pa for G=200 and 400 kg/m^{2}s. Thus, ΔP_f is increased by 83.1% for G raised from 200 to 400 kg/m^{2}s. The higher ΔP_f for a high refrigerant mass flux is attributed to the fact that both the speeds of the liquid and vapor flows in the tubes are directly proportional to the refrigerant mass flux. Finally, the frictional pressure drop is not affected to a noticeable degree by the imposed heat flux, as is evident from the results in Figs. 5.7 ~ 5.9. In fact, this change of the frictional pressure drop with the imposed heat flux is within the experimental uncertainty. We further note that for most cases the rise in the evaporation heat transfer coefficient with the imposed heat flux presented in Chapter 4 is rather significant, unlike the frictional pressure drop.

The ΔP_f data for the R-407C evaporation in the 2.0-mm tubes are shown in Figs. 5.10 ~ 5.18 for comparison. The results manifest that the effects of the refrigerant inlet vapor quality, saturated temperature, mass flux and heat flux on the frictional pressure drop associated with the R-407C evaporation in the 2.0-mm tubes qualitatively resemble those presented above for R-134a.

Contrasting the magnitudes of ΔP_f for the corresponding cases with the same T_{sat}, G and q shown in Figs. 5.1 ~ 5.18 between the R-134a and R-407C evaporation in the 2.0-mm tubes reveals that the frictional pressure drop in the R-134a flow is much higher. The higher ΔP_f for the R-134a evaporation is considered to result from the fact that R-134a has a much higher dynamic viscosity and a slighter lower latent

heat of vaporization.

5.2 Frictional Pressure Drop in the Smaller Tubes (D_i=0.83 mm)

The variations of the frictional pressure drops with x_{in}, T_{sat}, G and q for R-134a and R-407C evaporation in the smaller tubes with D_i=0.83 mm are presented in Figs. 5.19 ~ 5.36. These results qualitatively resemble those for the larger tubes with D_i=2.0 mm given in Figs. 5.1 ~ 5.18. Again the frictional pressure drops for both R-134a and R-407C in the smaller tubes increase significantly with the refrigerant inlet vapor quality, saturated temperature and mass flux. The effects of the imposed heat flux are small. Besides, the frictional pressure drop for R-134a is substantially higher than that for R-407C. Some quantitative data are given here to illustrate the effects of the important parameters on ΔP_f. For the typical case with T_{sat}=15℃, G=800 kg/m^{2}s and q=5 kW/m^2 the data in Figs. 5.19(a) & 5.28(a) show that for the inlet vapor quality raised from 0.2 to 0.8, the frictional pressure drop is significantly increased from 26,850 Pa to 30,400 Pa for R-134a (a 13.2% increase) and from 11,450 Pa to 13,390 Pa for R-407C (a 16.9% increase). Then Figs. 5.19(a) and 5.28(a) also show that the quality-averaged frictional pressure drops are reduced from 34,414 Pa to 28,316 Pa for R-134a and from 18,287 Pa to 12,360 Pa for R-407C when T_{sat} is increased from 5 to 15℃ for G=800 kg/m^{2}s and q=5 kW/m^2. These respectively correspond to 17.7% and 30% reduction in ΔP_f. Moreover, according to Figs. 5.22(c) and 5.31(c), the quality-averaged frictional pressure drops increase respectively from 28,316 to 31,607 Pa for R-134a and from 12,360 to 17,997 Pa for R-407C when G is raised from 800 to 1500 kg/m^{2}s for T_{sat}=15℃ and q=5 kW/m^2. These respectively correspond to 11.6% and 45.6% increases.

5.3 Correlation equation for Frictional Pressure Drops

Based on the present data for R-134a and R-407C evaporation in the 2.0-mm and 0.83-mm tubes, an empirical correlation for the dimensionless frictional pressure drop is proposed in terms of the friction factor. It is expressed as

$$f_{tp} = 1800 \cdot Re_{eq}^{-1.125} \cdot N_{conf}^{0.5} \tag{5.1}$$

where Re_{eq} is the equivalent Reynolds number for the evaporating flow and is defined as

$$Re_{eq} = \frac{G_{eq} \cdot D_i}{\mu_f} \tag{5.2}$$

in which

$$G_{eq} = G \cdot [(1 - x_{in}) + x_{in} \cdot (\frac{\rho_f}{\rho_g})^{0.5}] \tag{5.3}$$

Here G_{eq} is an equivalent mass flux which is a function of the R-134a and R-407C mass flux, mean vapor quality and density at the test condition. Besides, x_{in} is the inlet vapor quality of the flow. Figure 5.37 shows that more than 78% of the present data for f_{tp} fall within ±35% of Eq. (5.1), and the mean deviation between the present data for f_{tp} and the proposed correlation is about 27.6%.

5.4 Concluding Remarks

Experimental measurement has been carried out here to investigate how the frictional pressure drops of R-134a and R-407C evaporation in the small tubes are affected by the refrigerant saturated temperature, mass flux and imposed heat flux. The results show that the significant increase of the frictional pressure drop for R-134a and R-407C evaporation in the small tubes with the inlet vapor quality is almost linear and the increase is larger for a higher refrigerant mass flux. But an

opposite trend is noted for a rise in the refrigerant saturated temperature. Furthermore, the imposed heat flux exhibits a negligible effect on the frictional pressure drop. Finally, an empirical correlation is proposed to correlate the present data for the frictional pressure drop in terms of the friction factor.

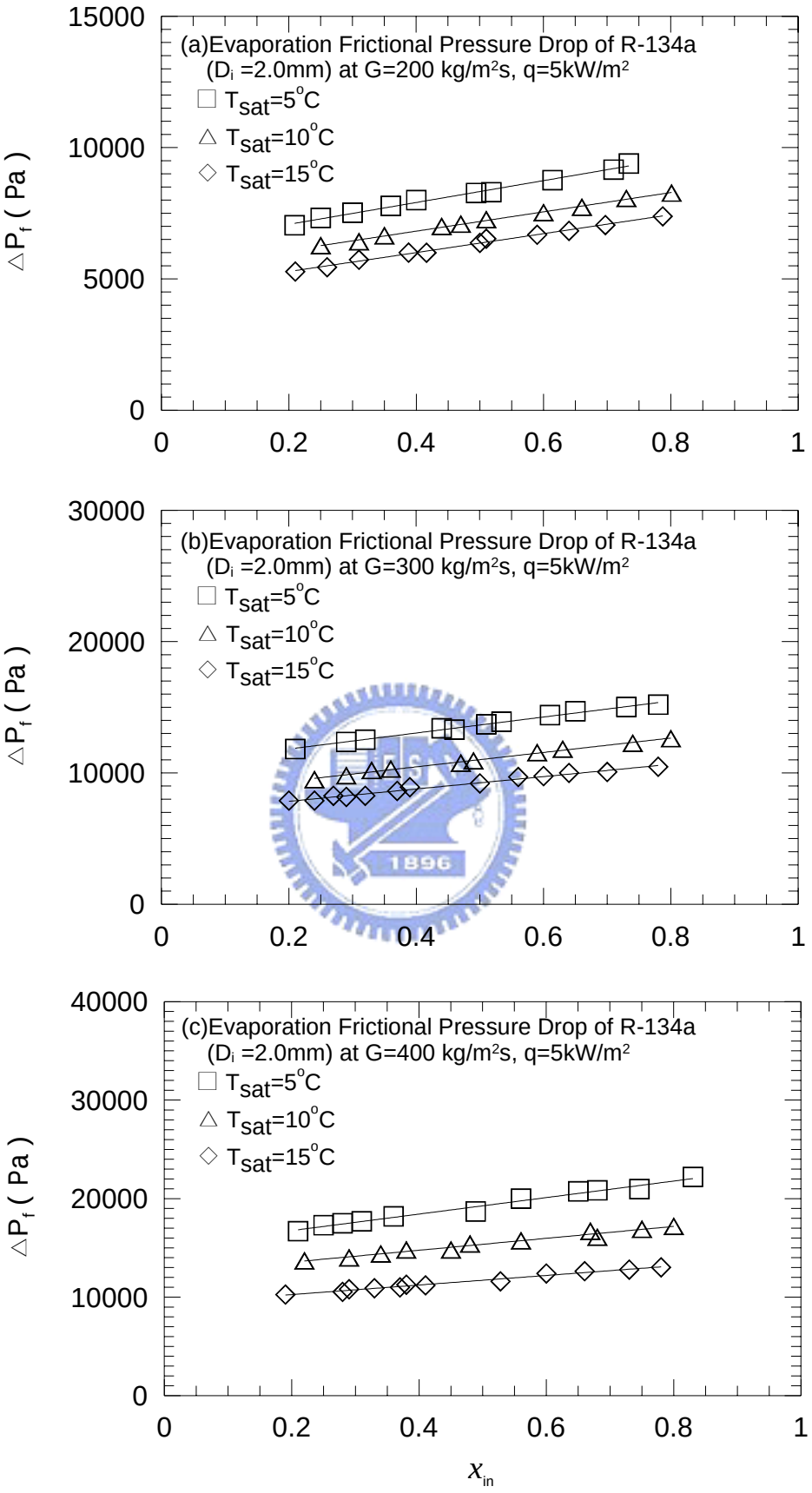

Fig. 5.1 Variations of R-134a frictional pressure drop with inlet vapor quality in 2.0-mm small tubes at q=5kW/m^2 for various T_{sat} for (a) G=200 kg/m^{2}s, (b) G=300 kg/m^{2}s, and (c) G=400 kg/m^{2}s.

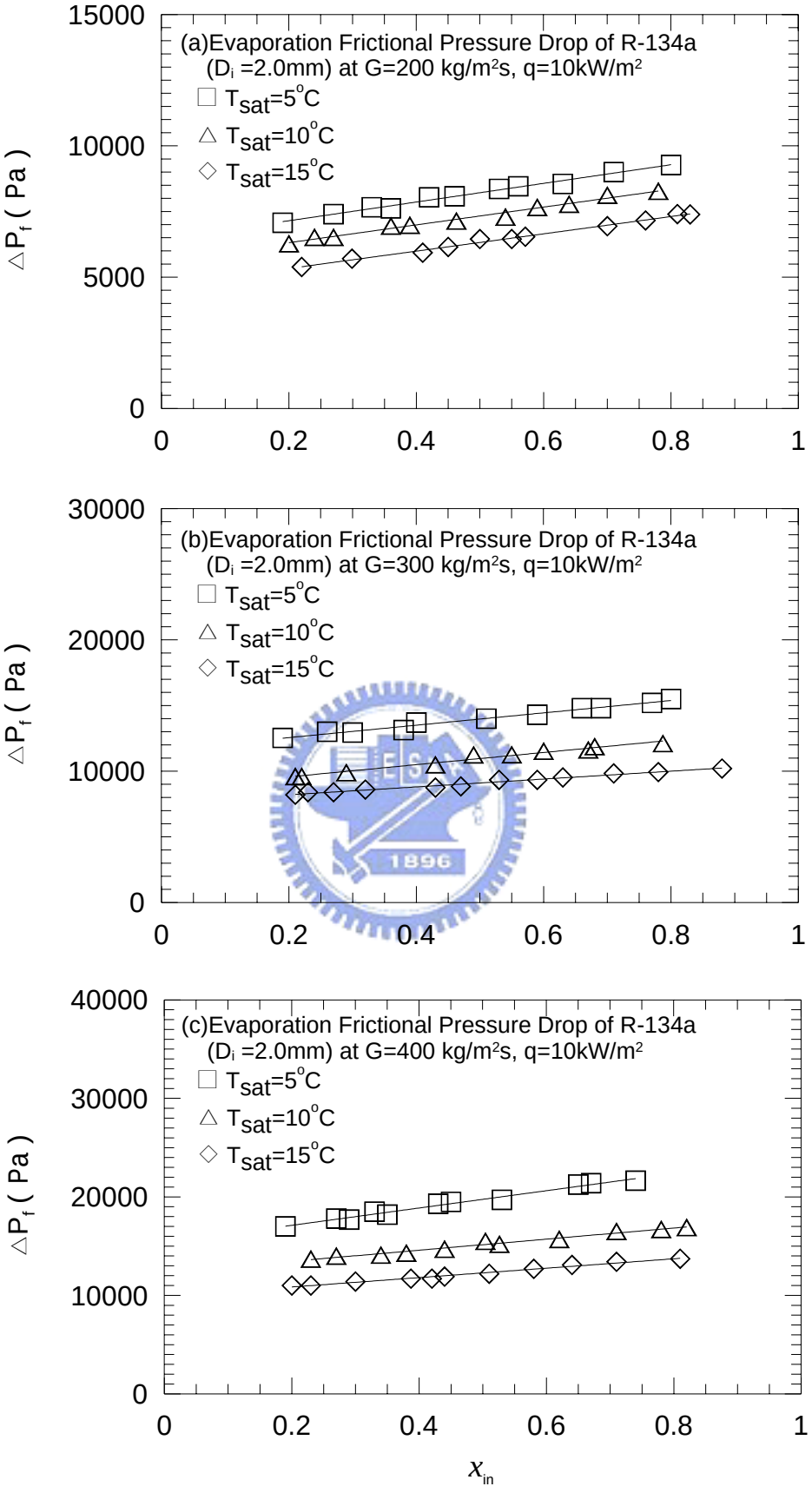

Fig. 5.2 Variations of R-134a frictional pressure drop with inlet vapor quality in 2.0-mm small tubes at q=10kW/m^2 for various T_{sat} for (a) G=200 kg/m^{2}s, (b) G=300 kg/m^{2}s, and (c) G=400 kg/m^{2}s.

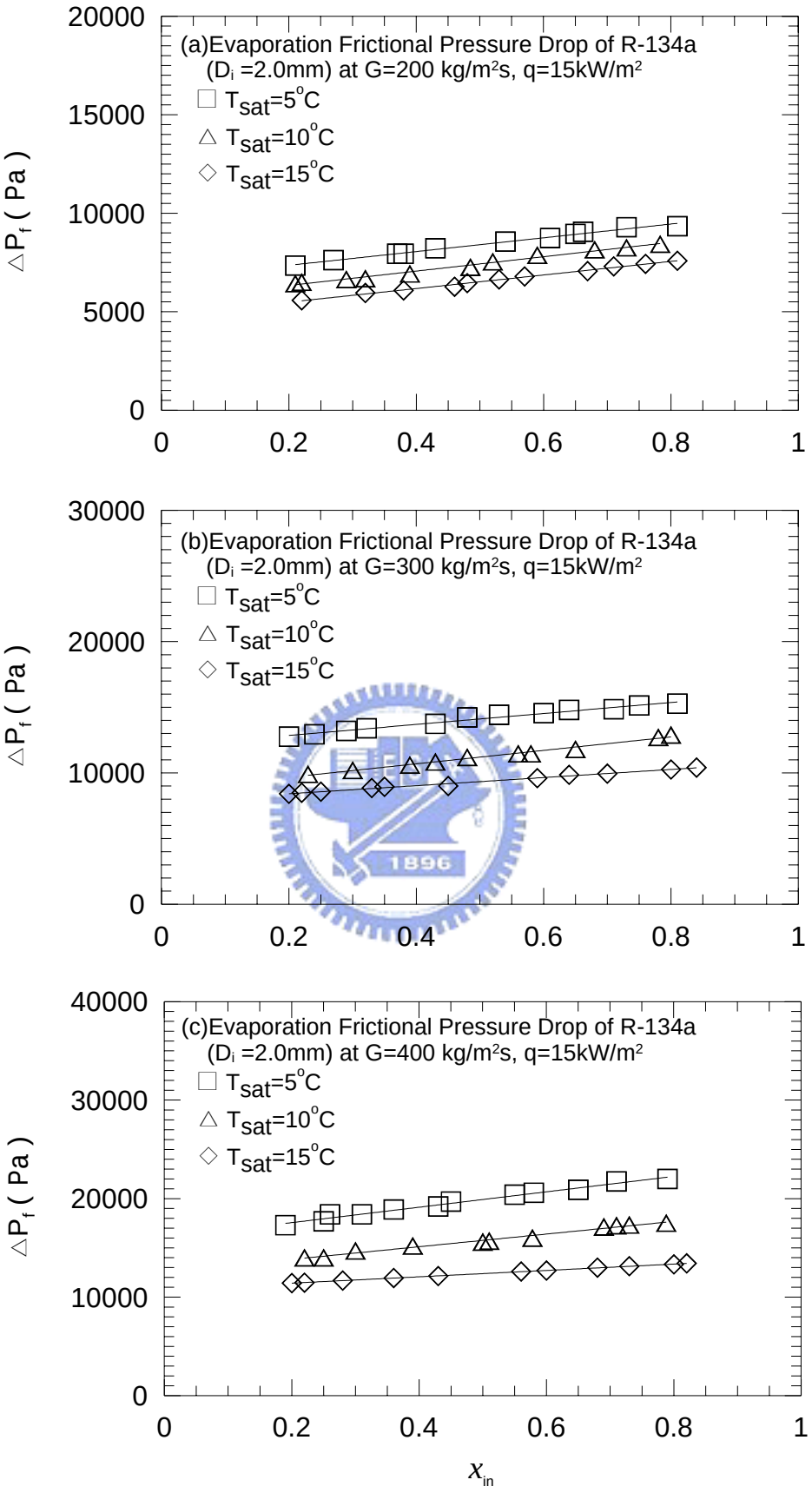

Fig. 5.3 Variations of R-134a frictional pressure drop with inlet vapor quality in 2.0-mm small tubes at q=15kW/m^2 for various T_{sat} for (a) G=200 kg/m^{2}s, (b) G=300 kg/m^{2}s, and (c) G=400 kg/m^{2}s.

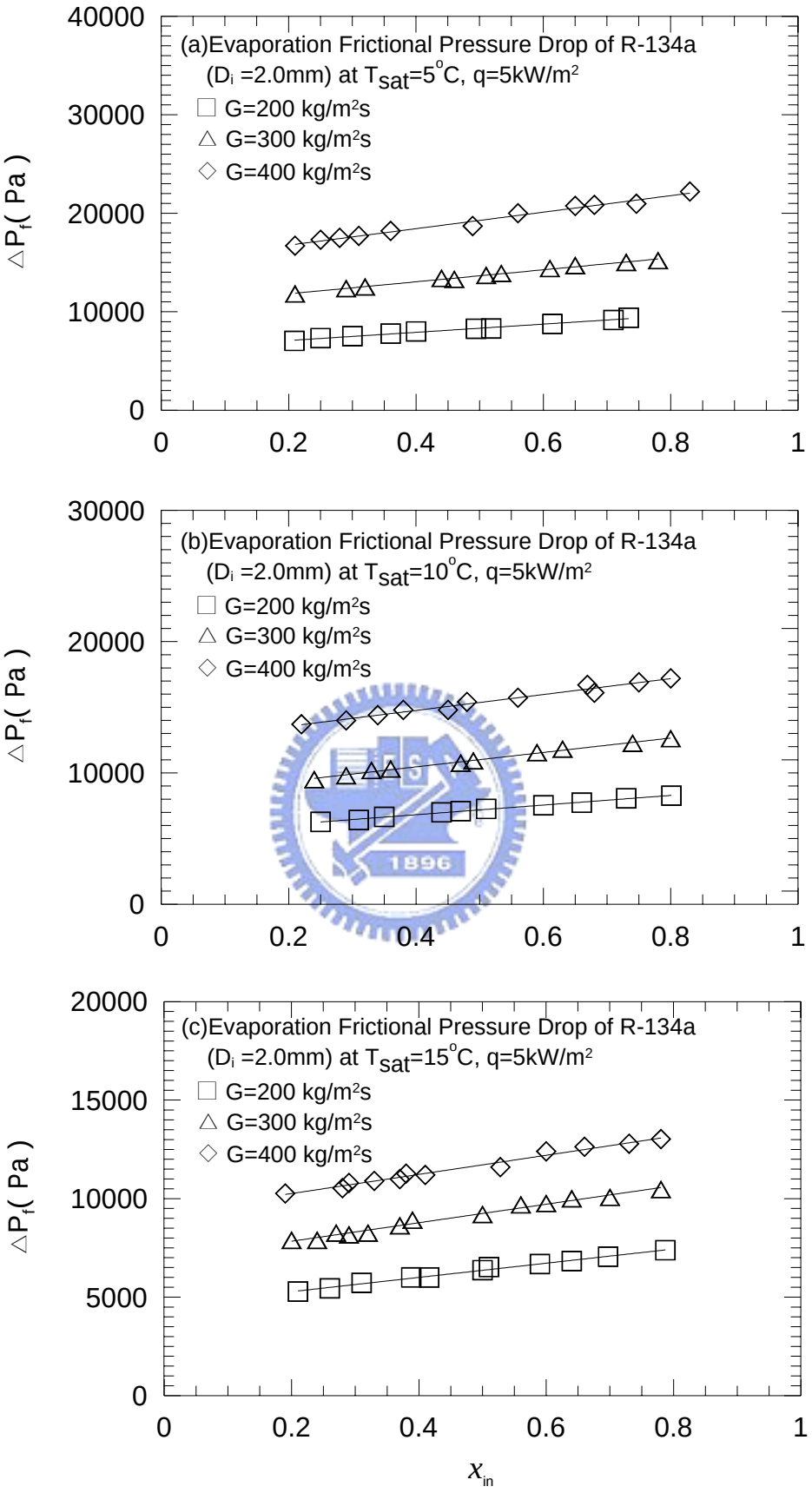

Fig. 5.4 Variations of R-134a frictional pressure drop with inlet vapor quality in 2.0-mm small tubes at q=5 kW/m^2 for various G for (a) T_{sat}=5℃, (b) T_{sat}=10℃, and (c) T_{sat}=15℃.

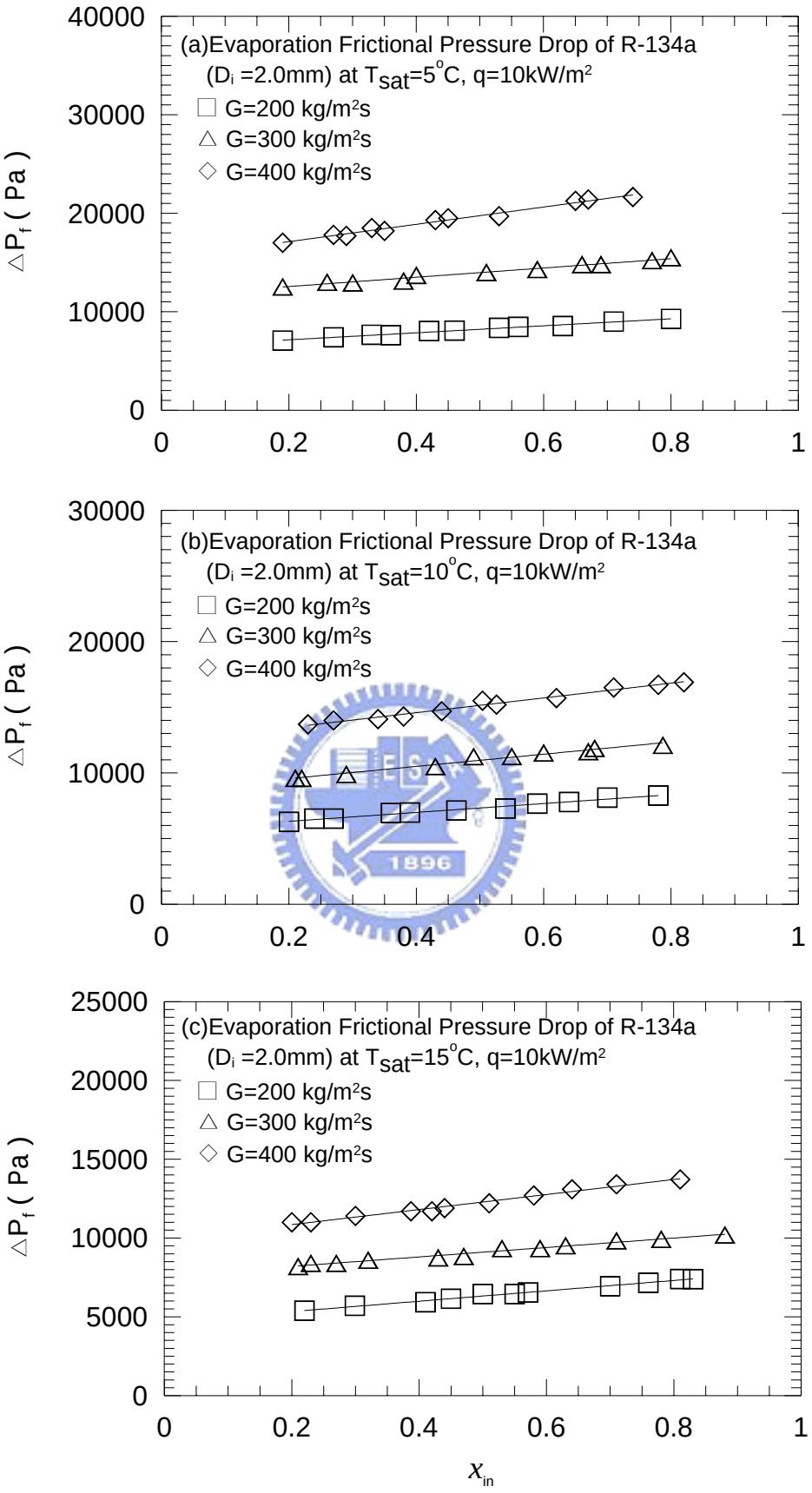

Fig. 5.5 Variations of R-134a frictional pressure drop with inlet vapor quality in 2.0-mm small tubes at q=10 kW/m^2 for various G for (a) T_{sat}=5℃, (b) T_{sat}=10℃, and (c) T_{sat}=15℃.

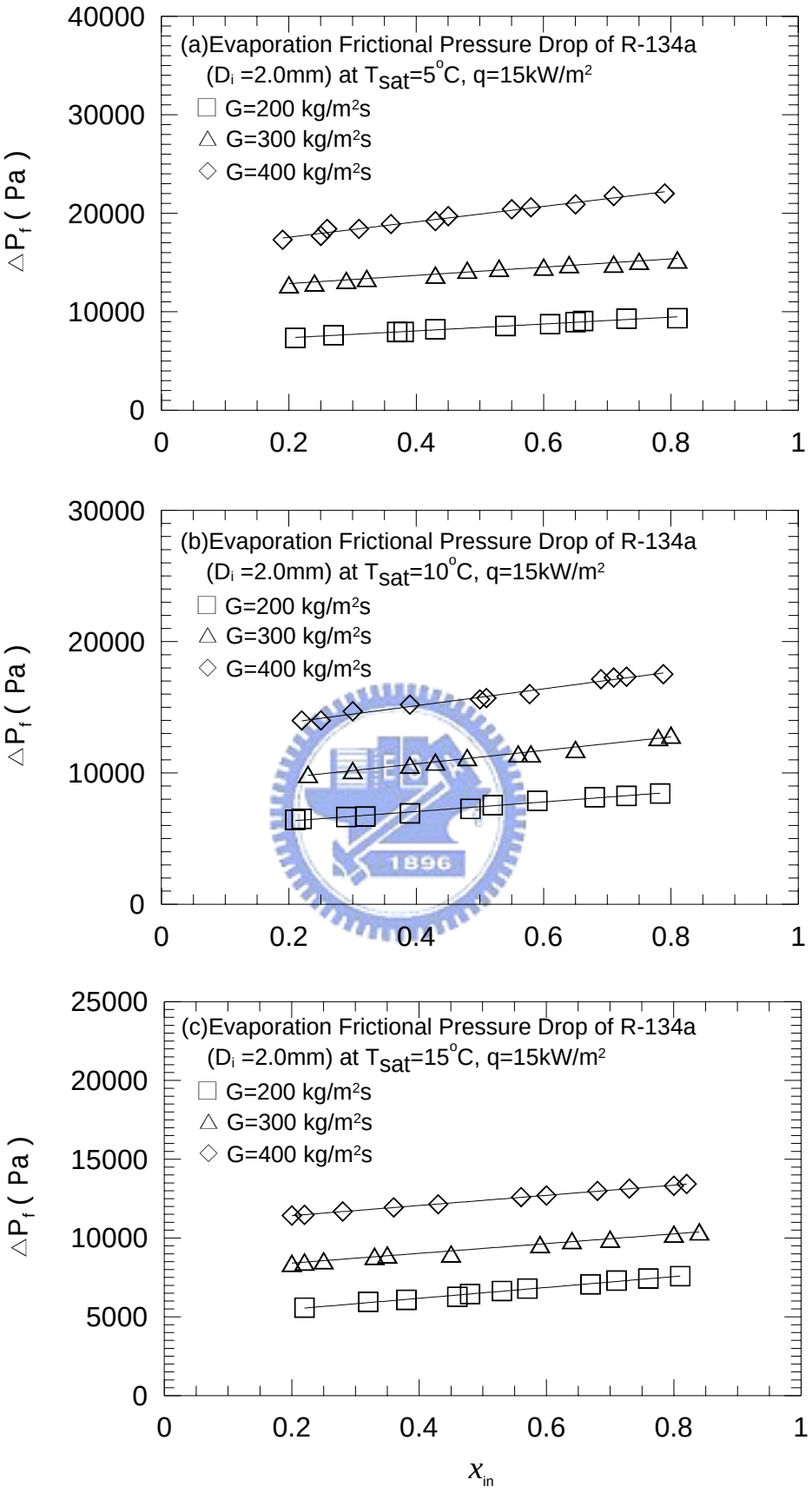

Fig. 5.6 Variations of R-134a frictional pressure drop with inlet vapor quality in 2.0-mm small tubes at q=15 kW/m^2 for various G for (a) T_{sat}=5℃, (b) T_{sat}=10℃, and (c) T_{sat}=15℃.

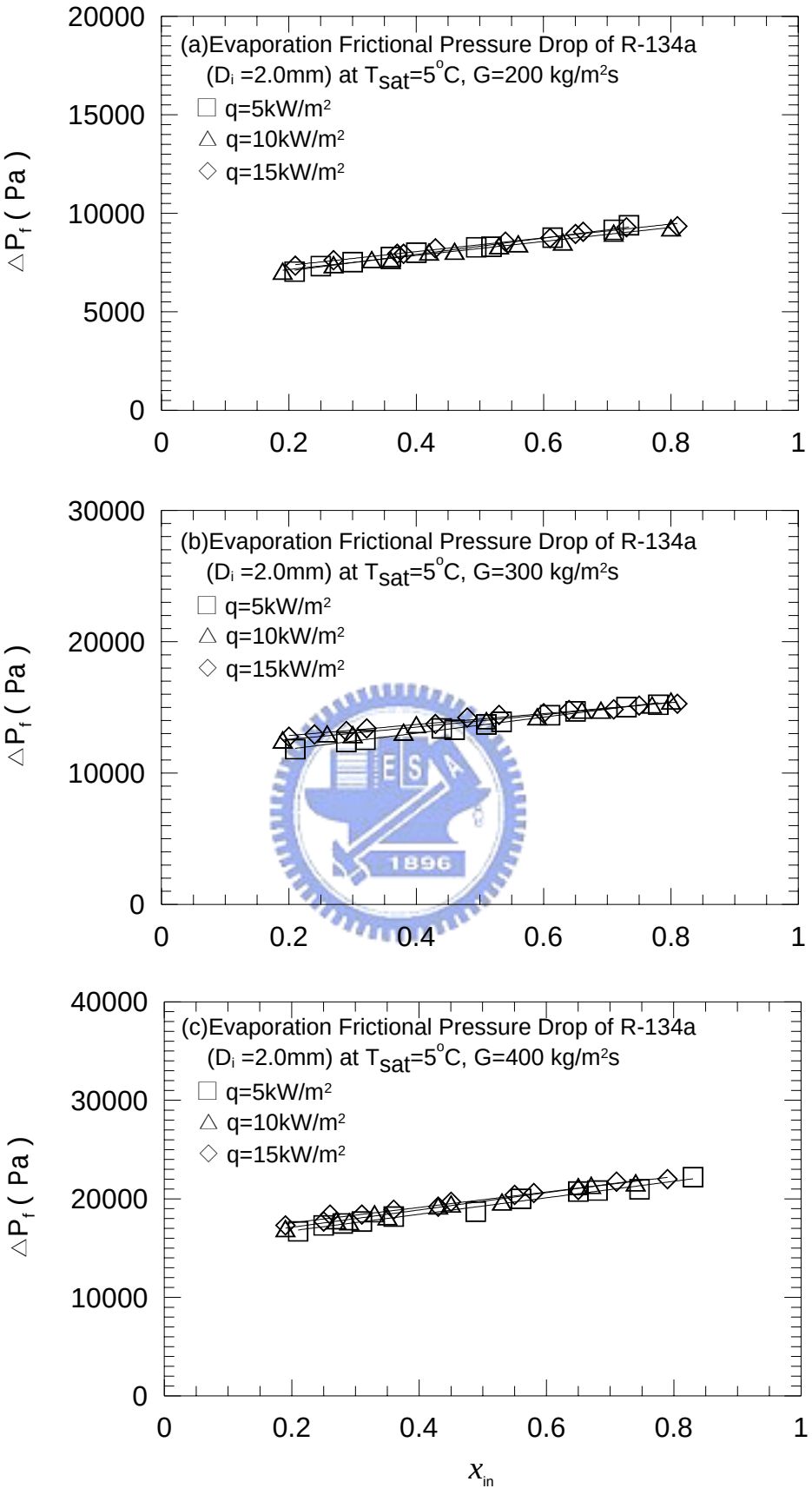

Fig. 5.7 Variations of R-134a frictional pressure drop with inlet vapor quality in 2.0-mm small tubes at T_{sat}=5℃ for various q for (a) G=200 kg/m^{2}s, (b) G=300 kg/m^{2}s, and (c) G=400 kg/m^{2}s.

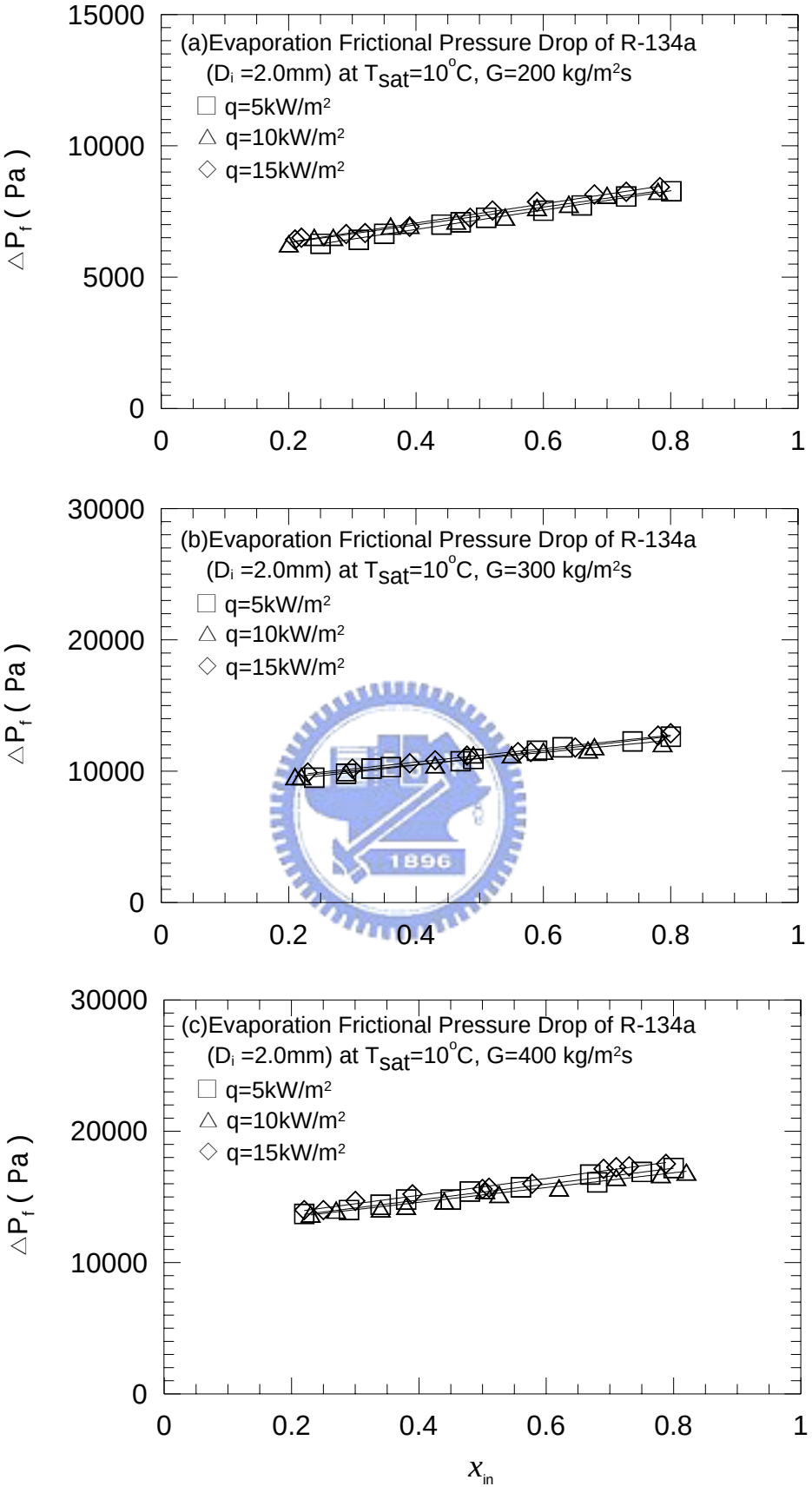

Fig. 5.8 Variations of R-134a frictional pressure drop with inlet vapor quality in 2.0-mm small tubes at T_{sat}=10℃ for various q for (a) G=200 kg/m^{2}s, (b) G=300 kg/m^{2}s, and (c) G=400 kg/m^{2}s.

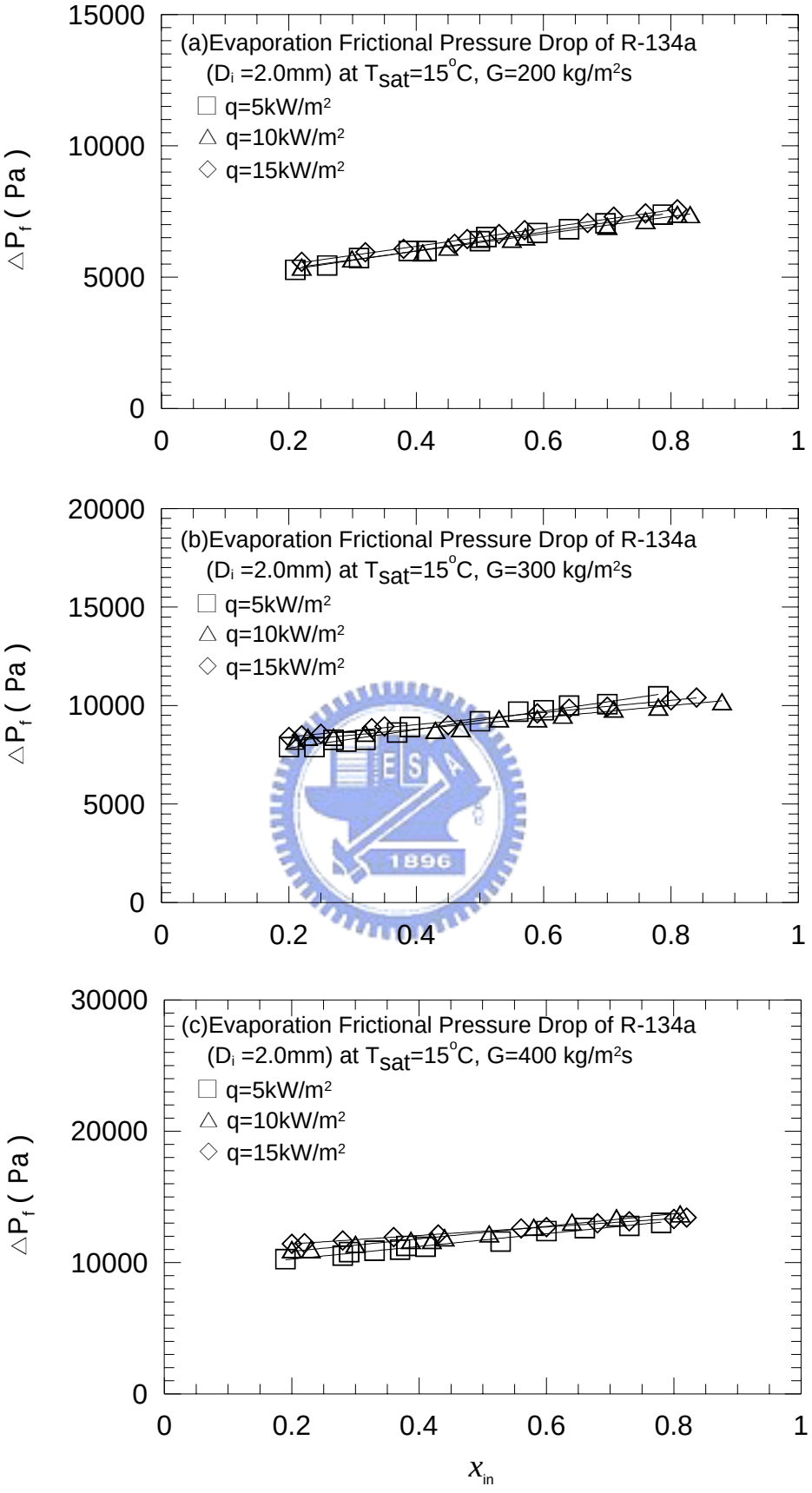

Fig. 5.9 Variations of R-134a frictional pressure drop with inlet vapor quality in 2.0-mm small tubes at T_{sat}=15℃ for various q for (a) G=200 kg/m^{2}s, (b) G=300 kg/m^{2}s, and (c) G=400 kg/m^{2}s.

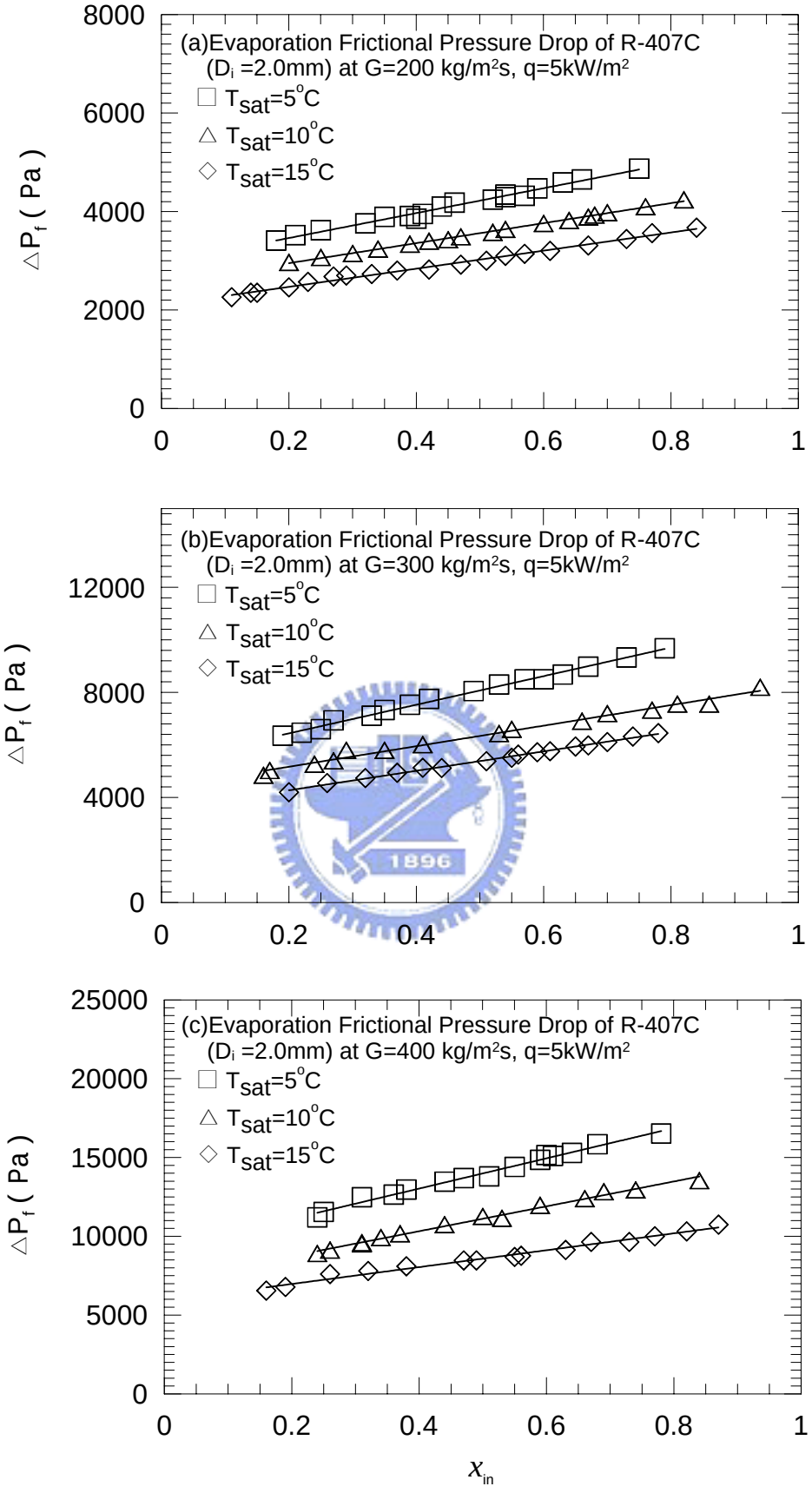

Fig. 5.10 Variations of R-407C frictional pressure drop with inlet vapor quality in 2.0-mm small tubes at q=5kW/m^2 for various T_{sat} for (a) G=200 kg/m^{2}s, (b) G=300 kg/m^{2}s, and (c) G=400 kg/m^{2}s.

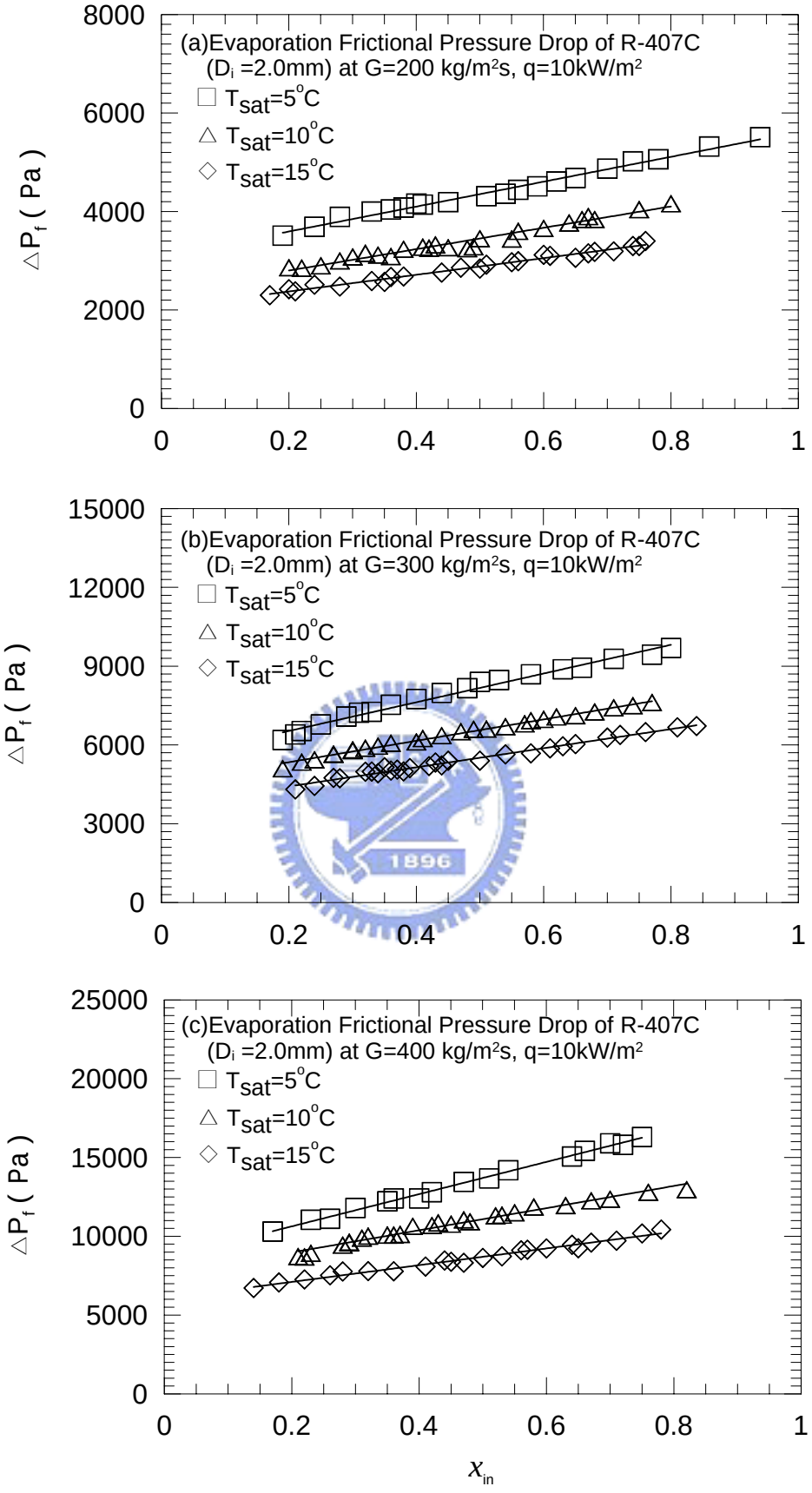

Fig. 5.11 Variations of R-407C frictional pressure drop with inlet vapor quality in 2.0-mm small tubes at q=10kW/m^2 for various T_{sat} for (a) G=200 kg/m^{2}s, (b) G=300 kg/m^{2}s, and (c) G=400 kg/m^{2}s.

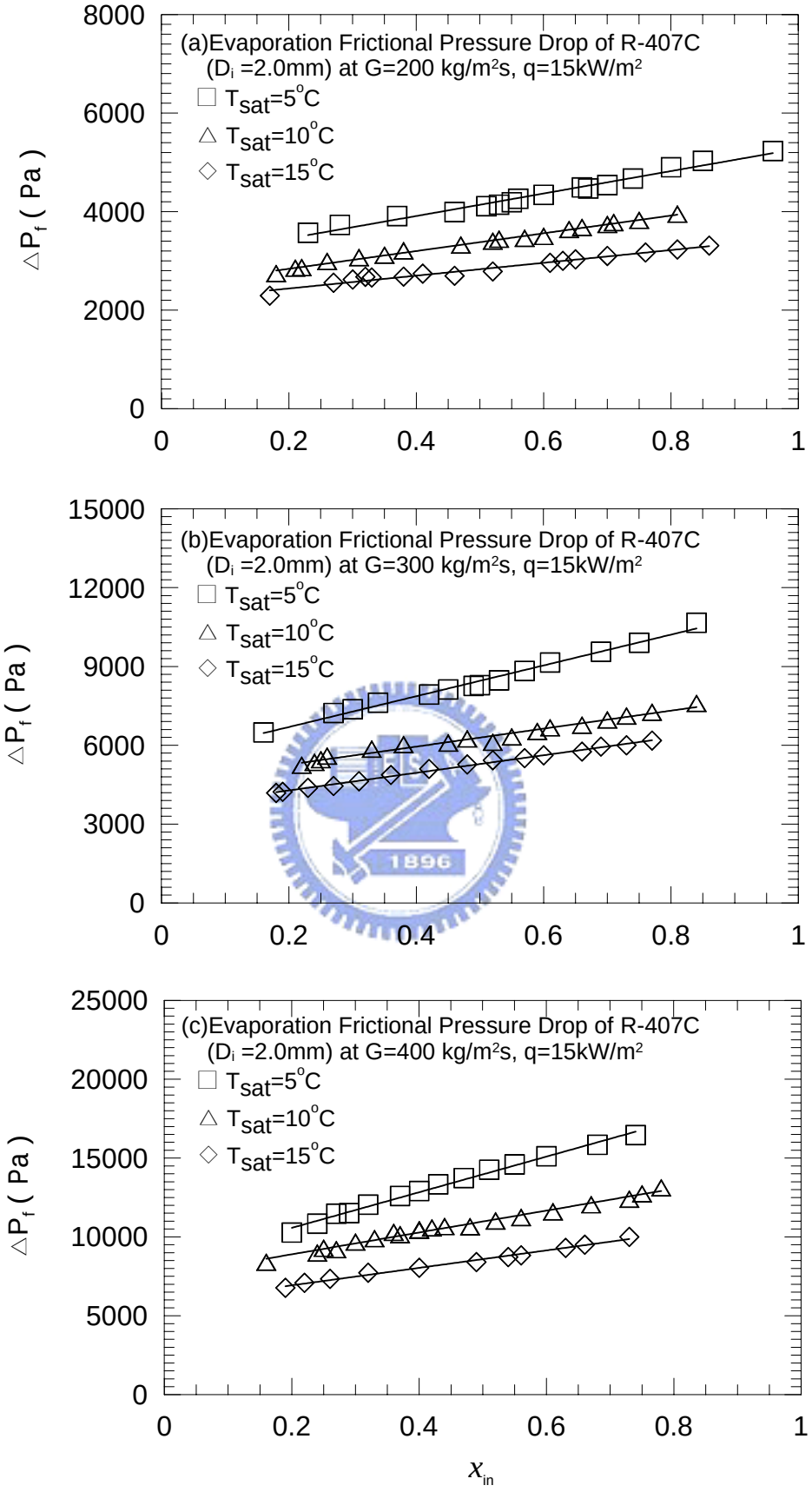

Fig. 5.12 Variations of R-407C frictional pressure drop with inlet vapor quality in 2.0-mm small tubes at q=15kW/m^2 for various T_{sat} for (a) G=200 kg/m^{2}s, (b) G=300 kg/m^{2}s, and (c) G=400 kg/m^{2}s.

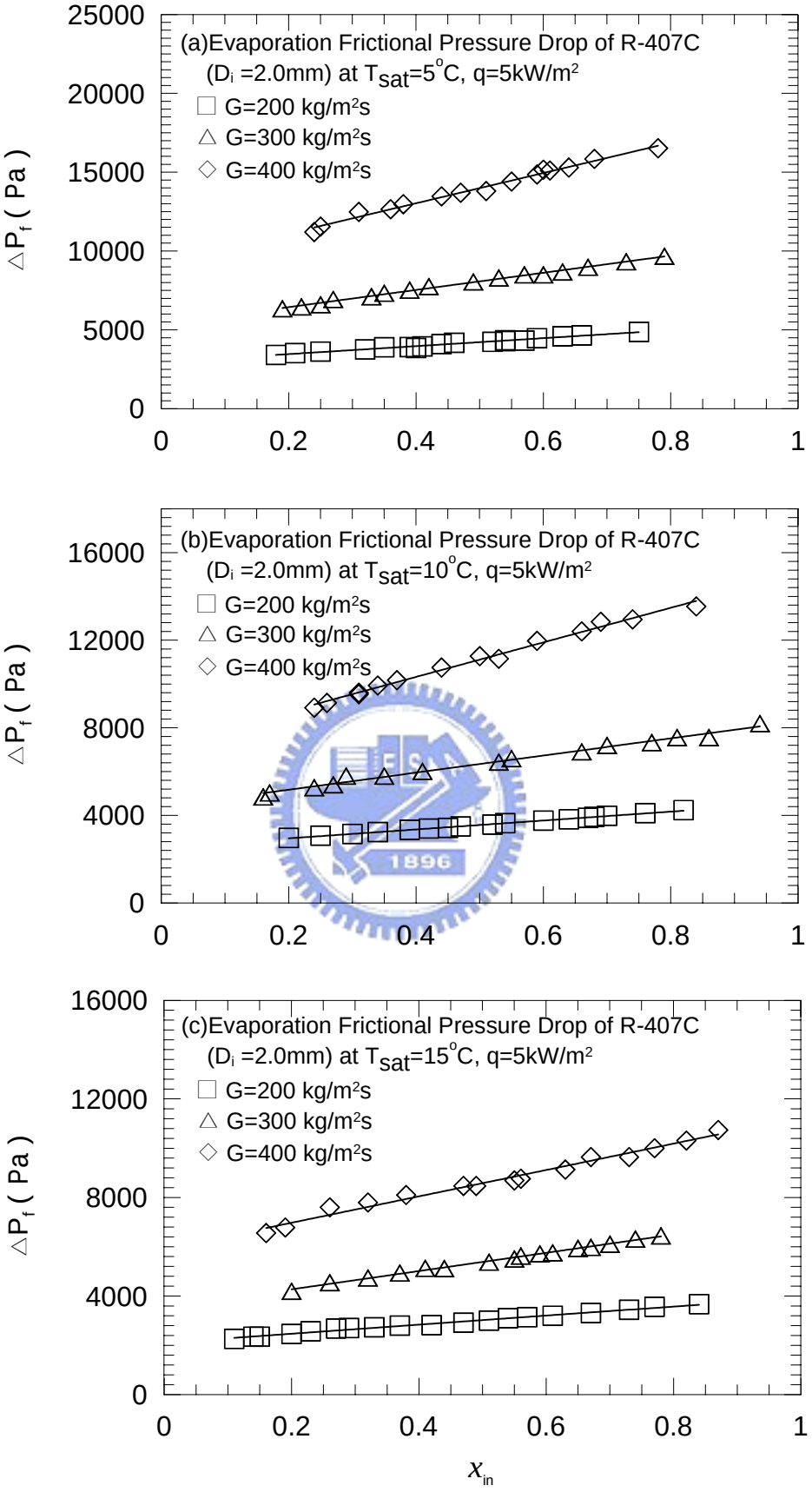

Fig. 5.13 Variations of R-407C frictional pressure drop with inlet vapor quality in 2.0-mm small tubes at q=5 kW/m^2 for various G for (a) T_{sat}=5°C, (b) T_{sat}=10°C, and (c) T_{sat}=15°C.

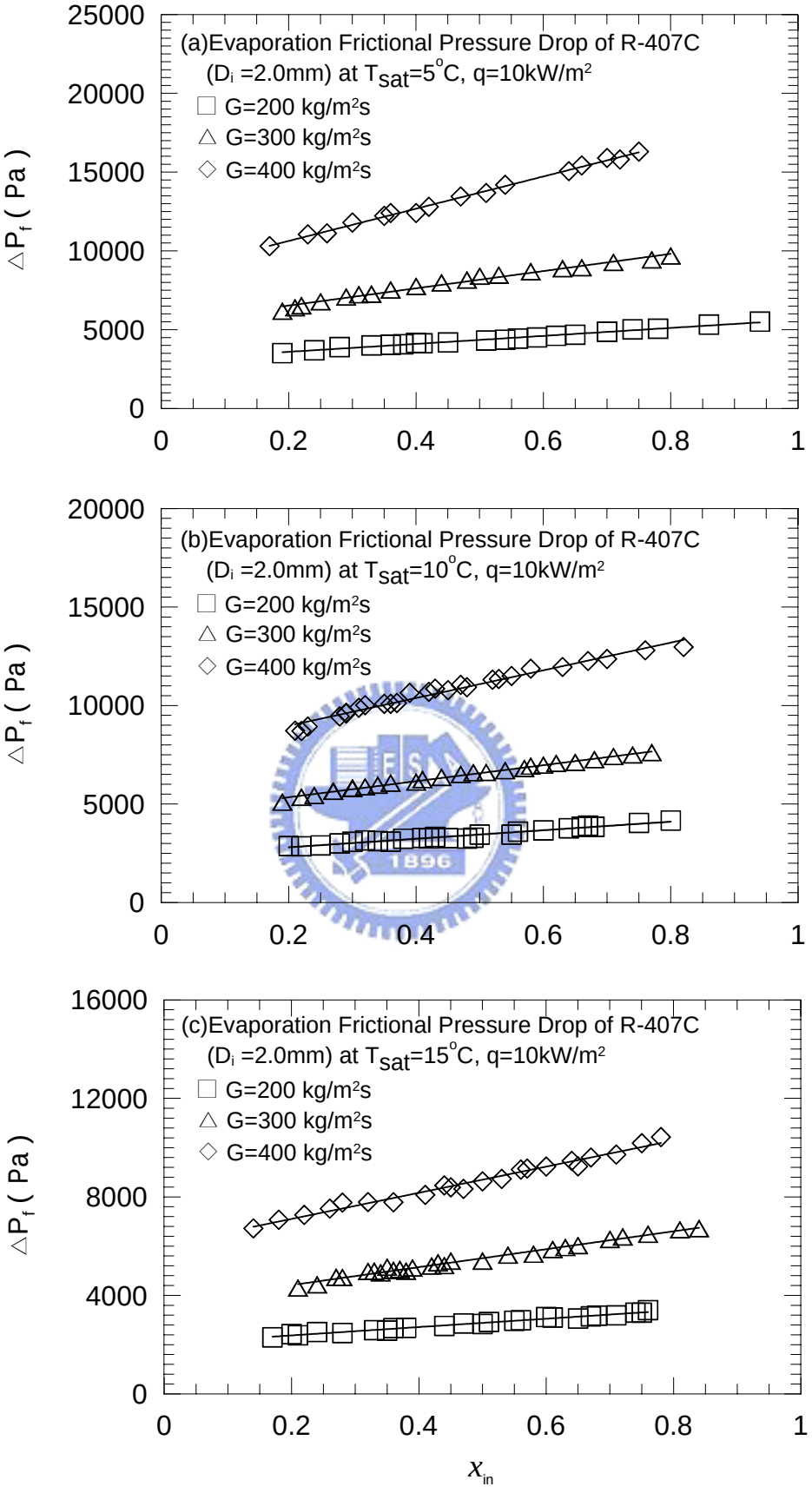

Fig. 5.14 Variations of R-407C frictional pressure drop with inlet vapor quality in 2.0-mm small tubes at q=10 kW/m^2 for various G for (a) T_{sat}=5℃, (b) T_{sat}=10℃, and (c) T_{sat}=15℃.

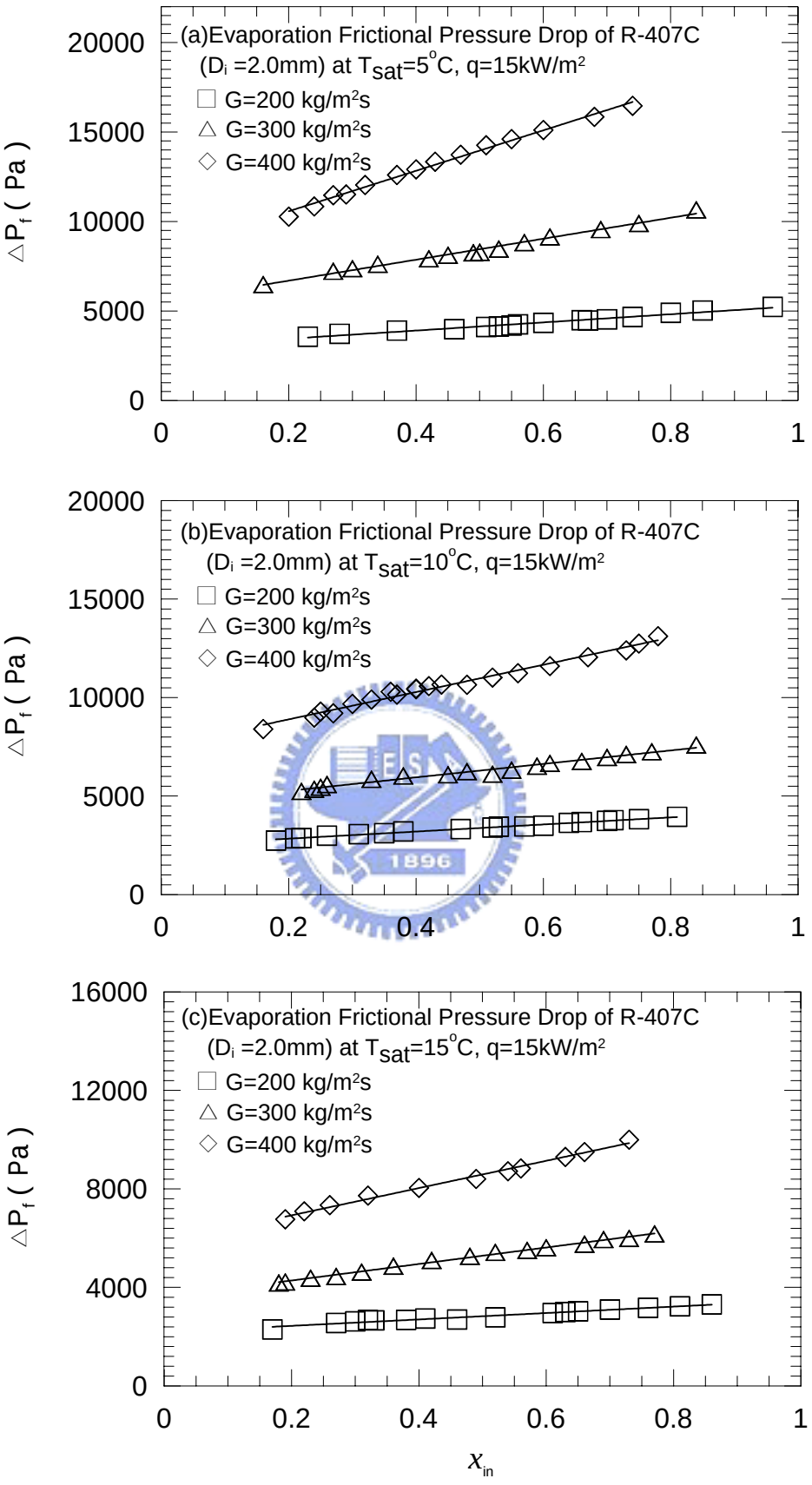

Fig. 5.15 Variations of R-407C frictional pressure drop with inlet vapor quality in 2.0-mm small tubes at q=15 kW/m^2 for various G for (a) T_{sat}=5℃, (b) T_{sat}=10℃, and (c) T_{sat}=15℃.

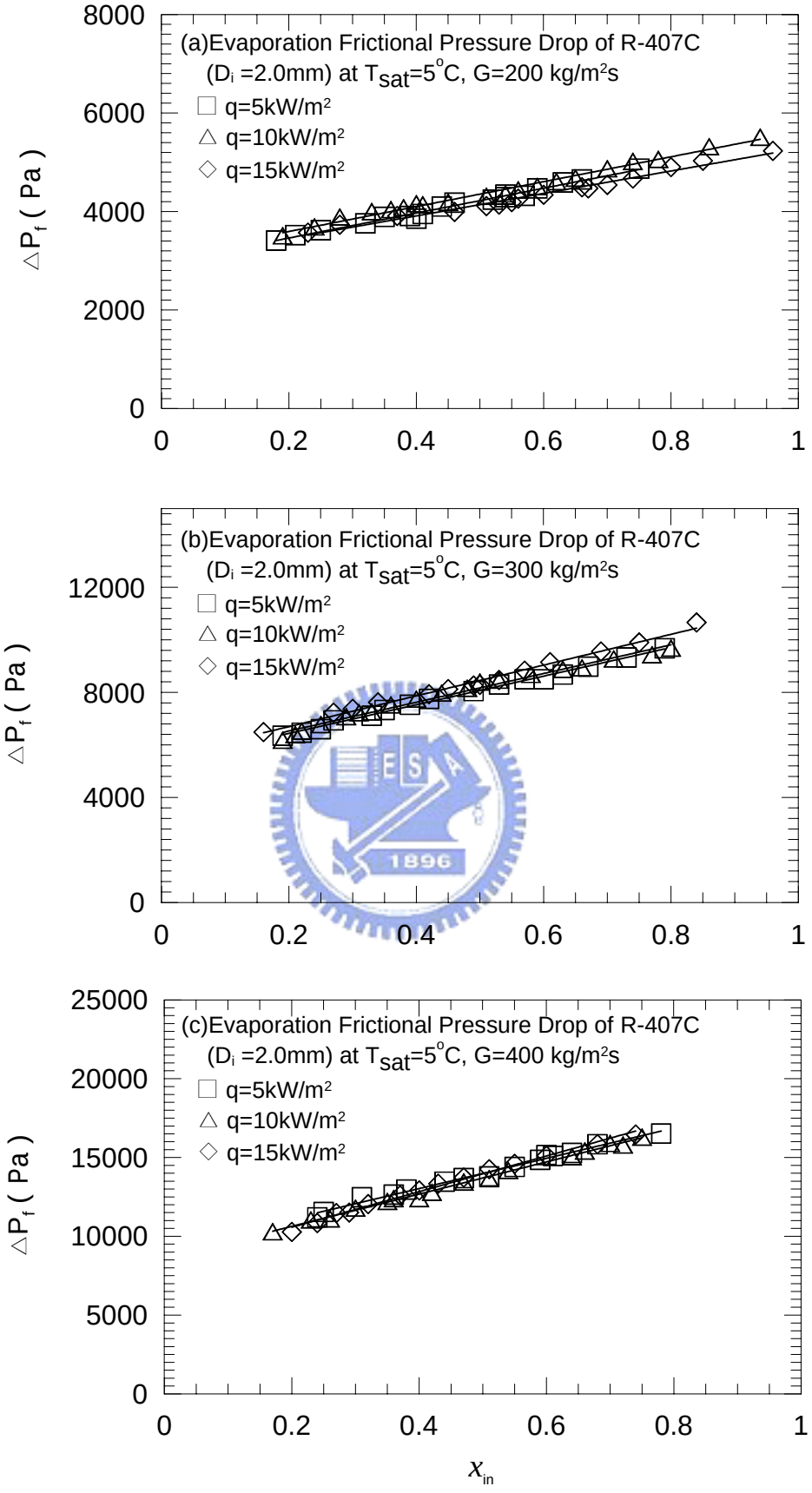

Fig. 5.16 Variations of R-407C frictional pressure drop with inlet vapor quality in 2.0-mm small tubes at T_{sat}=5℃ for various q for (a) G=200 kg/m^{2}s, (b) G=300 kg/m^{2}s, and (c) G=400 kg/m^{2}s.

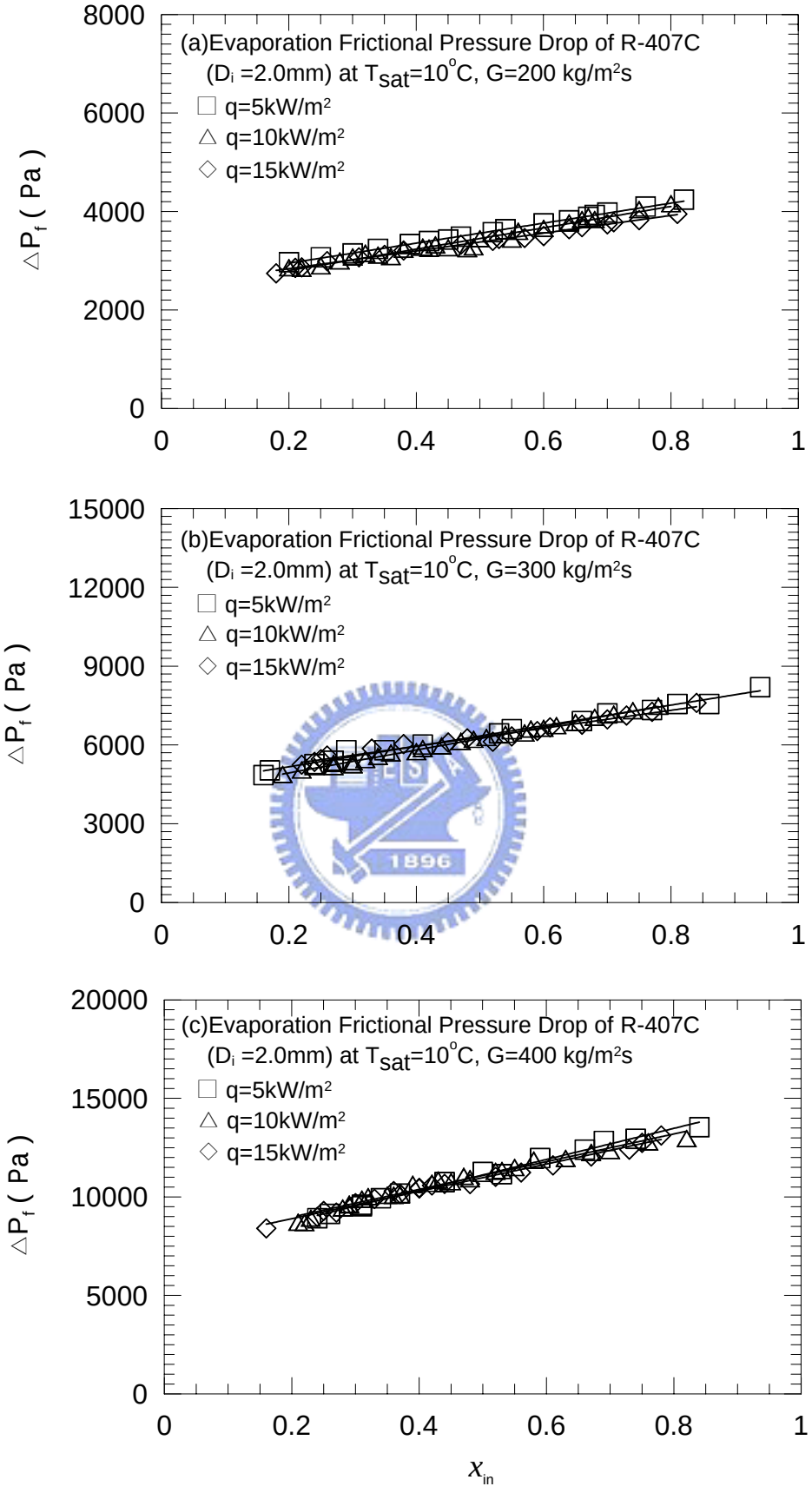

Fig. 5.17 Variations of R-407C frictional pressure drop with inlet vapor quality in 2.0-mm small tubes at T_{sat}=10℃ for various q for (a) G=200 kg/m^{2}s, (b) G=300 kg/m^{2}s, and (c) G=400 kg/m^{2}s.

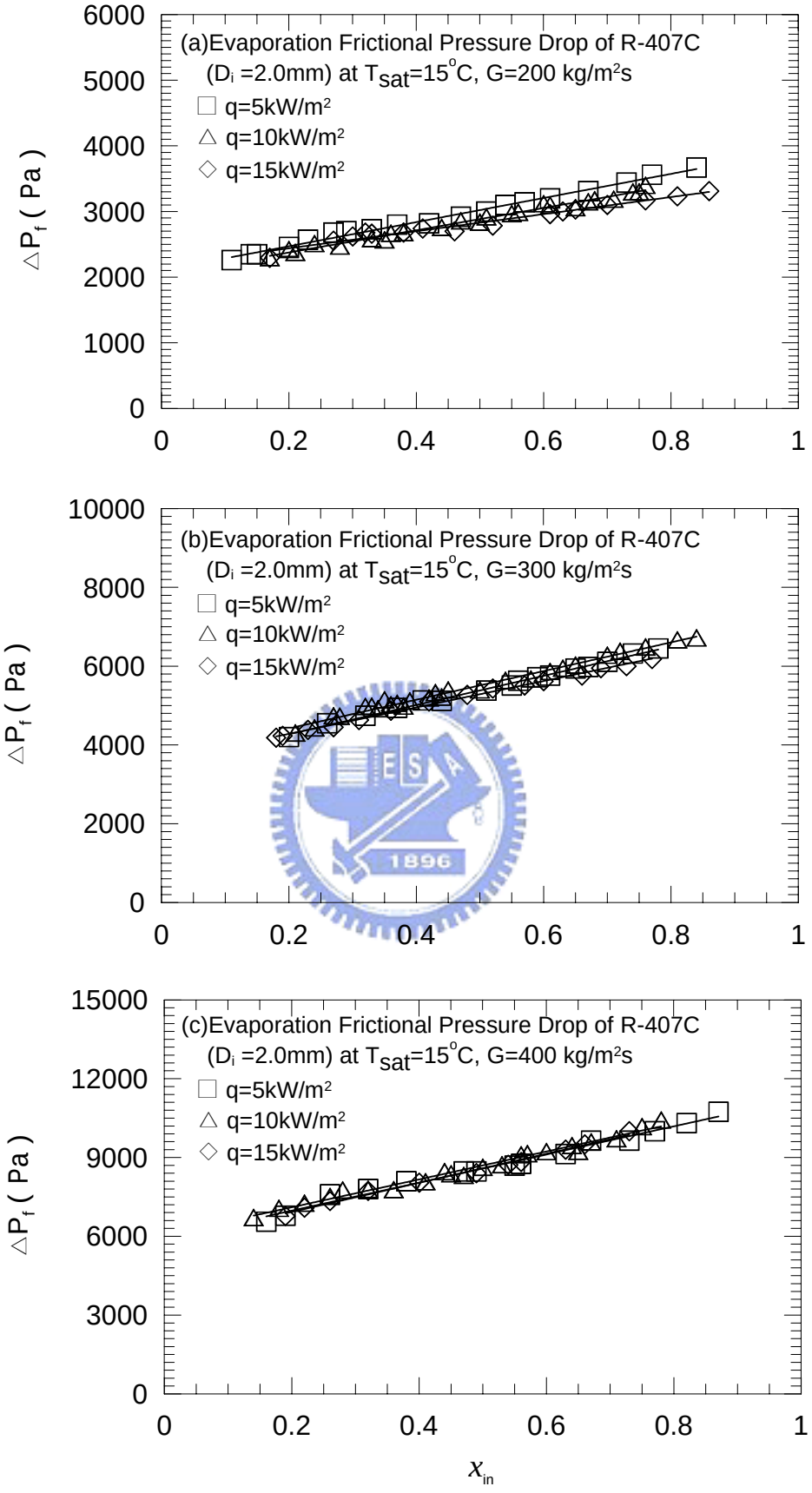

Fig. 5.18 Variations of R-407C frictional pressure drop with inlet vapor quality in 2.0-mm small tubes at T_{sat}=15℃ for various q for (a) G=200 kg/m^{2}s, (b) G=300 kg/m^{2}s, and (c) G=400 kg/m^{2}s.

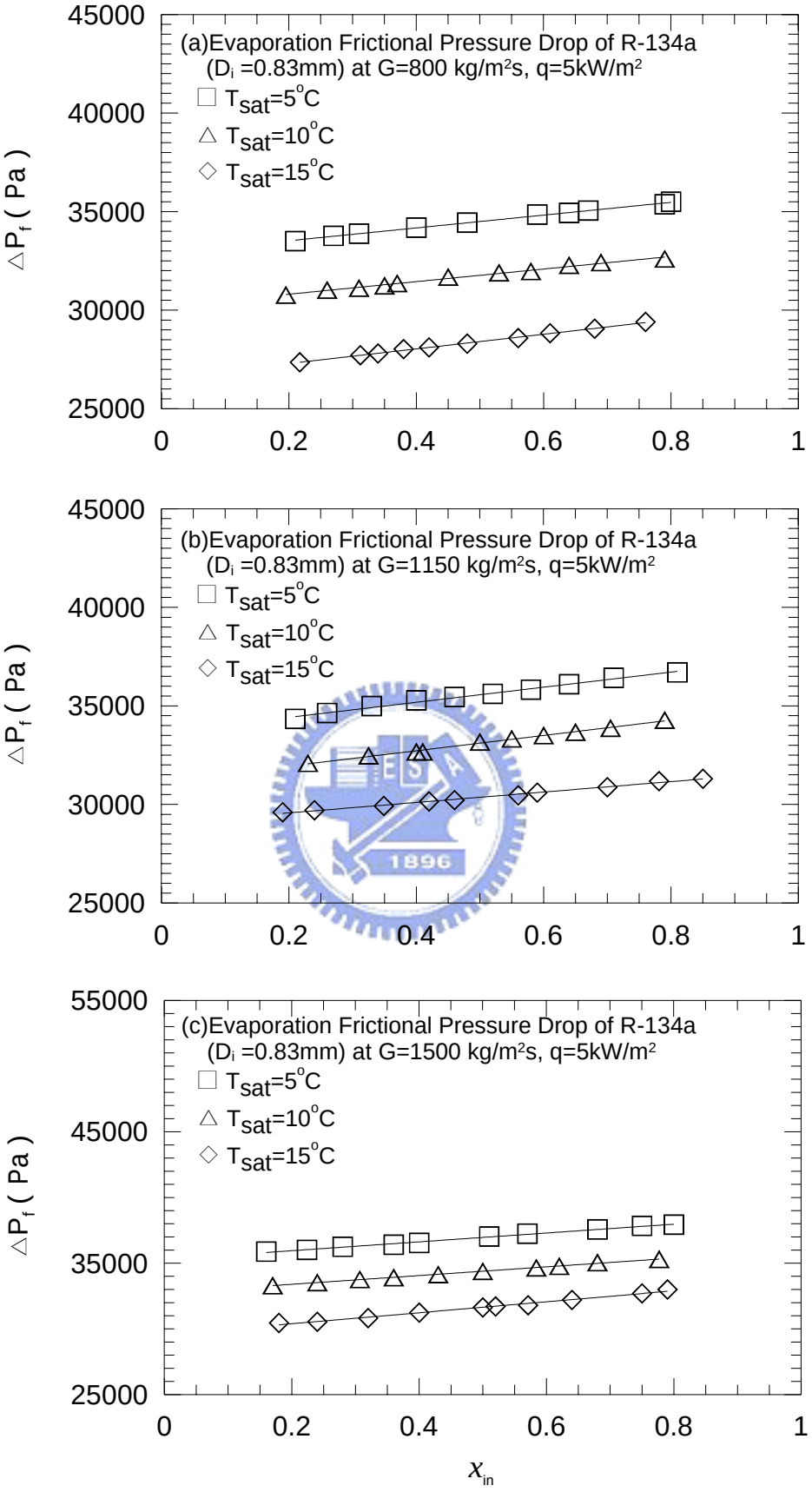

Fig. 5.19 Variations of R-134a frictional pressure drop with inlet vapor quality in 0.83-mm small tubes at q=5kW/m^2 for various T_{sat} for (a) G=800 kg/m^{2}s, (b) G=1150 kg/m^{2}s, and (c) G=1500 kg/m^{2}s.

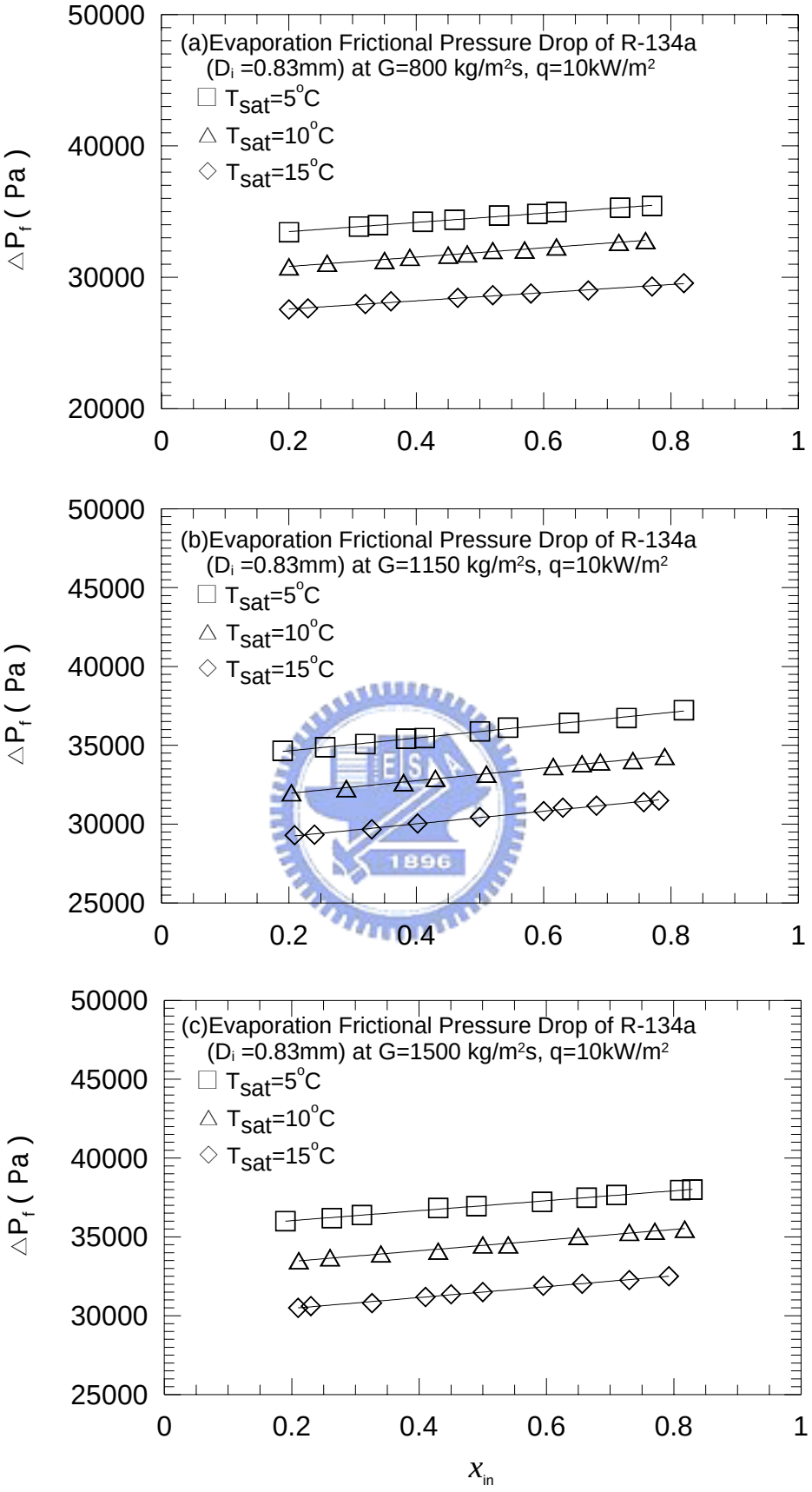

Fig. 5.20 Variations of R-134a frictional pressure drop with inlet vapor quality in 0.83-mm small tubes at q=10kW/m^2 for various T_{sat} for (a) G=800 kg/m^{2}s, (b) G=1150 kg/m^{2}s, and (c) G=1500 kg/m^{2}s.

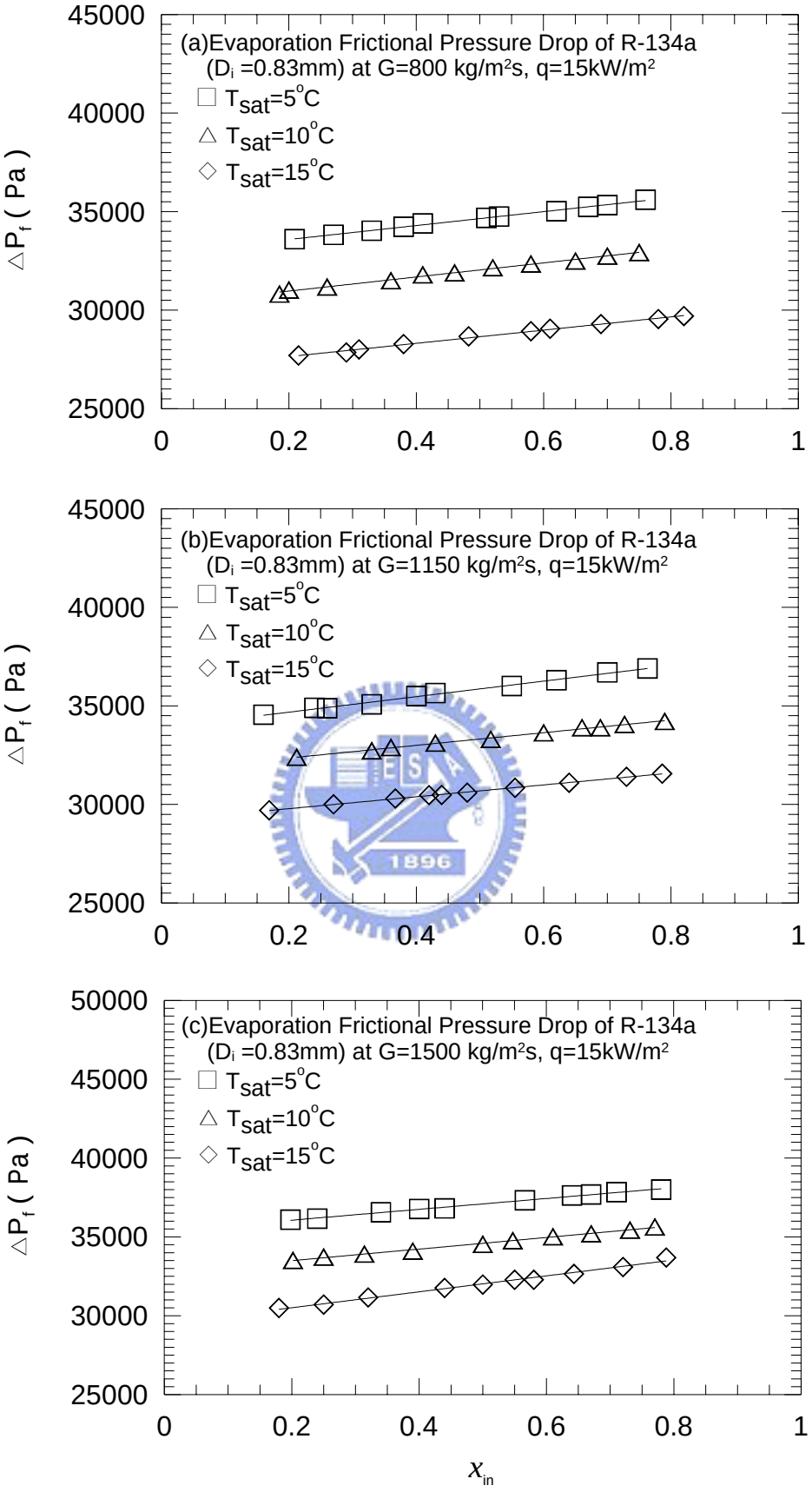

Fig. 5.21 Variations of R-134a frictional pressure drop with inlet vapor quality in 0.83-mm small tubes at q=15kW/m^2 for various T_{sat} for (a) G=800 kg/m^{2}s, (b) G=1150 kg/m^{2}s, and (c) G=1500 kg/m^{2}s.

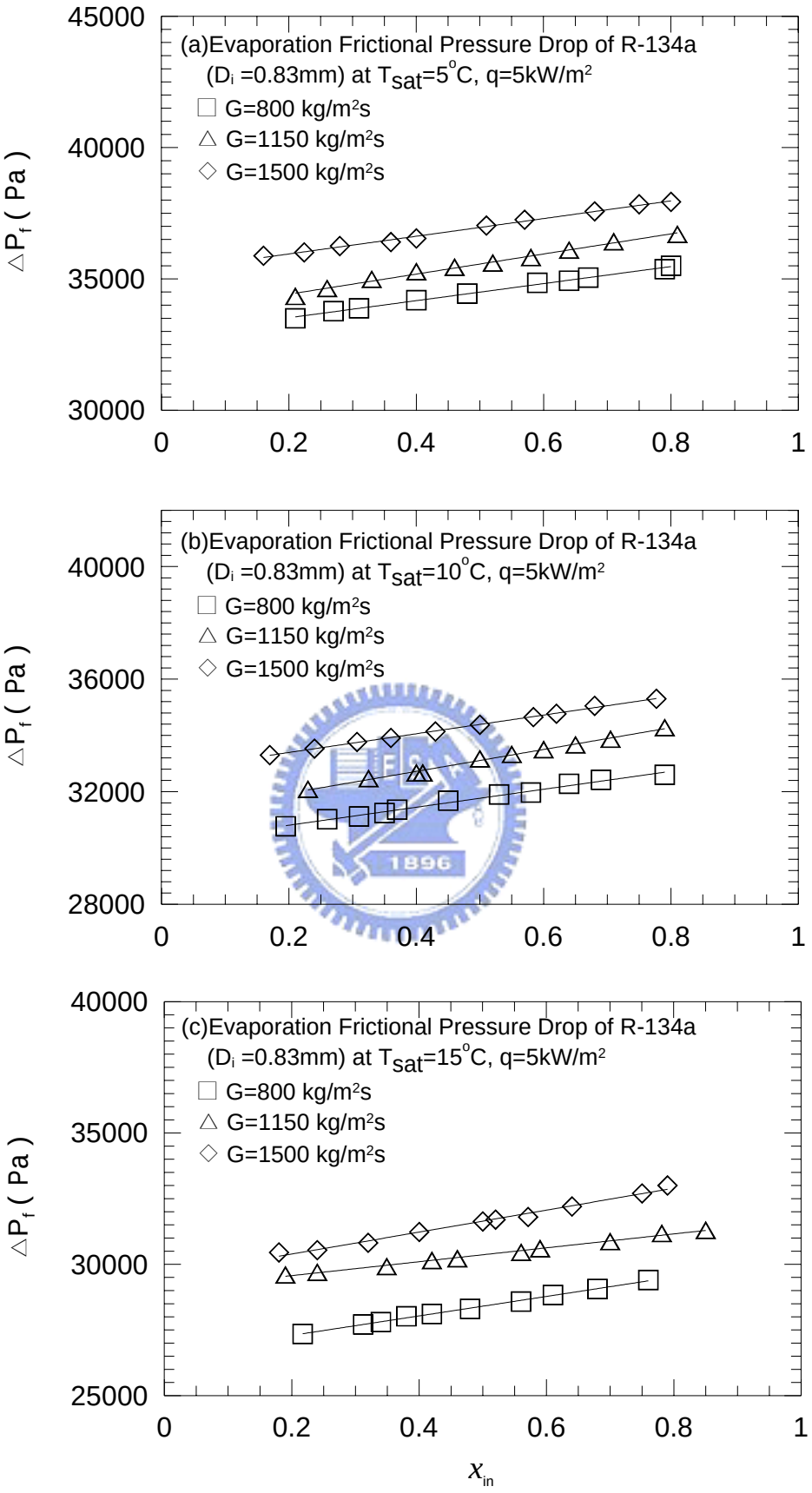

Fig. 5.22 Variations of R-134a frictional pressure drop with inlet vapor quality in 0.83-mm small tubes at q=5 kW/m^2 for various G for (a) T_{sat}=5℃, (b) T_{sat}=10 ℃, and (c) T_{sat}=15℃.

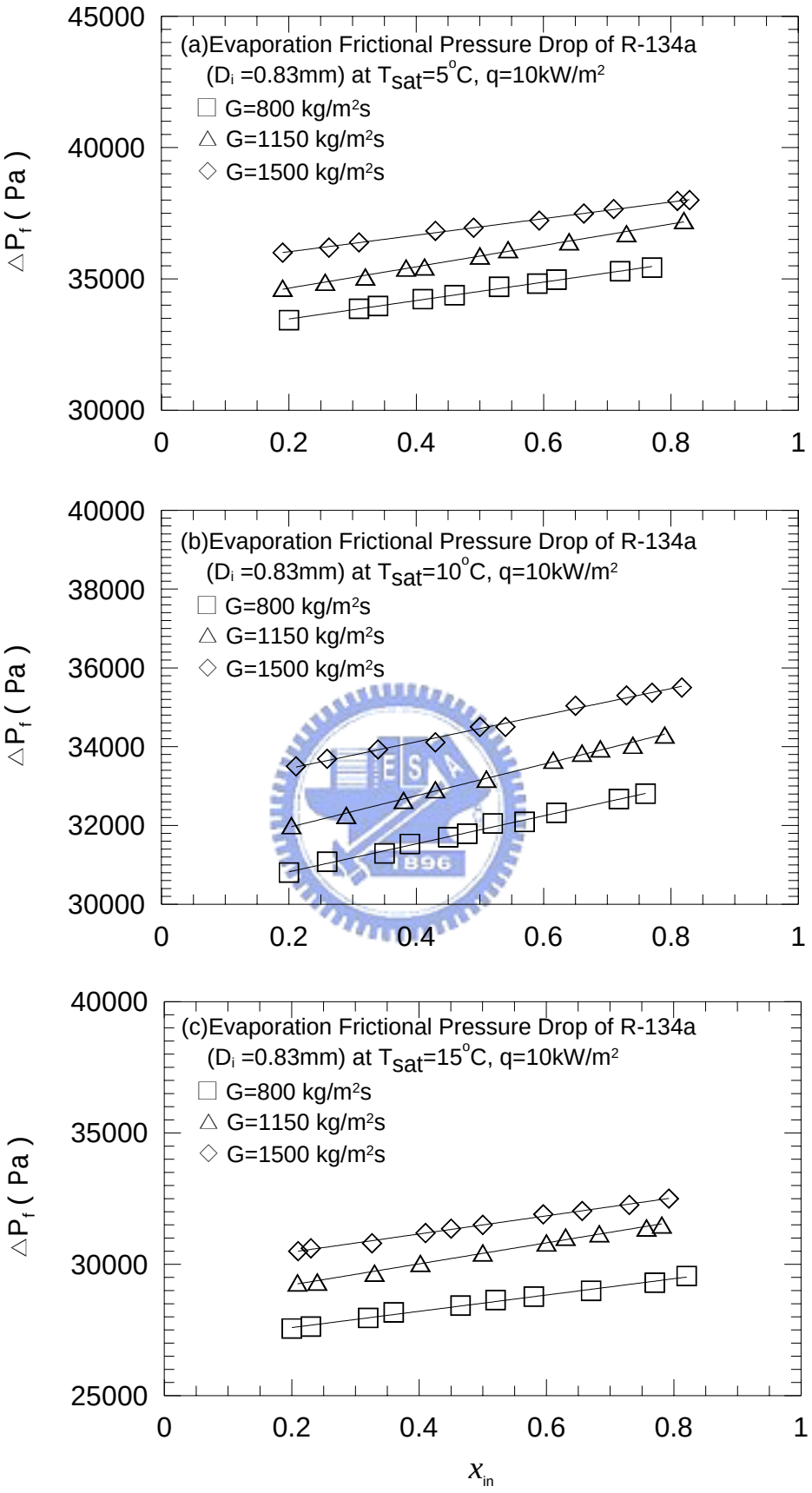

Fig. 5.23 Variations of R-134a frictional pressure drop with inlet vapor quality in 0.83-mm small tubes at q=10 kW/m^2 for various G for (a) T_{sat}=5℃, (b) T_{sat}=10 ℃, and (c) T_{sat}=15℃.

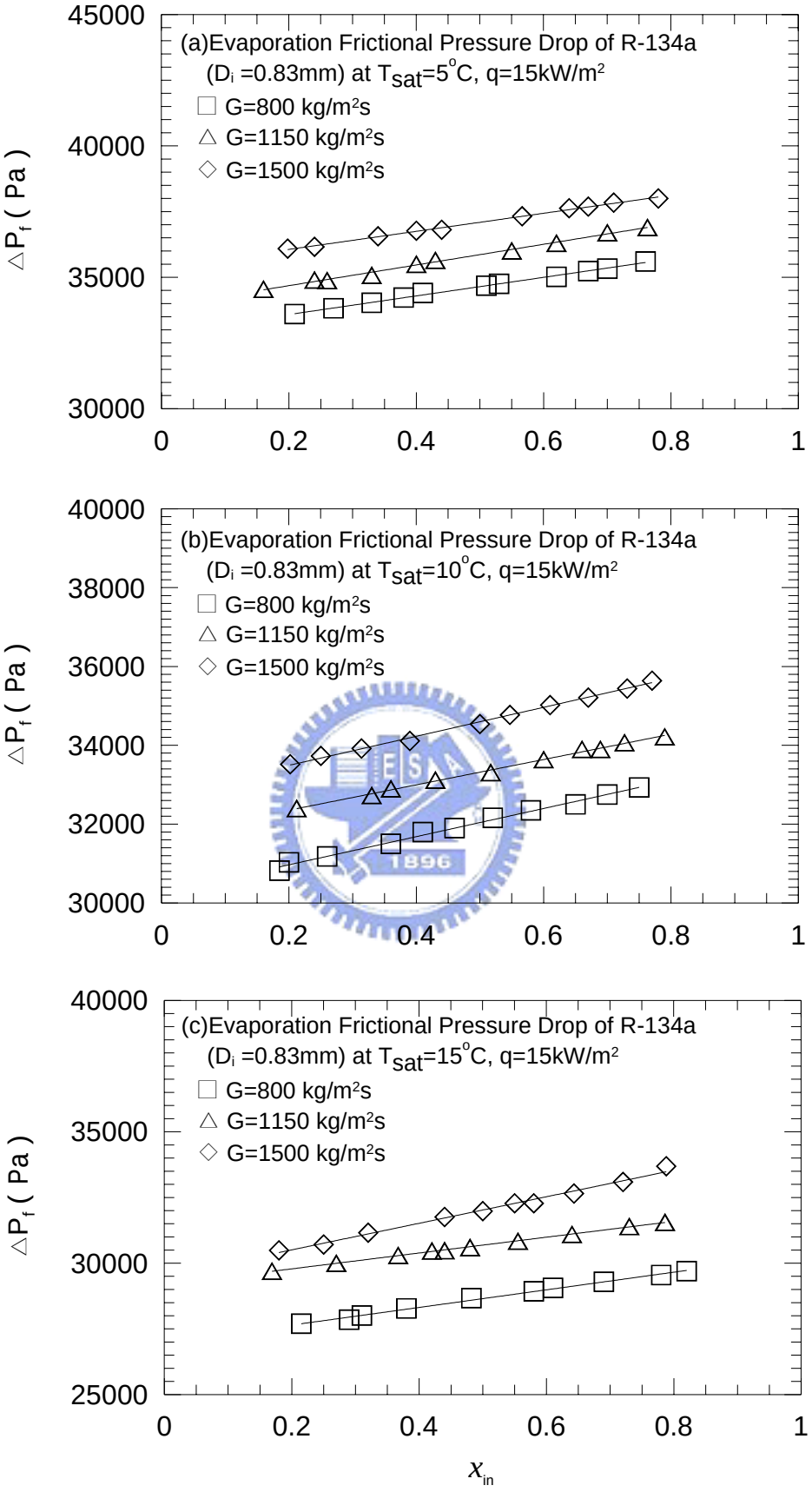

Fig. 5.24 Variations of R-134a frictional pressure drop with inlet vapor quality in 0.83-mm small tubes at q=15 kW/m^2 for various G for (a) T_{sat}=5℃, (b) T_{sat}=10 ℃, and (c) T_{sat}=15℃.

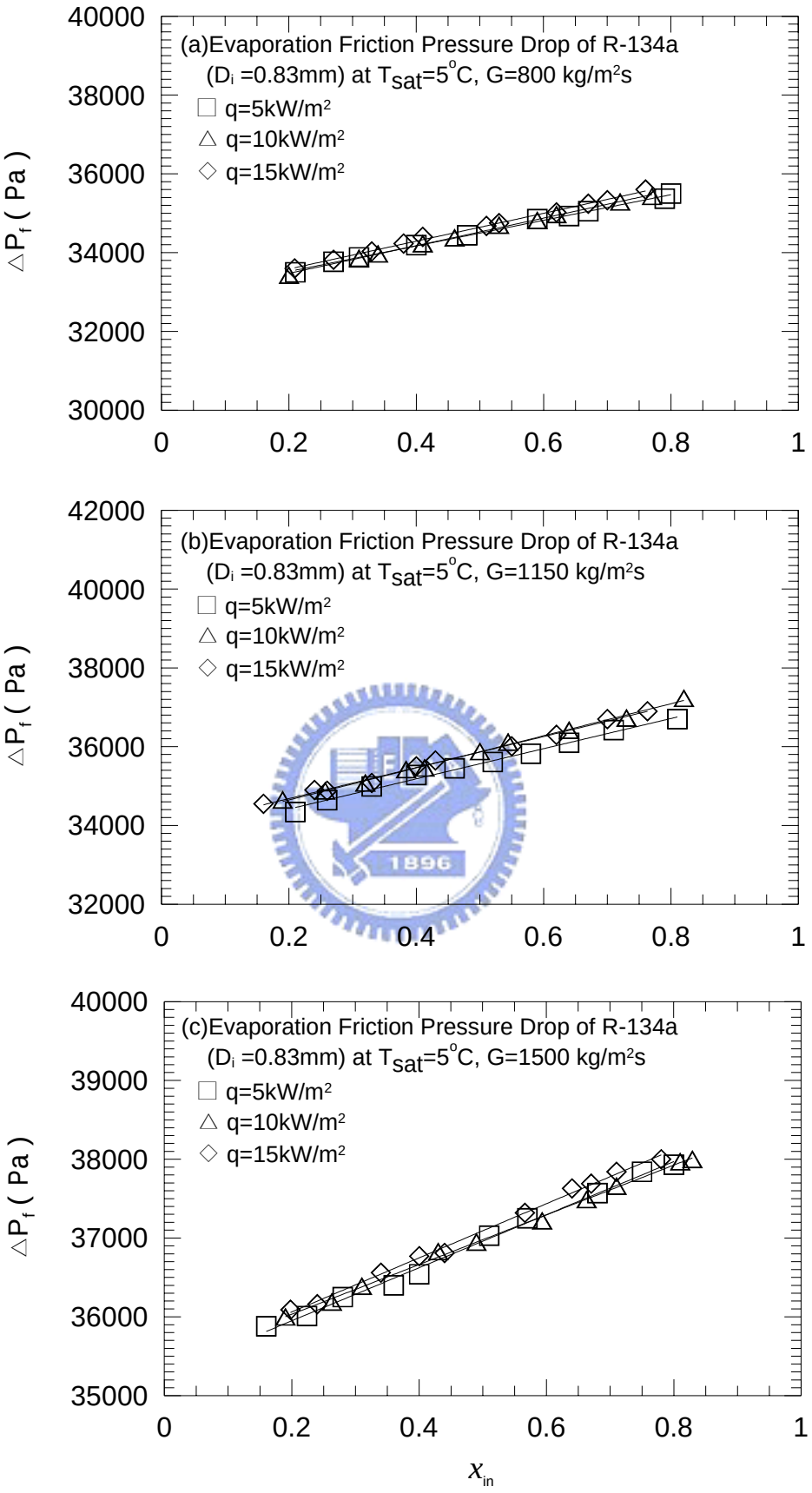

Fig. 5.25 Variations of R-134a frictional pressure drop with inlet vapor quality in 0.83-mm small tubes at T_{sat}=5°C for various q for (a) G=800 kg/m^{2}s, (b) G=1150 kg/m^{2}s, and (c) G=1500 kg/m^{2}s.

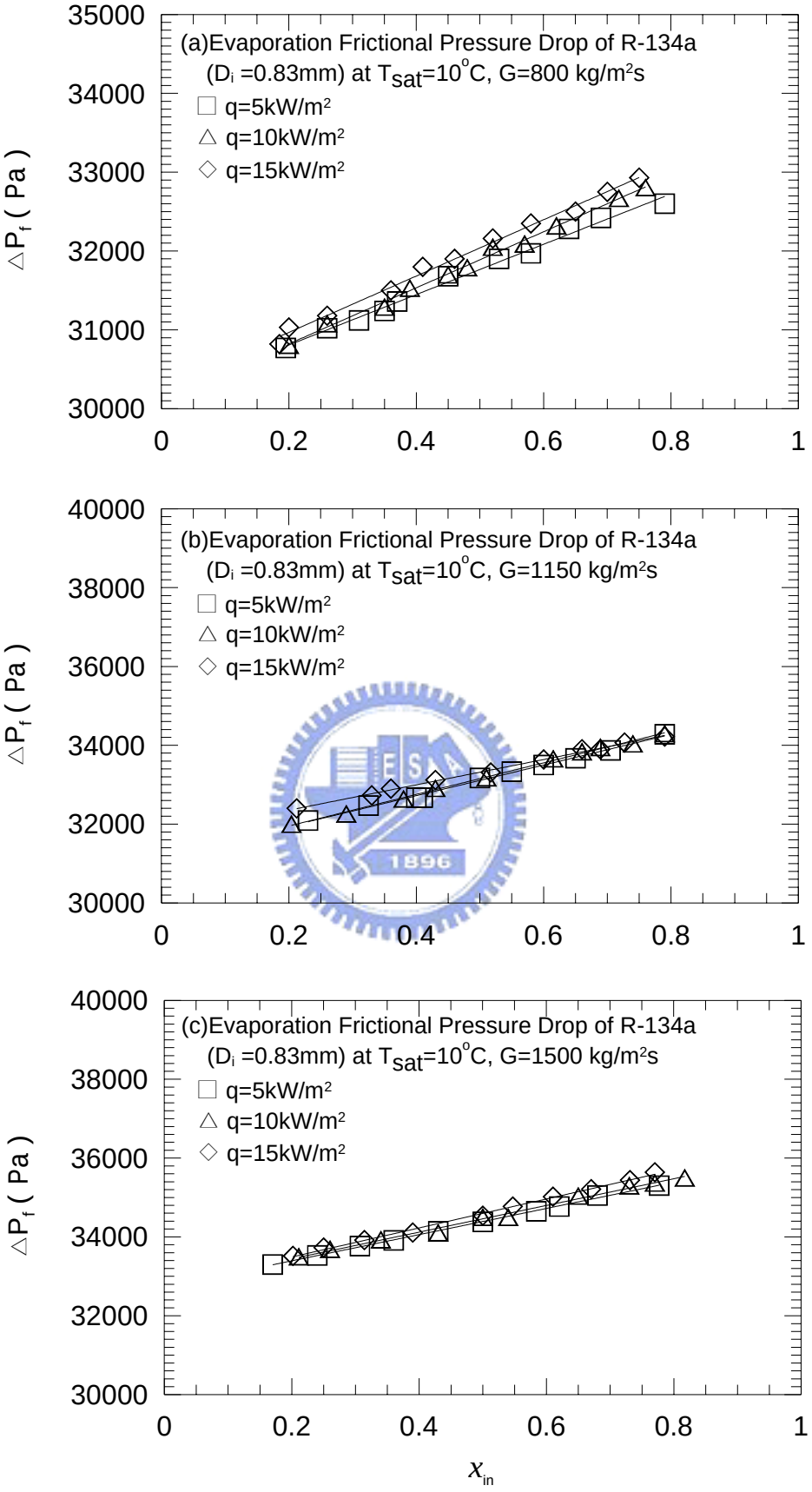

Fig. 5.26 Variations of R-134a frictional pressure drop with inlet vapor quality in 0.83-mm small tubes at T_{sat}=10℃ for various q for (a) G=800 kg/m^{2}s, (b) G=1150 kg/m^{2}s, and (c) G=1500 kg/m^{2}s.

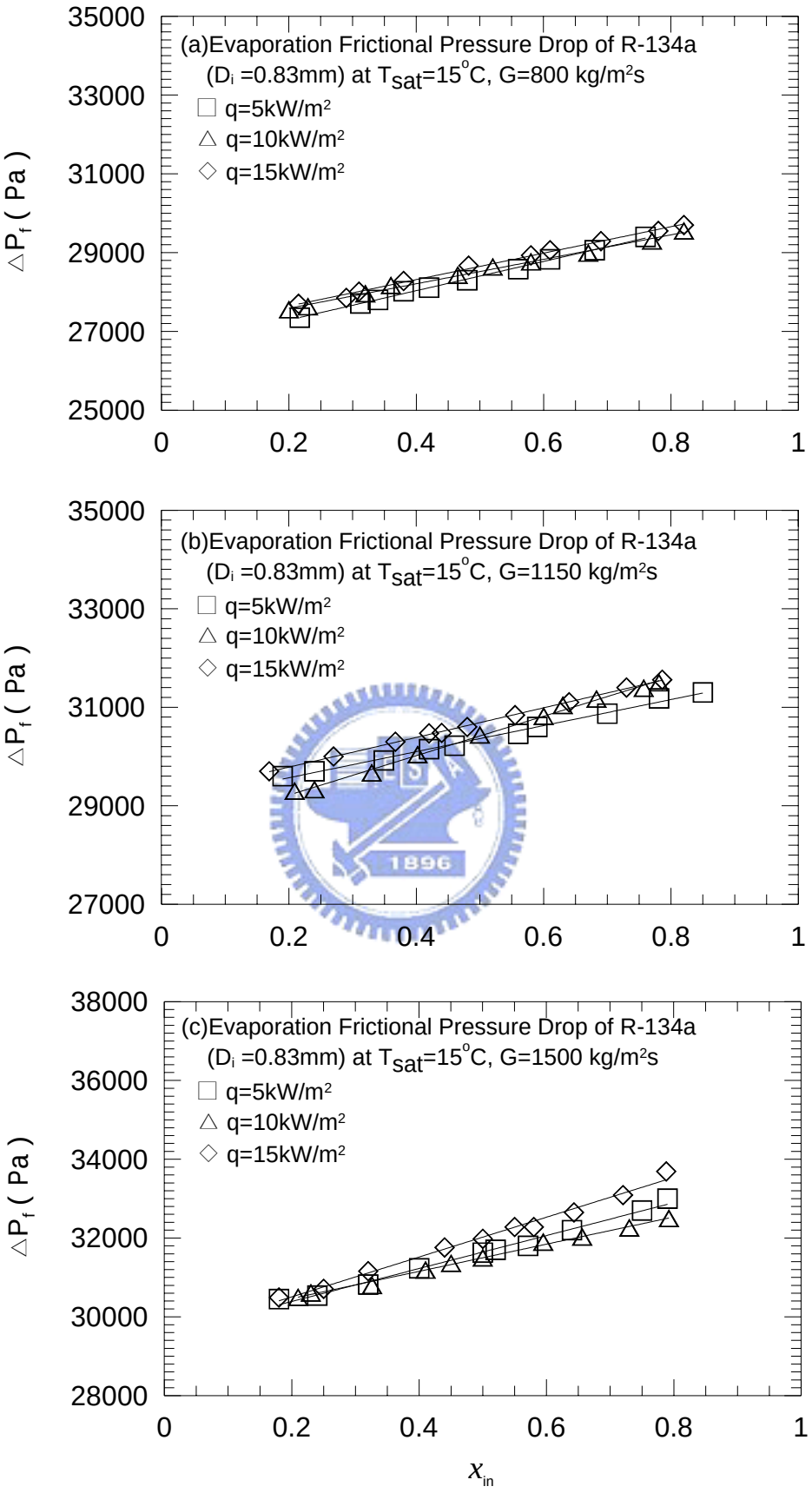

Fig. 5.27 Variations of R-134a frictional pressure drop with inlet vapor quality in 0.83-mm small tubes at T_{sat}=15℃ for various q for (a) G=800 kg/m^{2}s, (b) G=1150 kg/m^{2}s, and (c) G=1500 kg/m^{2}s.

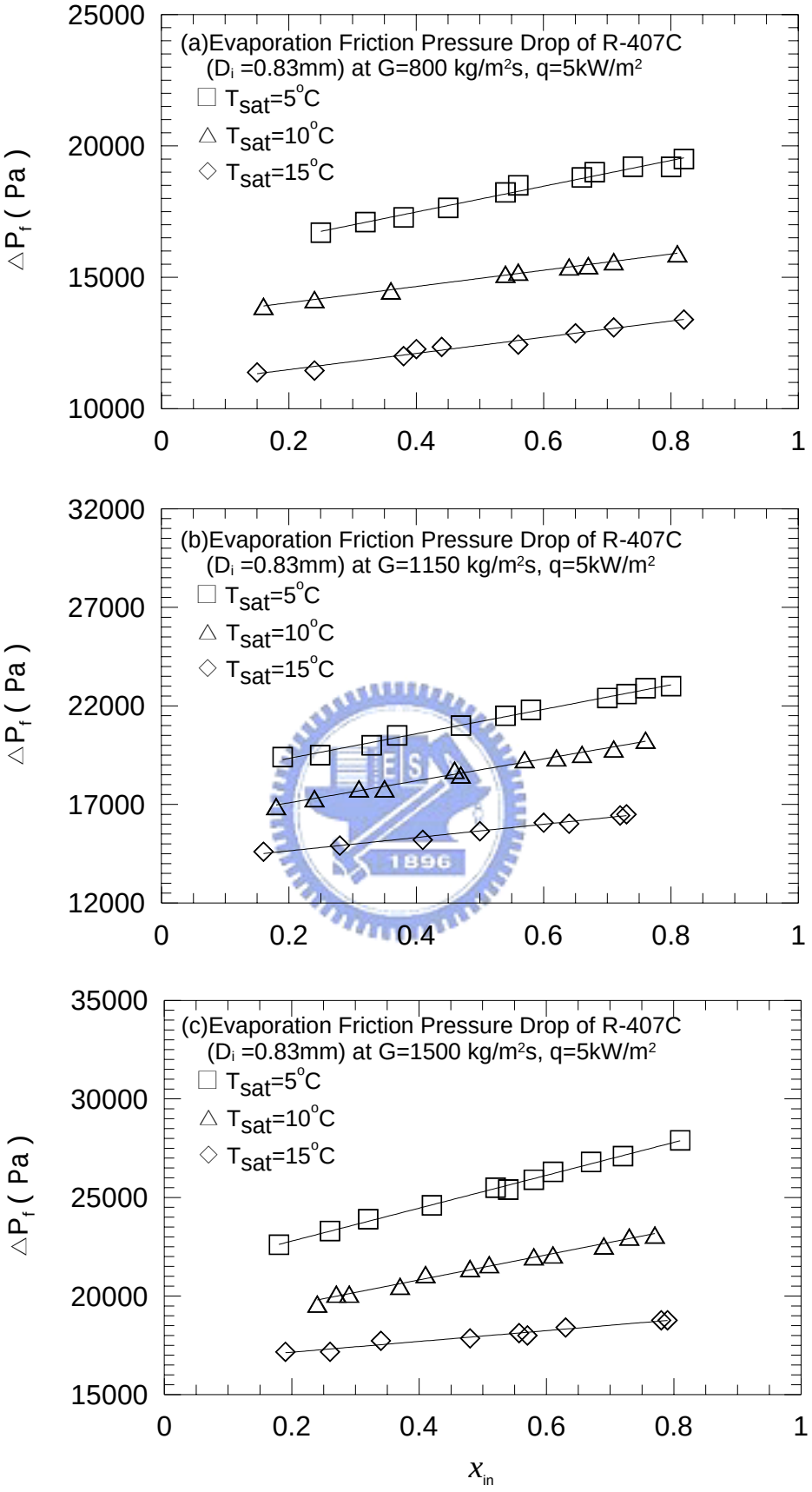

Fig. 5.28 Variations of R-407C frictional pressure drop with inlet vapor quality in 0.83-mm small tubes at q=5kW/m^2 for various T_{sat} for (a) G=800 kg/m^{2}s, (b) G=1150 kg/m^{2}s, and (c) G=1500 kg/m^{2}s.

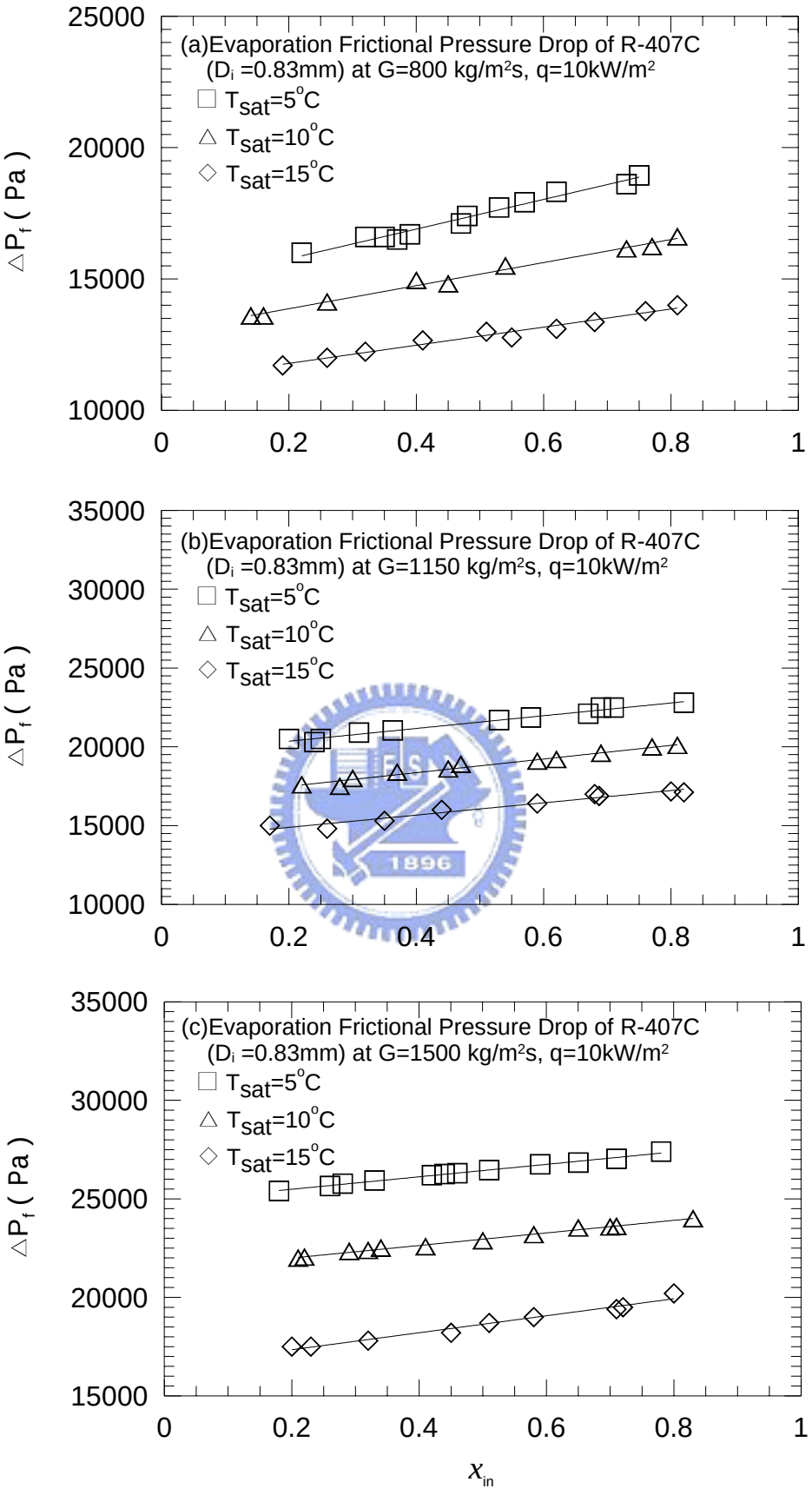

Fig. 5.29 Variations of R-407C frictional pressure drop with inlet vapor quality in 0.83-mm small tubes at q=10kW/m^2 for various T_{sat} for (a) G=800 kg/m^{2}s, (b) G=1150 kg/m^{2}s, and (c) G=1500 kg/m^{2}s.

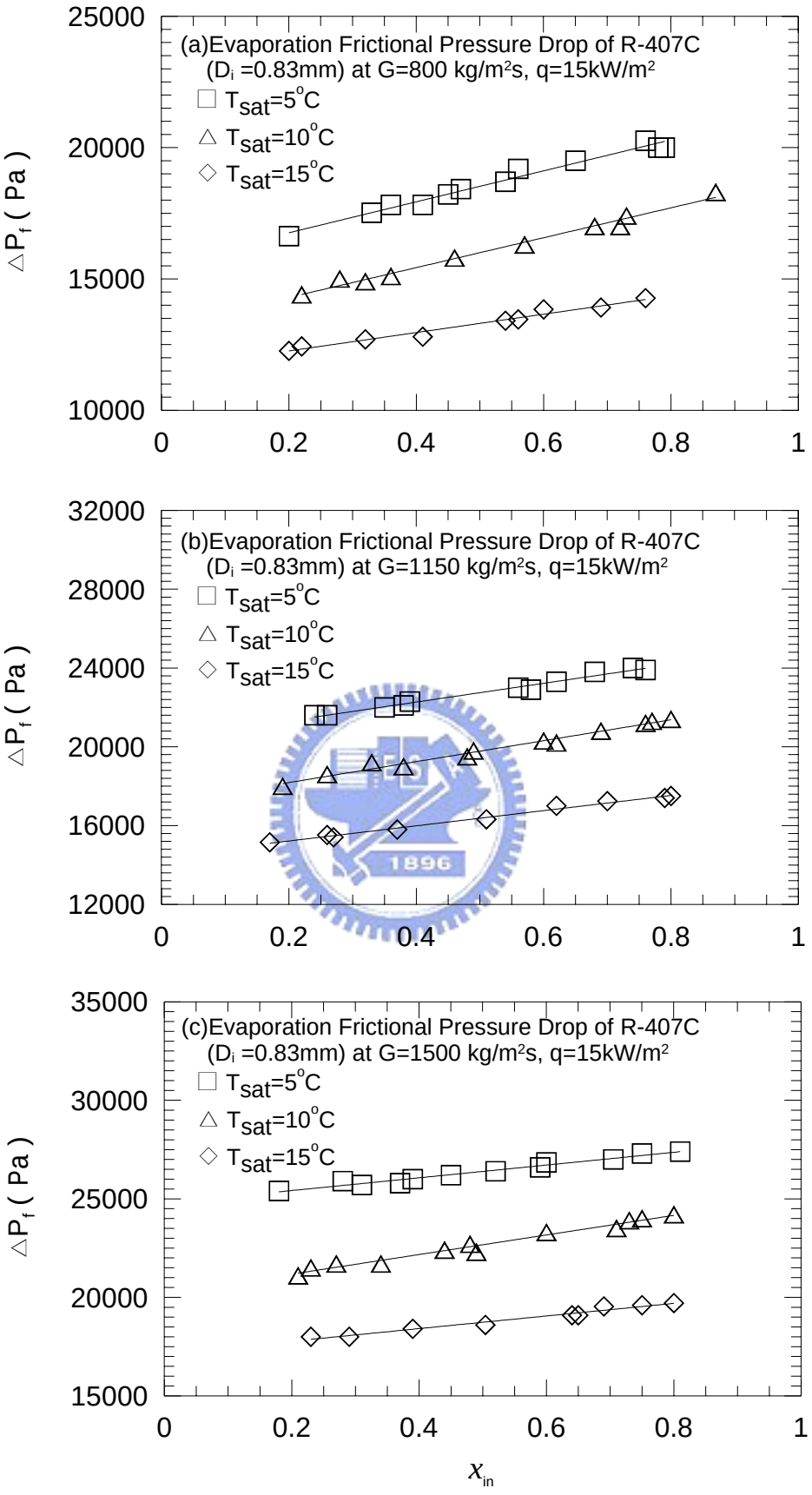

Fig. 5.30 Variations of R-407C frictional pressure drop with inlet vapor quality in 0.83-mm small tubes at q=15kW/m^2 for various T_{sat} for (a) G=800 kg/m^{2}s, (b) G=1150 kg/m^{2}s, and (c) G=1500 kg/m^{2}s.

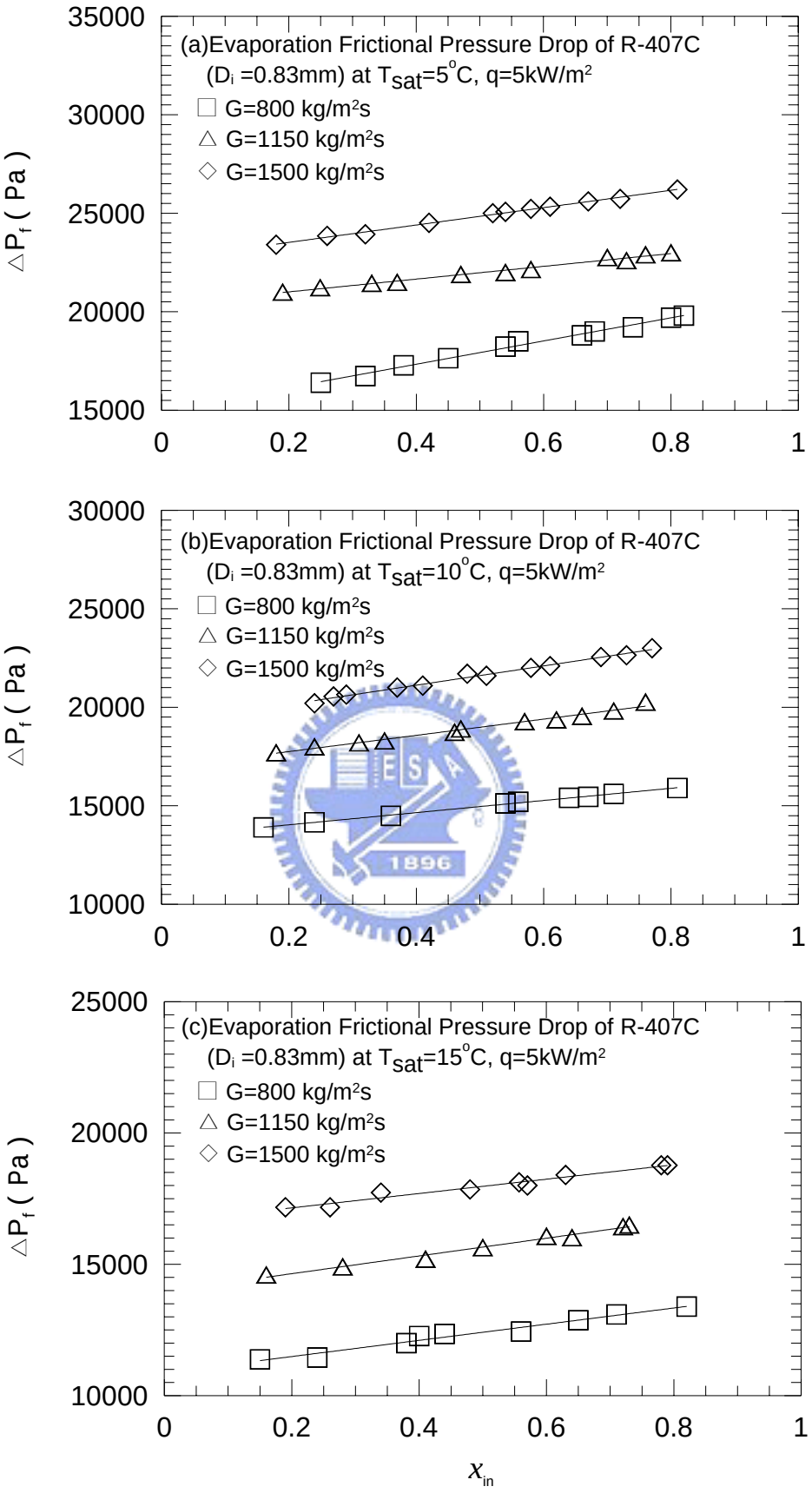

Fig. 5.31 Variations of R-407C frictional pressure drop with inlet vapor quality in 0.83-mm small tubes at q=5 kW/m^2 for various G for (a) T_{sat}=5℃, (b) T_{sat}=10 ℃, and (c) T_{sat}=15℃.

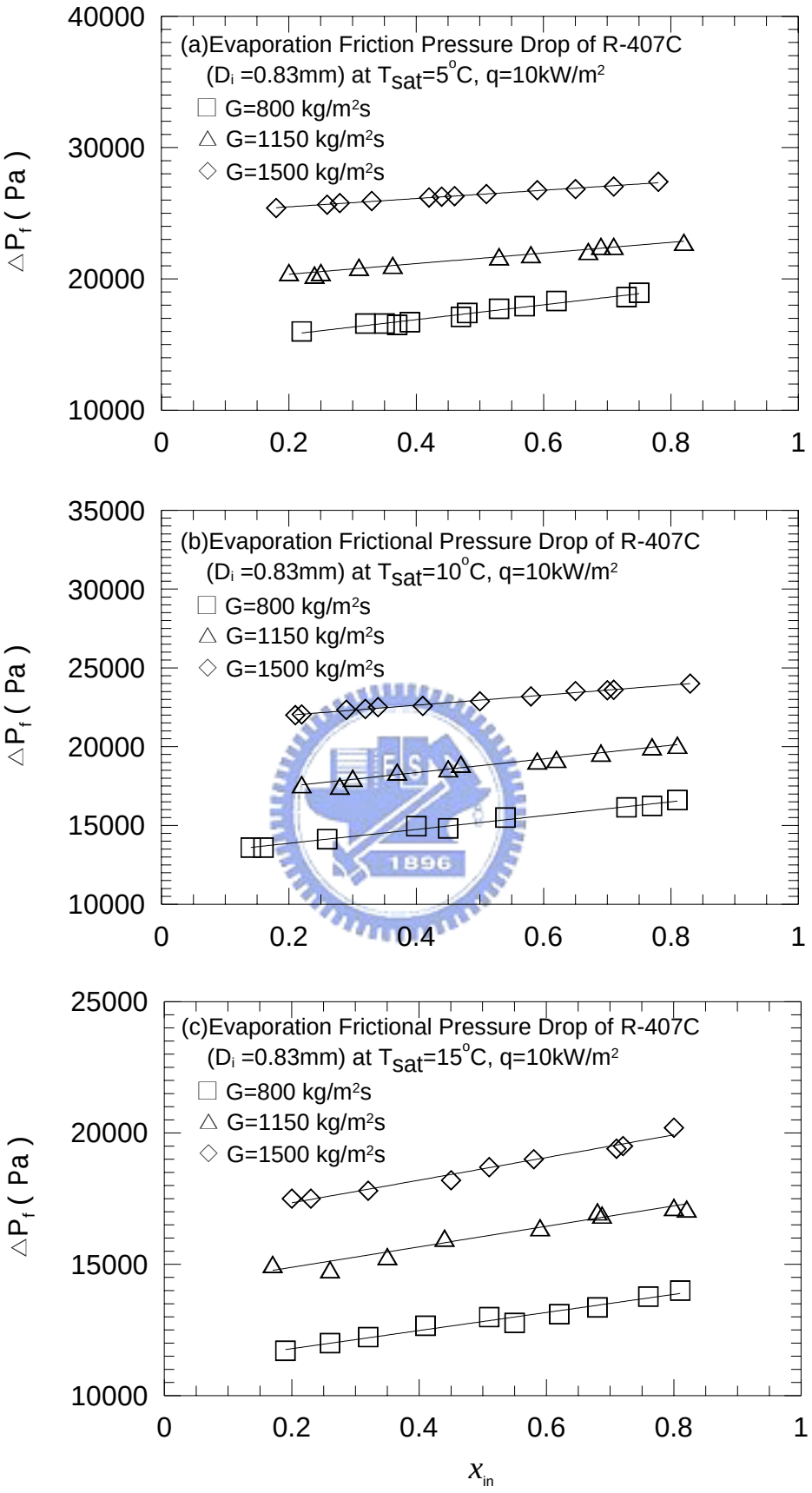

Fig. 5.32 Variations of R-407C frictional pressure drop with inlet vapor quality in 0.83-mm small tubes at q=10 kW/m^2 for various G for (a) T_{sat}=5℃, (b) T_{sat}=10 ℃, and (c) T_{sat}=15℃.

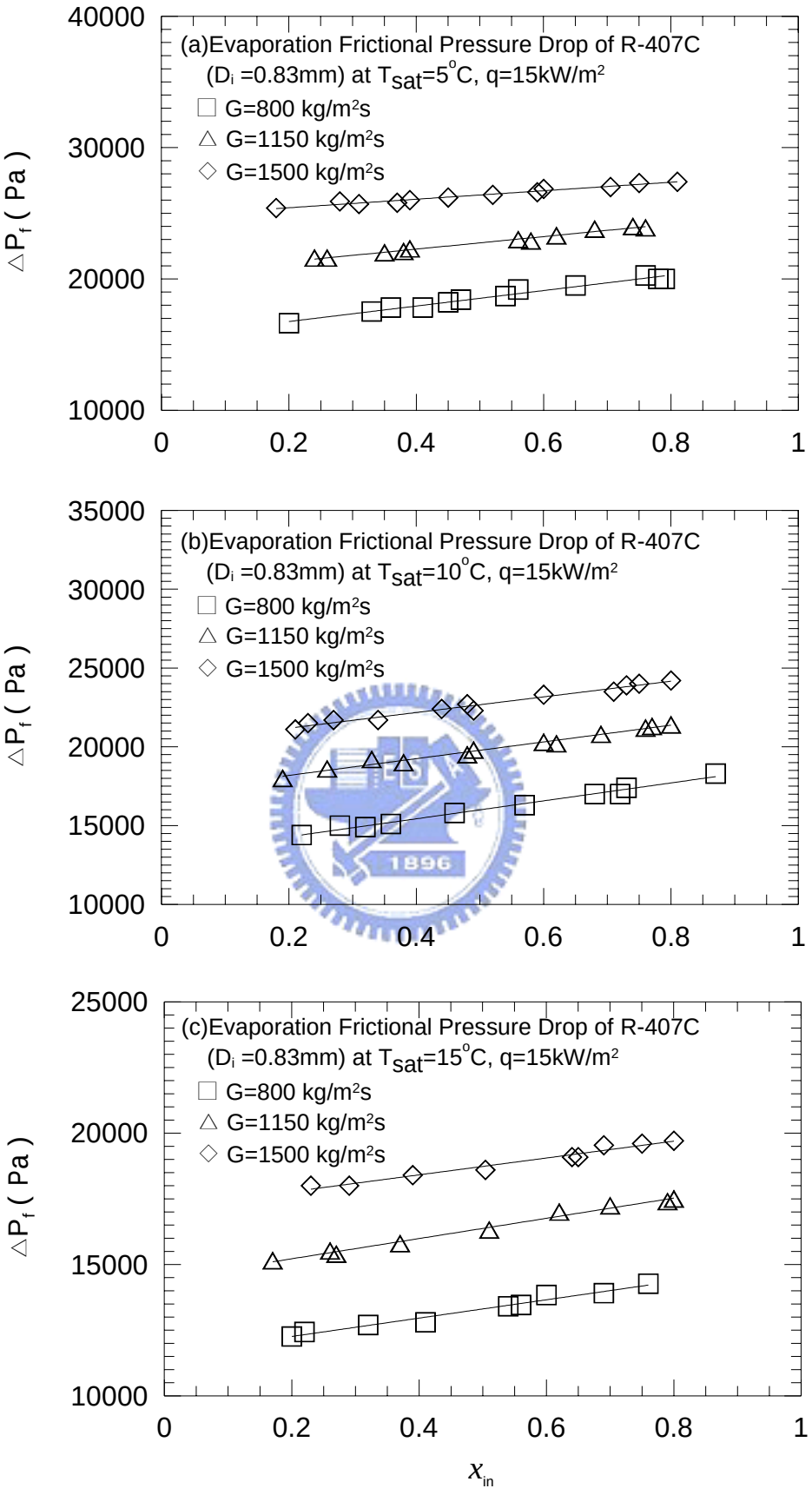

Fig. 5.33 Variations of R-407C frictional pressure drop with inlet vapor quality in 0.83-mm small tubes at q=15 kW/m^2 for various G for (a) T_{sat}=5℃, (b) T_{sat}=10 ℃, and (c) T_{sat}=15℃.

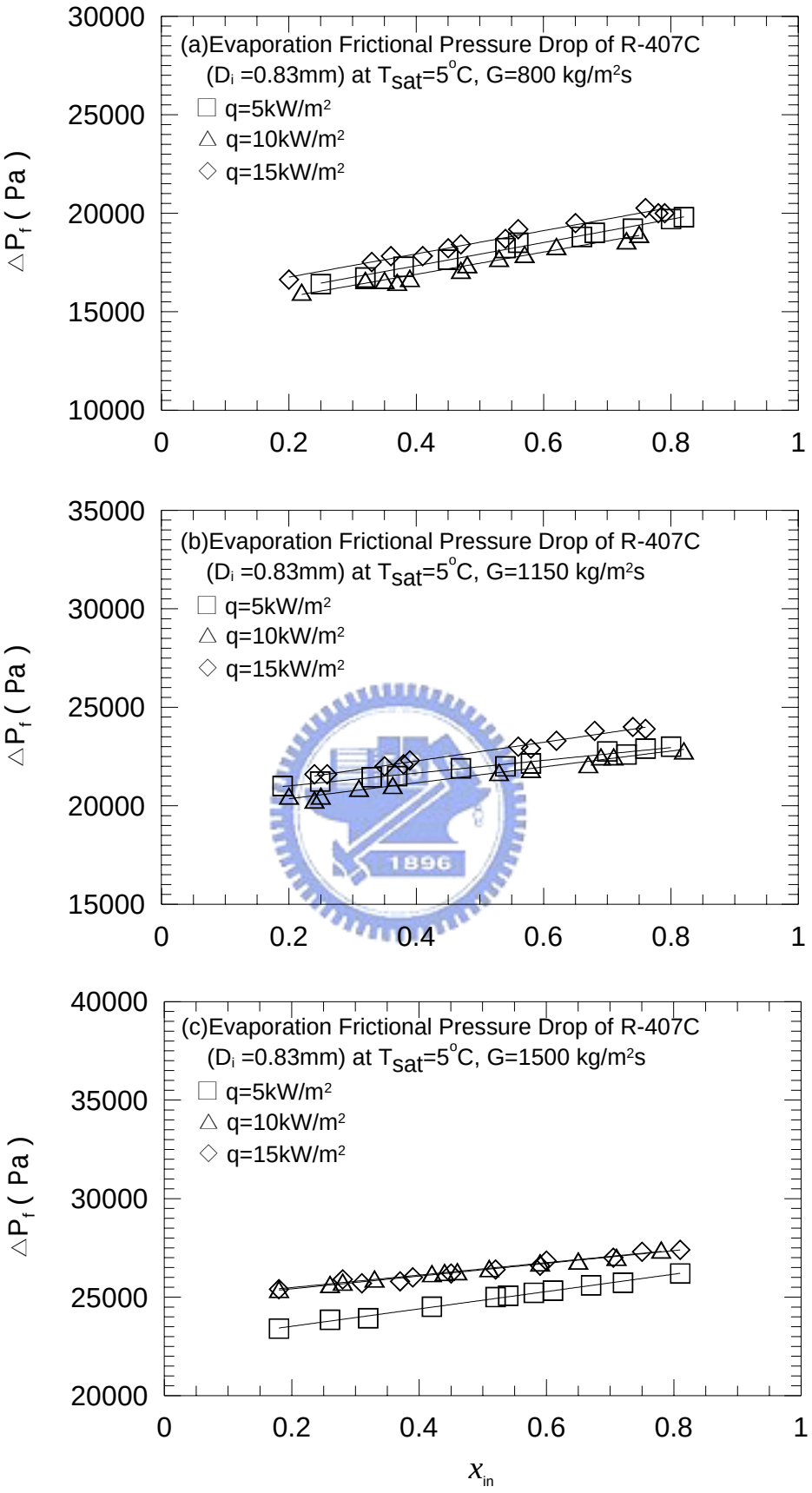

Fig. 5.34 Variations of R-407C frictional pressure drop with inlet vapor quality in 0.83-mm small tubes at T_{sat}=5°C for various q for (a) G=800 kg/m^{2}s, (b) G=1150 kg/m^{2}s, and (c) G=1500 kg/m^{2}s.

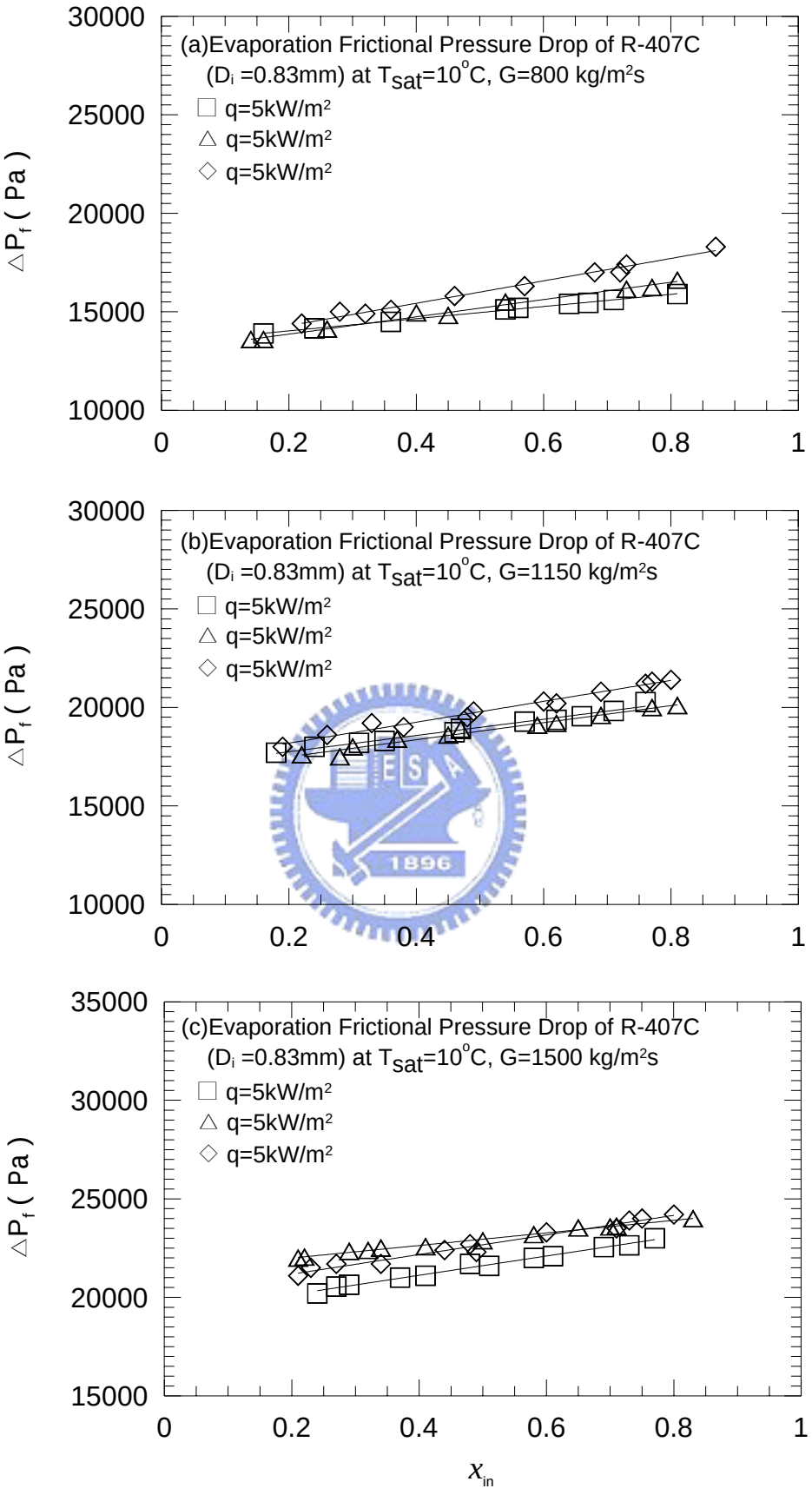

Fig. 5.35 Variations of R-407C frictional pressure drop with inlet vapor quality in 0.83-mm small tubes at T_{sat}=10℃ for various q for (a) G=800 kg/m^{2}s, (b) G=1150 kg/m^{2}s, and (c) G=1500 kg/m^{2}s.

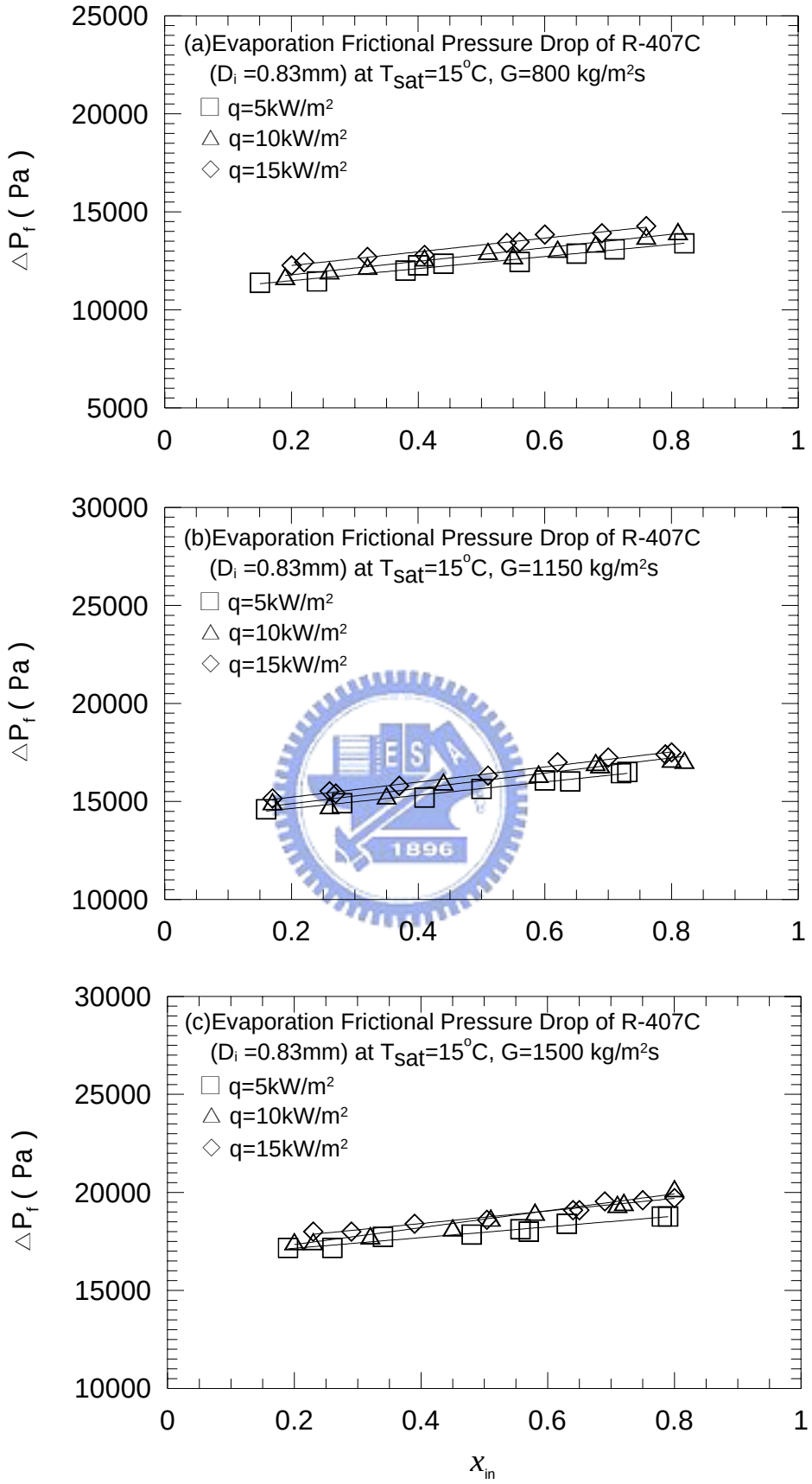

Fig. 5.36 Variations of R-407C frictional pressure drop with inlet vapor quality in 0.83-mm small tubes at T_{sat}=15℃ for various q for (a) G=800 kg/m^{2}s, (b) G=1150 kg/m^{2}s, and (c) G=1500 kg/m^{2}s.

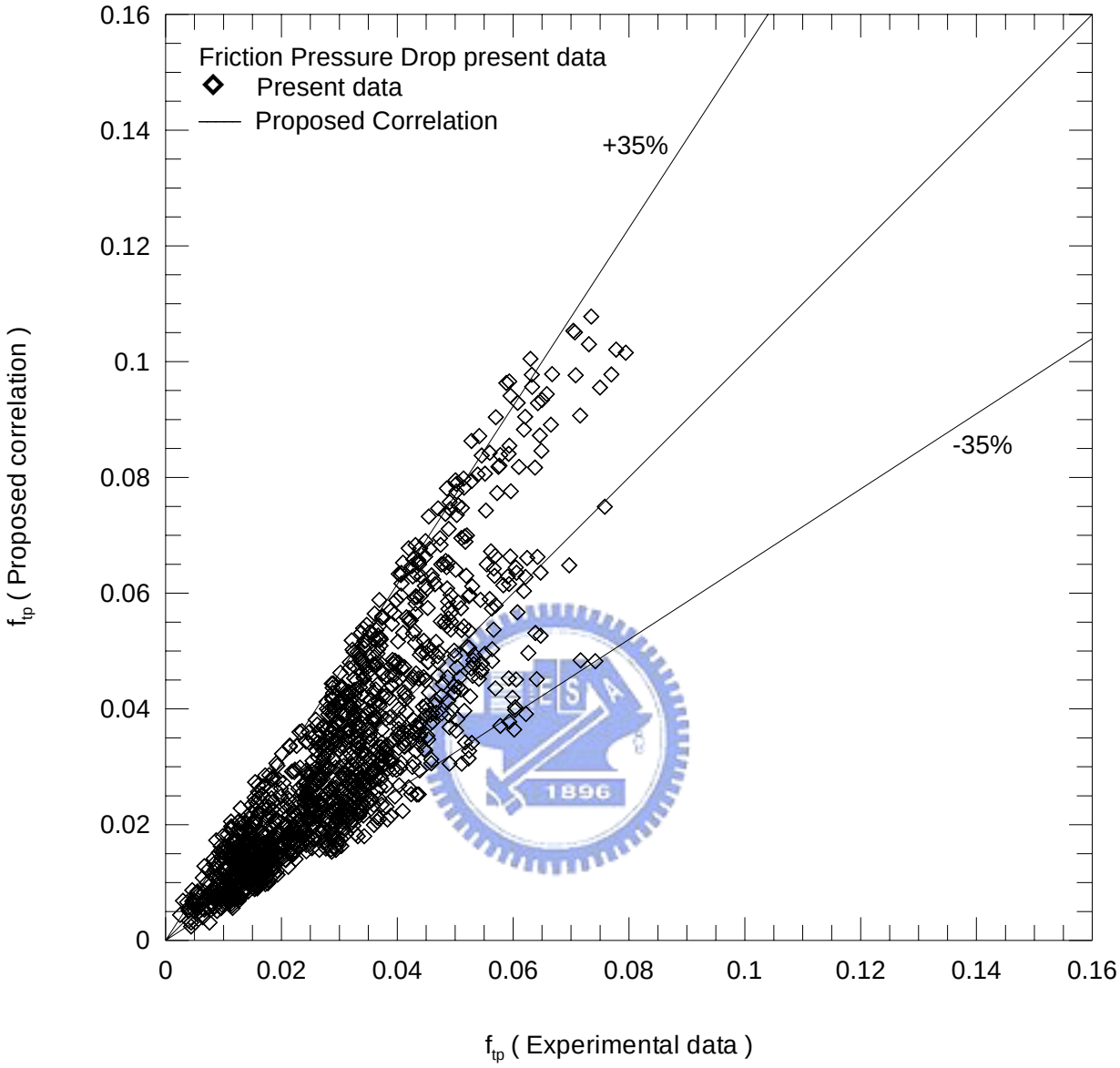

Fig. 5.37 Comparison of the measured data for frictional pressure drop coefficient in the evaporation of R-134a and R-407 in 0.83-mm and 2.0-mm small tubes with the proposed correlation.

CHAPTER 6

CONCLUDING REMARKS

In this study, we have experimentally measured the heat transfer coefficient and pressure drop for the R-134a and R-407C evaporation in the small circular tubes (D_i=0.83 & 2.0 mm). The influences of the refrigerant mass flux, heat flux, saturated temperature and vapor quality on the evaporation heat transfer and frictional pressure drop have been investigated in detail. The major results obtained here can be briefly summarized as follows.

(1). Both the R-134a and R-407C evaporation heat transfer coefficients and frictional pressure drops increase significantly with the mass flux and vapor quality except at low mass fluxes. A rise in the imposed heat flux results in a significant increase in the evaporation heat transfer coefficient for both R-134a and R-407C except at low heat fluxes. Nevertheless the influence of the imposed heat flux on the frictional pressure drop is rather slight. The increase in the saturated temperature of R-134a & R-407C results in a smaller increase in the evaporation heat transfer coefficient when compared that due to a rise in the mass flux. But the trend in the frictional pressure drop is opposite. The decrease in the R-134a & R-407C saturated temperature results in a noticeable increase in the frictional pressure drop. It is worth to note that for R-134a evaporation in the smaller tubes with D_i=0.83 mm partial dryout of the refrigerant can occur at high vapor quality, causing the evaporation heat transfer coefficient to decline at increasing quality. We also note that R-407C has higher latent heat of vaporization, higher thermal conductivity and lower viscosity than R-134a. Thus the evaporation heat transfer coefficient for R-407C is somewhat higher than that for R-134a. In the mean time the R-407C frictional pressure drop is

significantly lower.

(2). For the refrigerant vapor quality ranging from 0.2 to 0.8 the void fraction in the tube is high and heat transfer in the refrigerant flow is considered to be dominated by the vaporization of thin liquid film at the vapor-liquid interface. Therefore the refrigerant mass flux, saturated temperature, vapor quality and imposed heat flux all exhibit pronounced effects on the evaporation heat transfer coefficient in both the 2.0-mm and 0.83-mm tubes.

(3). Empirical correlations for the heat transfer coefficient and friction factor for the R-134a and R-407C evaporation in 0.83-mm and 2.0-mm small tubes were provided.

REFERENCES

1. V. Havelsky, Investigation of refrigeranting system with R12 refrigerant replacements, applied thermal engineering 20 (2) (2000) 133-140.
2. S. S. Mehenendale, A. M. Jacobi, and R. K. Shah, Fluid flow and heat transfer at micro- and meso-scale with application to heat exchanger design, Appl. Mech. Rev. 53 (2000) 175-193.
3. S. G. Kandlikar, Fundamental issues related to flow boiling in minichannels and microchannels, Experimental Thermal and Fluid Science 26 (2-4) (2000) 389-407.
4. X. F. Peng, B. X. Wang, G. P. Peterson and H. B. Ma, Experimental investigation of heat transfer in flat plates with rectangular microchannels, Int. J. heat Mass Transfer 38 (1) (1995) 127-137.
5. X. F. Peng and G. P. Peterson, Convective heat transfer and flow friction for water flow in microchannel structures, Int. J. Heat Mass Transfer 39 (12) (1996) 2599-2608.
6. B. Agostini, B. Watel, A. Bontemps and B. Thonon, Friction factor and heat transfer coefficient of R134a liquid flow in mini-channels, Applied Thermal Engineering 22 (16) (2002) 1821-1834.
7. Shah and London, Laminar Flow Forced Convection in Ducts, Acdemic Press, 1978.
8. V. Gnielinski, New equations for heat and mass transfer in turbulent pipe and channel flow, International Chemical Engineering 16 (2) (1976) 359-368.
9. F. W. Dittus, L. M. K. Boelter, Heat transfer in automobile radiator of the tube type, Publication in Engineering, University of California, Berkley, (2) (1930) 250.
10. W. Yu, D. M. France, M. W. Wambsganss and J. R. Hull, Two-phase pressure drop, boiling heat transfer, and critical heat flux to water in a small-diameter horizontal tube, International Journal of Multiphase Flow 28 (6) (2002) 927-941.
11. B. Sumith, F. Kaminaga and Kunihito Matsumura, Saturated flow boiling of water in a vertical small diameter tube, Experimental Thermal and Fluid Science 27 (7) (2003) 789-801.
12. Y. Y. Yan and T. F. Lin, Evaporation heat transfer and pressure drop of refrigerant R-134a in a small pipe, International Journal of Heat Transfer 41 (24) (1998) 4183-4194.
13. Y. Y. Yan and T. F. Lin, Reply to Prof. R.L. Webb's and Dr. J.W. Paek's comments, International Journal of Heat Transfer 46 (6) (2003) 1111-1113.
14. V. G. Nino, P. S. Hrnjak and T. A. Newell, Two-phase flow visualization of

R-134a in a multiport microchannel tube, Heat Transfer Engineering 24 (1) (2003) 41-52.

15. Y. Fujita, Y. Yang, N. Fujita, Flow boiling heat transfer and pressure drop in uniformly heated small tubes, Proceedings of the Twelfth International Heat Transfer Conference 3 (2002) 743-748.
16. G. M. Lazarek and S. H. Black, Evaporative heat transfer, pressure drop and critical heat flux in a small vertical tube with R-113, Int. J. Heat Mass Transfer 25 (7) (1982) 945-960.
17. S. Lin, P. A. Kew and K. Cornwell, Two-phase heat transfer to a refrigerant in a 1 mm diameter tube, International Journal of Refrigeration 24 (1) (2001) 51-56.
18. S. Lin, P. A. Kew and K. Cornwell, Flow boiling of refrigerant R141b in small tubes, Chemical Engineering Research & Design 79 (A4) (2001) 417-424.
19. K. Cornwell and P. A. Kew, Boiling in small parallel channels, in: Proc. of the Internat. Conf. on Energy Efficiency in Process Technology, Elsevier Applied Science, Athens, Greece, 1992, pp. 624-638.
20. P. A. Kew and K. Cornwell, Correlations for the prediction of boiling heat transfer in small-diameter channels, Applied Thermal Engineering 17 (8-10) (1997) 705-715.
21. T. N. Tran, M. W. Wambsganss and D. M. France, Small circular- and rectangular-channel boiling with two refrigerants, Int. J. Multiphase Flow 22 (3) (1996) 485-498.
22. Z. Y. Bao, D. F. Fletcher and B. S. Haynes, Flow boiling heat transfer of Freon R11 and HCFC123 in narrow passages, International Journal of Heat and Mass Transfer 43 (18) (2000) 3347-3358.
23. M. W. Wambsanss, D. M. France J. A. Jendrzejczyk and T. N. Tran, Boiling heat transfer in a horizontal small-diameter tube, Journal of heat transfer 115 (4) (1993) 963-972.
24. G. R. Warrier, V. K. Dhir, L. A. Momoda, Heat transfer and pressure drop in narrow rectangular channels, Experimental Thermal and Fluid Science 26 (1) (2002) 53-64.
25. H. Oh, M. Katsuta, K. Shibata, Heat transfer characteristics of R134a in a capillary tube heat exchanger, in: Proc. of 11th International Heat Transfer Conference, Vol. 6, 1998, pp. 131-136.
26. Jostein Pettersen, Flow vaporization of CO_2 in microchannel tubes, Experimental Thermal and Fluid Science 28 (2-3) (2004) 111-121.
27. S. M. Ghiaasiaan and S. I. Abdel-khalik, Two-phase flow in microchannels, Advances in heat transfer 34 (2001) 145-254.
28. John R. Thome, Boiling in microchannels: a review of experiment and theory,

International Journal of Heat and Fluid Flow 25 (2) (2004) 128-139.
29. C. B. Sobhan and S. V. Garimella, A comparative analysis of studies on heat transfer and fluid flow in microchannels, Microscale Thermophysical Engineering 5 (4) (2001) 293-311.
30. S. G. Kandkikar, Two-phase flow patterns, pressure drop, and heat transfer during boiling in minichannel flow passages of compact evaporators, Heat Transfer Engineering 23 (1) (2002) 5-23.
31. Satish G. Kandlikar, Heat transfer mechanisms during flow boiling in microchannels, J HEAT TRANS-T ASME 126 (1) (2004) 8-16.
32. B. Watel, Review of saturated flow boiling in small passages of compact heat-exchangers, International Journal of Thermal sciences 42 (2) (2003) 107-140.
33. C. C. Wang and C. S. Chiang, Two-phase heat transfer characteristics for R-22/R-407C in a 6.5-mm smooth tube, Int. J. Heat and Fluid 18 (6) (1997) 550-558.
34. J. Y Shin, M. S. Kim and S. T. Ro, Experimental study on forced convective boiling heat transfer of pure refrigerants and refrigerant mixtures in a horizontal tube, Int. J. Refrig. 20 (4) (1997) 267-275.
35. T. Y. Choi, Y. J. Kim, M. S. Kim and S. T. Ro, Evaporation heat transfer of R-32, R-134a, R-32/134a, and R-32/125/134a inside a horizontal smooth tube, International Journal of Heat and Mass Transfer 43 (19) (2000) 3651-3660.
36. M. H. Yu, T. K. Lin and C. C. Tseng, Heat transfer and flow pattern during two-phase flow boiling of R-134a in horizontal smooth and microfin tubes, International Journal of Refrigeration 25 (6) (2002) 789-798.
37. R. Yun Y. Kim M. S. Kim and Y. Choi, Boiling heat trasfner and dryout phenomenon of CO_2 in a horizontal smooth tube, International Journal of Heat and Mass Transfer 46 (2003) (13) 2353-2361.
38. T. N. Tran, M. C. Chyu, M. W. Wambsganss and D. M. France, Two-phase pressure drop of refrigerants during flow boiling in small channels: an experimental investigation and correlation development, International Journal of Multiphase Flow 26 (11) (2000) 1739-1754.
39. W Qu. And I. Mudawar, Measurement and prediction of pressure drop in two-phase micro-channel heat sinks, International Journal of Heat and Mass Transfer 46 (15) (2003) 2737-2753.
40. J. C. Chen, A correlation for boiling heat transfer to saturated fluids in convective flow, Ind. Engng. Chem. Proc. Des. Dev., (5) (1966) 322-329.
41. Y. Fujita, H. Ohta, S. Uchida and K. Nishikwa, Nucleate boiling heat transfer and critical heat flux in narrow space between rectangular surfaces. Int. J. Heat Mass

Transfer 31 (2) (1988) 229-239.
42. C. Xia, Z. Guo, W. Hu, Mechanism of boiling heat transfer in narrow channels, Two-Phase Flow and Heat Transfer, Proc. Of the ASME Heat Transfer Division 197 (1992) 111-119.
43. K. E. Gungor, R. H. S. Winterton, A general correlation for flow boiling in tubes and annuli, International Journal of Heat and Mass Transfer (29) (1986) 351-368.
44. Z. Liu, R. H. S. Winterton, A general correlation for saturated and subcooled boiling in tube and annuli, based on a nucleate pool boiling equation, International Journal of Heat and Mass Transfer (34) (1991) 2759-2766.
45. S. G. Kandlikar, Ageneral, correlation for saturated two-phase flow boiling heat transfer inside horizontal and vertical tubes, Transaction of the ASME Journal of Heat Transfer (112) (1990) 219-228.
46. S. G.. Kandlikar, Development of a flow boiling map for subcooled and saturated flow boiling of different fluids inside circular tubes, transactions of the ASME Journal of Heat Transfer (113) (1991) 190-200.
47. S. G. Kandlikar and M. E. Steinke, Flow Boiling Heat transfer coefficient in minichannels – correlation and trends, Proceedings of the Twelfth International Heat Transfer Conference 3 (2002) 785-790.
48. S. G. Kandlikar and M. E. Steinke, Predicting heat transfer during flow boiling in minichannels and microchannels, ASHRAE Transactions 109 (1) (2003) 667-676.
49. I. Y. Chen, K. S. Yang, C. C. Wang, An empirical correlation for two-phase frictional performance in small diameter tubes, International Journal of Heat and Mass Transfer (45) (2002) 3667-3671.
50. J. G. Collier, Convective boiling and condensation, McGraw-Hill International Book Company, 2nd ed (1972) p.32, p.90-93, p.341.
51. S. M. Zivi, Estimation of steady state steam void-fraction by means of principle of minimum entropy production, Transaction of the ASME Journal of Heat Transfer 86 (1964) 237-252.
52. Wataru Nakayama, Flow boiling in advanced geometries and applications, in: S.G. Kandlikar, M Shoji, V.K. Dhir (Eds.), Handbook of boiling and condensation, Taylor and Francis, NY, 2000, Chapter 16, 403-441.
53. S. J. Kline, F. A. Mcclintock, Describing uncertainties in single-sample experiments, mechanical Engineering 75 (1953) 3-8.